STUDIES IN BONE LEAD

STUDIES IN BONE LEAD: A NEW ^{109}CD K-XRF MEASUREMENT SYSTEM; MODELING BONE LEAD METABOLISM; INTERPRETING LOW CONCENTRATION DATA

by

Nie, Huiling, M.Sc.

A Thesis Submitted to the School of

Graduate Studies in partial fulfillment of

the requirements for the degree:

Doctor of Philosophy

McMaster University

DOCTOR OF PHILOSOPHY (2005) McMaster University
(Medical Physics) Hamilton, Ontario

TITLE: Studies in Bone Lead: A New ^{109}Cd K-XRF Measurement System;

Modeling Bone Lead Metabolism; Interpreting Low Concentration Data

AUTHOR: Nie, Huiling

SUPERVISOR: Dr. David R. Chettle

NUMBER OF PAGES: xii, 191

ABSTRACT

Source induced K x-ray fluorescence (XRF) has been used for *in vivo* bone lead measurement for more than two decades. Recently, the need for the improvement of this system has been emphasized due to the increased awareness of effects of low level lead exposures, the need to examine potentially sensitive populations, such as children and pregnant woman, for whom minor exposure might be important, and the necessity to distinguish relatively small differences between groups in different exposure categories.

In this thesis, a new XRF *in vivo* bone lead measurement system will be studied. The new system consists of a cloverleaf-shaped detector system made of four detectors, and four sets of electronics. The projected performance of this system was investigated in my Master's program. The result showed an overall minimum detectable limit (MDL) improvement of a factor of about 3.6. Two such systems were purchased in our group. Three different types of electronics were tested to get the optimal setup for the system. After the initial system testing, a dosimetry study was carried out to investigate the dose delivered to the measured individual by using this system. Three age groups were involved in this dosimetry study. The doses were predicted by calculations, MC simulations, and experiments. The result shows that the dose delivered is small, even for 5 years old children (effective dose: ~9μSv). An approval to conduct human measurements on this system has been received from the Research Ethics Board of Hamilton Health Sciences based on this study. Twenty volunteers had their tibia bone measured by both the new system and the conventional system for 30 minutes clock time. The median MDLs for the conventional system and the new system are 8.75 μg/g bone mineral and 3.48 μg/g bone mineral. The source strength used for the new system is

2.45GBq, and this could go up to 10GBq. So the extrapolated median MDL for the new system is 1.74 μg/g bone mineral.

Two other minor projects were also described in the thesis. One is about an investigation of a model of lead metabolism in human body. The study shows that one of the current lead metabolism models cannot correctly reflect lead transfer between blood and bone. KXRF bone lead measurement data were used to regulate the transfer rates and the result shows a great improvement. The other is about a statistical approach for the analysis of the KXRF bone lead measurement data. Some left-censoring methods were discussed in this project and the study shows that left-censoring is a good way to handle the censored data.

ACKNOWLEDGEMENTS

I am grateful to so many people, who make my life for the past four years so peaceful, fruitful, and enjoyable. But first of all, I would like to thank my supervisor, Dr. David Chettle, for his great guidance as a supervisor, and his unconditional kindness as a friend. David is a knowledgeable, experienced, and helpful mentor. He has a way to explore my merit and to cover my shortness, and that is how he turns me from an ordinary student, whose only goal is to find a job, to a maturing research scientist. I cannot thank enough to him, for shaping me not only to a better researcher, but also to a better person.

For the consistent help and consultancy, special thanks to my other committee members, Dr. Fiona McNeill, Dr. Joanne O'Meara, Dr. Colin Webber, and my "over-enrollment" committee member Dr. William Prestwich.

My gratitude also goes to Wendy Malarek, Fiona Ahlang, Vera Iarossi, Kristina Trollip, and Nancy Brand, for making my life outside the research so much easier.

I would like to thank Jason Falladown, John Cave, Steve Staniek, and Scott McMaster for their help with the affiliated devices for the system for my research. Specially, I want to thank Norbert Boehling for his great help with the computer problems.

My special thanks go to Liqiang Luo, Soo-Hyun Byun, Zhengfeng Liu, Marija Popovic, Ryan Studinski, Rao Khan, and Mehran Goharian, for their help with my life, research, language, career decision, etc. My gratitude also goes to my other fellow graduate students, Jovica Atanackovic, Daria Comsa, Zhaoyang Fan, Joanna Grinyer,

Lorna Ryan, Kara Schnarr, Jeroen Thompson, Fabiola Vallejo, Heping Xu, Mariangela Zamburlini, Xiaoli Zhang, and Xin Zhang, for helping each other and having fun.

Last, but not least, I want to thank my husband Baozeng Zhang for his unlimited support and care, my little baby Richard for making me a very proud mother, and my dear mother for taking care of the baby, so I can get my hands off for the research and thesis. I would also like to thank my family in China for their blessings from the other side of the earth.

TABLE OF CONTENTS

Abstract iii

Acknowledgements v

Table of Contents vii

List of Figures x

List of Tables xi

Chapter 1: Introduction 1
1.1 Lead 1
1.2 Impact of lead on human health 3
1.2.1 Systemic effects 3
1.2.1.1 Hematological effects 3
1.2.1.2 Renal effects 4
1.2.1.3 Neurological effects 5
1.2.1.4 Reproductive effects 7
1.2.2 Debatable Health effects related with lead exposure 7
1.2.2.1 Cardiovascular effects 7
1.2.2.2 Immunological effects 8
1.2.2.3 Musculoskeletal effects 8
1.2.2.4 Carcinogenic effects 9
1.2.3 Health effects of low-level lead exposure 9
1.3 Tests to determine lead exposure 10
1.3.1 Blood lead measurement 10
1.3.2 Lead measurement in soft tissues 11
1.3.3 Lead measurement in hair, teeth, and bone *in vitro* 11
1.3.4 *In vivo* bone lead measurement 11
1.4 Lead metabolism in human body 12
1.5 X-ray fluorescence (XRF) 13
1.5.1 Interactions of photons with specimen 13
1.5.2 *In vivo* XRF bone lead measurement systems 17
1.5.2.1 *In vivo* L XRF bone lead measurement systems 17
1.5.2.2 *In vivo* KXRF bone lead measurement systems 19
1.5.3 ^{109}Cd γ-ray induced KXRF bone lead measurement 20
1.6 Brief introduction of the thesis 24
1.7 Purpose of the projects 26

Chapter 2: Design, performance, and tests of the new system 28
2.1 Conventional system and new system 28
2.1.1 ^{109}Cd γ-ray induced XRF bone lead measurement system – conventional system 28
2.1.2 ^{109}Cd source 30

2.1.3 New system set up 32
2.2 Electronics 33
2.2.1 Comparison of Canberra DSA-2000 and XIA Polaris 34
2.2.1.1 Experimental design 34
2.2.1.2 Results 37
2.2.2 Comparison of DSA-2000 and DSA-1000 38
2.2.2.1 Experimental design 38
2.2.2.2 Results 40
2.3 New system 41
2.3.1 Throughputs and resolutions 42
2.3.2 Summary of the predicting approaches and results 45
2.3.2.1 Calculations 45
2.3.2.2 MC simulations 46
2.3.2.3 Single-detector experiments 47
2.4 New system experiments and results 48
2.5 Discussion 51

Chapter 3: Dosimetry study **54**
3.1 Introduction 54
3.2 Materials and methods 55
3.2.1 Experiments 57
3.2.2 MC simulation 58
3.2.3 Calculation 59
3.3 Results 63
3.4 Discussion 70

Chapter 4: *In vivo* bone lead measurement by using the new system **71**
4.1 System setup 71
4.2 Experiments 72
4.3 Results 74
4.4 Discussion 87
4.5 Future work 90

Chapter 5: Lead metabolism modeling **92**
5.1 Lead metabolism models 92
5.2 Method 94
5.2.1 Bone lead measurement and subject population 94
5.2.2 Lead metabolism simulation by Leggett's model 94
5.2.3 The new model 96
5.2.4 The bone and blood compartments in Leggett's model and the new model 98
5.3 Results/Discussion 99
5.3.1 The predicted bone lead concentrations based on Leggett's model compared to the measured bone lead concentrations 99
5.3.2 The estimated transfer rates by the new model 101

5.3.3 The predicted bone lead concentrations based on Leggett's model with new transfer rates, compared to the measured bone lead concentrations 104
5.4 Conclusion/Future work 108

Chapter 6: Left censoring: a statistical approach for XRF bone lead data analysis 110
6.1 Left censoring 110
6.2 Methods 111
6.2.1 IVW method 112
6.2.2 KM method 113
6.2.3 NA method 116
6.2.4 RM method 117
6.2.5 Mean and uncertainty of the mean 118
6.2.6 Log-normal distribution 119
6.3 Measurements and populations 119
6.4 Results/discussion 121
6.5 Conclusion 126

References 127

Appendices Introduction/Comments/Description 134

Appendix I Papers 135
paper 1 A study of MDL improvement for the in vivo measurement of lead in bone 137-141
paper 2 An investigation of ^{109}Cd γ-induced K-x-ray fluorescence (XRF) bone lead measurement calibration procedure 142-151

Appendix II Initial work in calculating the dose absorption fraction for ^{14}C and tritium in trabecular bone by Monte Carlo (MC) simulation 152

Appendix III Fitting programs 162

List of figures

Figure 1-1	Effects of lead on heme biosynthesis	4
Figure 1-2	Process of x-ray fluorescence	14
Figure 1-3	^{109}Cd XRF bone lead measurement system	20
Figure 1-4	Spectrum for ^{109}Cd KXRF lead measurement	22
Figure 2-1	System setup	28
Figure 2-2	Conventional system setup	29
Figure 2-3	System setup for tibia measurement	29
Figure 2-4	Decay scheme of ^{109}Cd source	30
Figure 2-5	Size of the source holder for the conventional system	31
Figure 2-6	Scheme diagram for the four detectors	32
Figure 2-7	Experimental design for the new system	32
Figure 2-8	New system setup	41
Figure 2-9	Single-detector setup	47
Figure 3-1	New source holder	55
Figure 3-2	Back side of the Panasonic UD-803AS TLD	56
Figure 3-3	TLD setup for the experiments	57
Figure 3-4	The cross section of the lower leg for the dose distribution	59
Figure 3-5	Geometries to calculate exposure rate at point A	60
Figure 3-6	MC simulation for the bone marrow dose	66
Figure 3-7	Irradiated skin area	69
Figure 5-1	The simplified model proposed in this study, based on the available data	97
Figure 5-2	Bone and blood compartments in Leggett's model of lead metabolism	99
Figure 5-3	Predicted and measured bone and blood lead concentrations for subject #270	100
Figure 5-4	Predicted and measured bone and blood lead concentrations for 9 retired workers	101
Figure 5-5	Z-distribution of the differences between the predicted and measured bone lead concentration	103
Figure 5-6	Predicted and measured bone and blood lead concentrations for subject #270	105
Figure 5-7	Predicted and measured bone and blood lead concentrations for 9 retired workers by using the new bone to blood transfer rates in Leggett's model	106
Figure 6-1	Histogram of bone lead concentrations for 67 people	114
Figure 6-2	Histogram of bone lead concentrations for the referent young adult women	125
Figure 6-3	PDFs estimated by the four left-censoring methods for bone lead concentration measurements for the referent young adult women	125

LIST OF TABLES

Table 1-1	Energies of lead K x-rays and their characteristics	21
Table 2-1	Attenuation factors for 88, 25, and 22 keV photons through 0.7 mm Cu filter	31
Table 2-2	Summary of six sets of spectra	35
Table 2-3	Parameter setup and some characteristics of the spectra for DSA-2000 and Polaris	36
Table 2-4	Calculated MDLs for DSA2000 and Polaris	37
Table 2-5	Ratio of MDLs (DSA-2000/Polaris) for K_α, K_β, and the weighted estimate	38
Table 2-6	Summary of three sets of spectra	39
Table 2-7	Parameter setup and some characteristics of the spectra for DSA-1000 and DSA-2000	40
Table 2-8	Calculated MDLs for DSA-1000 and DSA-2000	40
Table 2-9	Ratios of MDLs (DSA-1000/DSA-2000)	41
Table 2-10	Energy resolution for detector #1 with low and high ICR	43
Table 2-11	Energy resolution for detector #2 with low and high ICR	43
Table 2-12	Energy resolution for detector #3 with low and high ICR	44
Table 2-13	Energy resolution for detector #4 with low and high ICR	44
Table 2-14	MDL_{new}/MDL_{old} ratios by MC simulations and single-detector experiments	48
Table 2-15	Calculated MDLs for the new system	50
Table 2-16	Ratios of the MDLs of the new system and the old system	50
Table 2-17	Factors that affect the improvement of the new system	52
Table 3-1	The sizes of the lower legs for the three sets of human phantoms	56
Table 3-2	Characteristic of Panasonic UD-803AS TLD	57
Table 3-3	Proportion of the elements in H_2O, Air, Compact bone, Muscle, plaster of Paris, and Wax	62
Table 3-4	Exposure rate of some key organs for the three sets of human phantoms	63
Table 3-5	Skin, bone surface, bone marrow, and the midcalf exposure rate for 5-year old	65
Table 3-6	Calculated skin, bone surface, bone marrow, and midcalf exposure rate and dose for 5-year old, 10-year old, and adult	66
Table 3-7	The comparison of the bone marrow dose rate from calculation and from the MC simulation	67
Table 3-8	The equivalent bone dose, bone marrow dose, and tissue dose for the three age groups by MC simulation for 1 hour lead measurement	67
Table 3-9	Effective bone dose and bone marrow dose for 1 hour bone lead measurement	68
Table 3-10	Whole body dose for the three age groups	69
Table 4-1	Setup parameters selected for the conventional system and the new system	71
Table 4-2	Age and sex of the 20 volunteers	73
Table 4-3	Concentration from α and β fittings for the old system	75

Table 4-4	Concentrations from α and β fittings for the new system, det#1	76
Table 4-5	Concentrations from α and β fittings for the new system, det#2	77
Table 4-6	Concentrations from α and β fittings for the new system, det#3	78
Table 4-7	Concentrations from α and β fittings for the new system, det#4	79
Table 4-8	Bone lead concentrations measured by the four detectors of the new system	80
Table 4-9	Lead concentrations and uncertainties measured by both systems	82
Table 4-10	Regression results between concentration and age for both systems	83
Table 4-11	Averages and standard deviations of Z values	85
Table 4-12	MDLs for the conventional system and the new system and their ratios	86
Table 4-13	MDLs for the new system for 2.45GBq and 10GBq sources	87
Table 5-1	Calculated transfer rates for five age groups based on the simplified model	102
Table 5-2	Calculated and modeled lead concentrations in cortical and trabecular bones	107
Table 6-1	Bone lead concentrations for 67 people	113
Table 6-2	The cumulative distribution (CD) and the probability distribution (PD) of the bone lead concentrations by KM method	114
Table 6-3	Mean and SEM calculated from reduced sample, IVW, and KM method	116
Table 6-4	Characteristics of the populations	120
Table 6-5	Mean, Error of the mean (EM), or standard error of the mean (SEM) determined by inverse variance weighted (IVW) averaging, KM, NA, RM, and Minitab	122
Table 6-6	Difference between means of the given populations	123

Chapter 1

INTRODUCTION

1.1 Lead

Lead is a naturally occurring bluish-gray metal found in small amounts in the earth's crust. It has no taste or smell. Some natural and manufactured substances contain lead but do not look like lead in its metallic form, which is one of the reasons for people being exposed to lead without being aware of it. Lead occurs naturally in the environment. However, most of the high levels found throughout the environment come from human activities. The use of lead can be traced back to five thousand years ago, when it was used as an artistic material. In modern times, the most important use of lead is in the production of some types of batteries. It is also used in the production of ammunition, in metal products (such as sheet lead, solder, brass and bronze products, pipes etc.), and in ceramic glazes. Tetraethyl lead and tetramethyl lead were introduced in 1926 as gasoline additives to increase gasoline octane and counter engine "knock". Fortunately, leaded gasoline was phased out in most of the developed countries since the 1990s, which include Canada. However, in many developing countries, lead in gasoline remains a serious problem related with public health. Other chemicals containing lead are used in paint, which now becomes a big concern of lead exposure for children. Lead is also used in a large variety of medical equipment (radiation shields, electronics, ceramic parts of ultrasound machines, intravenous pumps, fetal monitors, and surgical equipment), scientific equipment (circuit boards for computers and other electronic circuitry), and

military equipment (military tracking systems). Most lead used by industry comes from mined ores ("primary") or from recycled scrap metal or batteries ("secondary"). Because of the mining, refining, as well as the use of leaded gasoline and other leaded products, lead has been spread very widely in the environment and the ecosystem and causes many kinds of problems to human health.

Lead intoxication in human beings has been documented since the second century B.C. (Perazella 1996). Lead can be transferred to human body through many ways: by eating foods or drinking water that contain lead; by spending time in area where leaded paints have been used and are deteriorating; by working in jobs where lead is used; by using health-care products that contain lead; or by having hobbies in which lead may be used; etc.. Many measures have been performed to reduce the exposure of lead during the last several decades, which include the reduction and elimination of lead from gasoline, elimination of lead solder from canned food, removal of lead from paint, and abatement of housing containing lead-based paint. Nevertheless, the health effects of lead is still an important issue, especially for children and women, for whom even very low level of exposure may have a significant effect. The health effects for low level lead exposure will be explained in detail in section 1.2.3.

1.2 Impact of lead on human health

1.2.1 Systemic effects

1.2.1.1 Hematological effects

The effects of lead on the hematopoietic system include increased urinary porphyrins, coproporphyrins, δ-aminolevulinic acid (ALA), erythrocyte protoporphyrin (EP), free erythrocyte protoporphyrin (FEP), erythrocyte zinc protopophyrin (ZPP), and anemia. Lead interferes with heme biosynthesis by altering the activity of three enzymes: δ-aminolevulinic acid synthetase (ALAS), δ-aminolevulinic acid dehydratase (ALAD), and ferrochelatase (Much of this section 1.2 draws on the data and overview presented in the report entitled "Toxicological Profile for Lead", Research Triangle Institute, 1999, and other reports referenced therein. Additional bibliographic sources will be identified specifically in this text).

Figure 1-1 shows the effects of lead on heme biosynthesis (EPA 1986). As shown in the figure, lead indirectly stimulates the mitochondrial enzyme ALAS, which catalyzes the condensation of glycine and succinyl-coenzyme A to form ALA. At the same time, lead inhibits the zinc-containing cytosolic enzyme ALAD, which catalyzes the condensation of two units of ALA to form porphobilinogen. Inhibition of ALAD and derepression of ALAS result in accumulation of ALA. Lead also decreases the activity of the zinc-containing mitochondrial enzyme ferrochelatase, which catalyzes the insertion of iron (II) into the protoporphyrin ring to form heme, by binding to the vincinal sulfhydryl groups of the active site. Lead may also affect the heme synthesis through impaired transport of iron in the mitochondrion, due to disruption of mitochondrial structure. All

these interferences with heme synthesis result in a reduction of the hemoglobin concentration in blood. Decreased hemoglobin production, coupled with an increase in erythrocyte destruction, results in a hypochromic, normocytic anemia with associated reticulocytosis.

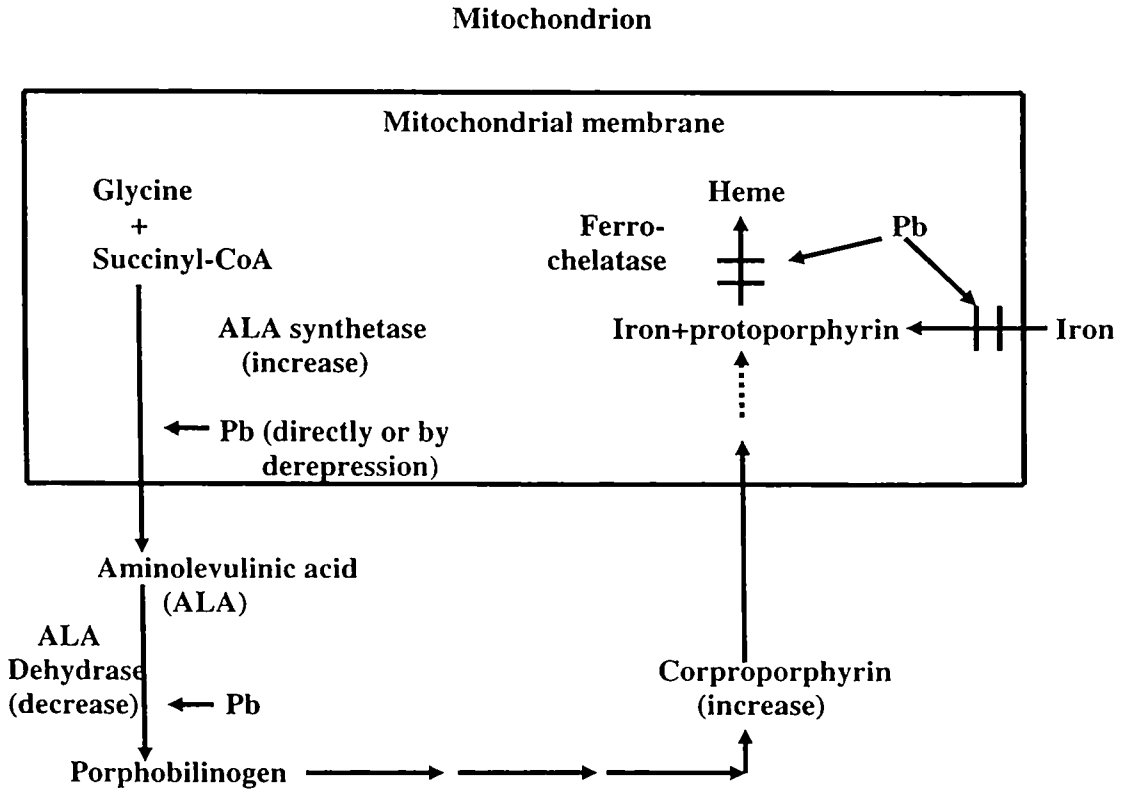

Figure 1-1 Effects of lead on heme biosynthesis

1.2.1.2 Renal effects

The effects of acute lead-induced nephropathy in humans include nuclear inclusion, mitochondrial changes, and cytomegaly of the proximal tubular epithelial cells; dysfunction of the proximal tubules (Fanconi's syndrome) manifested as aminoaciduria, glucosuria, and phosphaturia with hypophosphatemia; and increased sodium and

decreased uric acid excretion. The effects of chronic lead nephropathy include progressive interstitial fibrosis, dilation of tubules and atrophy or hyperplasia of the tubular epithelial cells, reduction in glomerular filtration rate, and azotemia.

There are high-affinity cytosolic zinc- and lead-binding proteins in the kidneys (or brain). These proteins moderate the inhibition of ALAD by lead through chelating lead and donating zinc, and by translocating lead to the nucleus, where it may influence gene expression. Lead can also attach to kidney cell membranes and alter membrane permeability, hence it affects the release of N-acetyl-D-glucosaminidase (NAG) from renal tubular cells. NAG is a lysosomal enzyme present in renal tubular cells that has been shown to be a sensitive indicator of early subclinical renal tubular disease. Some other ways for lead to affect kidney function include affecting rennin release from the kidney by changing calcium ion fluxes in the juxtaglomerular cells, and decreasing circulating levels of the active form of vitamin D (1,25-dihydroxy-vitamin D) in children by affecting the formation process which involves the renal tubule.

1.2.1.3 Neurological effects

The fact that lead is potentially toxic to the nervous system has been recognized for nearly 200 years. The most severe neurological effect of lead is lead encephalopathy, which is a term to describe various diseases that affect brain function. It can cause dullness, irritability, poor attention span, headache, muscular tremor, loss of memory and ability to concentrate, hallucinations, delirium, convulsions, paralysis, coma, and death.

Lead blocks the voltage-regulated calcium channels, inhibiting the influx of calcium and release of neurotransmitter, thus inhibiting synaptic transmission. Lead also decreases the activity of tyrosine hydroxylase in brain, the rate-limiting enzyme in catecholamine biosynthesis. In glutamatergic systems, lead inhibits depolarization-evoked glutamate release and in the astroglia, lead inhibited high affinity glutamate uptake and glutamine synthetase activity, which catalyzes the formation of glutamine from glutamate. Lead may act as a calcium substitute in the activation of protein kinase C, which is important in cell growth and differentiation, including the differentiation of brain endothelial cells. Lead also has been shown to substitute for calcium in the activation of calmodulin, which regulates the activity of certain enzymes and transporters. Another mechanism by which lead affects the nervous system is through its effect on neuronal cell adhesion molecules (NCAMs), membrane-bound cell-recognition molecules that regulate cell-cell interactions, including synapse formation. Chronic, low-level lead exposure impairs the desialylation of NCAMs during postnatal periods that coincide with synapse formation. This interference with sialylation pattern may perturb synapse selection, thus contributing to learning deficits. As discussed previously under renal effects, high-affinity cytosolic zinc- and lead-binding proteins are also identified in the brain, which cause lead-induced encephalopathy. The nervous system can also be affected indirectly through lead's inhibition of heme synthesis.

1.2.1.4 Reproductive effects

Increasing evidence indicates that lead exposure cause adverse effects on both male and female human reproductive functions. Both exposed men and women experienced diminished fertility. Women exposed to lead during pregnancy experienced increased frequency of low-weight babies, miscarriages, and stillbirths. The effects of lead exposure to men include lower sperm counts, lower libido etc.

The mechanisms underlying these effects are unknown at this time. Factors that may contribute to such results include indirect effects of lead on maternal nutrition or hormonal status before and during pregnancy and more direct gametogenic effects.

1.2.2 Debatable health effects related with lead exposure

1.2.2.1 Cardiovascular effects

There is considerable scientific debate as to whether lead exposure has cardiovascular effects. Some studies show that lead exposure causes hypertension and electrocardiographic (ECG) abnormalities, while others claim that the relationship is not significant.

The following are possible mechanisms for lead's purported effects on cardiovascular system: the effects of lead on several hormonal and neural regulatory systems, changes in vascular smooth muscle reactivity, cardiac muscle contractility, changes in cell membrane cation transport systems, and possible effects on vascular endothelial cells (Victery 1988).

1.2.2.2 Immunological effects

The data on immunological effects in humans following exposure to lead are inconsistent and limited. Studies show that people exposed to lead had immunologic problems (e.g. more colds and infections, depression of the lymphocytes, impaired cell-mediated immunity) than a control group (Ewers et al. 1982, Alomran and Shleamoon 1988, Fischbein et al. 1993). These effects are believed to be associated with the suppression of secretory immunoglobulin A (IgA) and changing of the lymphocyte transformation.

1.2.2.3 Musculoskeletal effects

There are very few studies on lead induced musculoskeletal effects. Adachi et al. show possible relationships between bone lead and Paget's disease as well as osteoprosis (1998). Gruber et al. show increased osteoid coverage of trabecular surfaces and increased osteoclasts in trabecular lacunae for lead exposed people (1997). Although little research has been performed in this area, a number of mechanisms have been proposed for lead toxicity to bone. Lead may affect bone indirectly through alteration of the circulating levels of hormones, particularly 1,25-dihydroxyvitamin D, that modulate calcium homeostasis and bone cell function (Pounds et al. 1991; Puzas et al. 1992). In addition, lead may alter the responses of bone cells to these hormones, and disrupt many aspects of calcium homeostasis and signaling at the cellular level (Pounds et al. 1991). Lead could also increase bone resorption activity.

1.2.2.4 Carcinogenic effects

The studies regarding the association of occupational exposure to lead with increased cancer risk are not sufficient to determine the carcinogenic effects of lead exposure, partly because of some controversial results, partly because of the potential exposure to other chemicals for the workers. Suggested mechanisms for the carcinogenesis of lead include an alteration of genetic function by lead in association with the high-affinity lead-binding protein following translocation to the nucleus, tumor promotion by activation of protein kinase C, and stimulation of cellular proliferation or cystic hyperplasia (Goyer 1993).

1.2.3 Health effects of low-level lead exposure

People used to think that there is a threshold for lead to induce health effects to humans and that only occupationally exposed workers should be concerned in terms of lead poisoning. Childhood lead poisoning was first discovered in Brisbane, Australia in 1894. In the United States, it was believed that if a lead-poisoned child did not die, they recovered with no residue. This was disproved by R.K. Byers in 1943. In the 1960's, the defined toxic level of lead in the blood was 60 micrograms/dl. Studies of lower lead exposure began to be published in the early 1970's (Needleman 1993). Numerous studies show that low-level lead induces many health effects, especially in children and newborns; these effects include high blood pressure (more often in adults), lower IQ, deficits in the neurobehavioral-cognitive performance, decrease in auditory sensitivity and visuomotor performance, lower learning ability etc. (more often in children). In

October 1991, the Centers for Disease Control and Prevention issued new lead guidelines, dramatically lowering the intervention level from 25 micrograms/dL of lead in blood to 10 micrograms/dL (Schonfeld DJ 1993). Although there is still some debate on low-level lead exposure induced health effects, it is believed that there is no threshold for lead toxicity, especially to the nervous system, and the effects are considered irreversible.

1.3 Tests to determine lead exposure

1.3.1 Blood lead measurement

The methods currently used to determine blood lead are flame atomic absorption spectrometry (AAS), graphite furnace atomic absorption spectrometry (GFAAS), anode stripping voltametry (ASV), inductively coupled plasma-atomic emission spectroscopy (ICP-AES), and inductively coupled plasma mass spectrometry (ICP-MS). The most reliable and commonly used method for the determination of lead at low concentrations is ICP-MS. Measurement of lead in blood is the most common method of assessing exposure, due to its sensitivity and availability. Other advantages of blood lead measurements include easy sample collecting and quick analysis process. However, the half-life of lead in human blood is about 30 days, so the lead levels in blood only reflect relatively recent exposure. Therefore, blood lead levels cannot serve as exact measures of lead exposure or the total body lead burden. In addition, the relationship between blood lead and lead exposure is nonlinear, such that the proportional increase in blood lead concentration is less at high exposure levels than at low exposure levels. Nevertheless, blood lead measurement is the most widely used method to determine lead exposure.

1.3.2 Lead measurement in soft tissues

Lead can be measured in liver, kidney, brain, heart, lung, and muscle. Techniques for measuring lead in these tissues are similar to those used for blood. The disadvantages of measuring lead in these tissues are that it has to be done in postmortem, and the amounts of lead accumulated in these tissues are relatively small.

1.3.3 Lead measurement in hair, teeth, and bone in vitro

ICP-MS and x-ray fluorescence (XRF) were used to measure lead in hair, teeth, and bone samples. Hair has been used as an indicator for intermediate exposure in children (Wilhelm et al. 1989). However, artificial hair treatment and external surface contamination make it difficult to differentiate between externally and internally deposited lead. For *in vitro* teeth and bone lead measurement, the disadvantage again is that it has to be done posthumously, or by using a biopsy, which is a painful process.

1.3.4 In vivo bone lead measurement

XRF is the only way to measure lead in bone *in vivo* so far. It is noninvasive, relatively sensitive, and above all, bone lead reflects long term lead exposure. The half life of lead in bone is measured in decades, and more than 95% of the lead will be accumulated in bone after a fairly short time. So bone lead indicates total body burden and exposure history of the person. Many studies suggest that bone lead levels are better predictors of certain health outcomes than are contemporary blood lead concentrations

(Gonzalez-Cossio et al. 1997; Hu et al. 1995, 1996). The techniques will be described in detail in section 1.5.

1.4 Lead metabolism in human body

The lead metabolism has been extensively studied in both animals and humans. While some of the precise pharmacokinetic mechanisms that control the metabolism process are unknown, available data can be used to quantify the uptake and deposition of lead in the human body for various populations. Several lead metabolism models have been built based on different data sets. Some of these models will be described in Chapter 5, section 1. While these models are useful in understanding the toxicokinetics of lead with their own ways, recent progress in analytical methods has raised some questions for these models. The *in vivo* bone lead measurement is one of these analytical methods. For example, endogenous release of lead from bone to blood in retired workers has been investigated (Brito et al. 2002, Fleming et al. 1997, Bleeker et al. 1995, Gerhardsson et al. 1993, Erkkilä et al. 1992), and it is believed that endogenous exposure plays an important role in retired lead workers. Studies also show that the kinetic parameters of human lead metabolism may vary with age and exposure level. In Chapter 5, a study to investigate the relationship between the kinetic parameters and age will be described.

1.5 X-ray fluorescence (XRF)

1.5.1 Interactions of photons with specimen

When a beam of x-ray photons falls onto a given specimen, four basic phenomena may result (Knoll G F, 1999).

a) Photoelectric absorption

In the photoelectric absorption process, a photon undergoes an interaction with an absorber atom in which the photon completely disappears and an orbital electron is ejected by the atom from one of its bound shells. The photoelectron can be ejected from K, L, M etc. shells. The whole process has to meet energy conservation as well as momentum conservation, so it can not take place with free electrons. For photons of sufficient energy, the most probable origin of the photoelectron is the most tightly bound K shell of the atom. Part of the incident photon energy is used to overcome the binding energy of the photoelectron, and the other part is converted to the energy of the photoelectron. So the energy of the photoelectron can be described as:

$$E_e = h\nu - E_b \quad \ldots\ldots\ldots\ldots (1.1)$$

where E_b represents the binding energy of the photoelectron and hν is the energy of the incident photon.

In addition to the photoelectron, the interaction also creates an ionized atom with a vacancy in one of its bound shells. This vacancy will be filled through rearrangement of electrons from other shells of the atom and eventually a free electron will be captured from the medium. Therefore, one or more characteristic x-ray photons may be generated. In some cases, the emission of an electron from another shell may substitute for the

characteristic x-ray in carrying away the atomic excitation energy, and this electron is called an Auger electron. The incident photon could knock out an electron from K shell, L shell, M shell... So the vacancy could be present in these shells with certain proportions. If the vacancy is in K shell, then the characteristic x-ray ejected while the electron jumps from other shells to the vacancy is called a K-series x-ray. If the vacancy is in L shell, then the x-ray generated is called an L-series x-ray, and so on. There are K_αs and K_βs depending from which shell and layer of the shell the electron that fills the vacancy originates. The energy of the x-ray is determined by the binding energies of atomic electron shells, which are determined by the charge, or atomic number, of the nucleus. So we can determine the type and concentration of the element by measuring the energy and intensity of the characteristic x-rays. This is the basic principle of XRF measurement for a sample. Figure 1-2 shows the process of x-ray fluorescence.

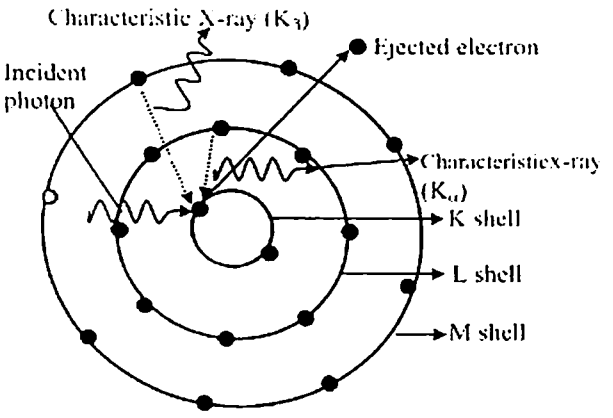

Figure 1-2 Process of x-ray fluorescence

b) Compton scattering

In the Compton scattering process, a photon interacts with an absorber atom in which the photon is deflected through an angle θ with respect to its original direction and at the same time transfers a portion of its energy to an electron. The electron is called a recoil electron. If the target electron is treated as free and stationary, the energy of the scattered photon hν' can be described as:

$$h\nu' = \frac{h\nu}{1 + \frac{h\nu}{m_e c^2}(1 - \cos\theta)} \quad \ldots\ldots\ldots\ldots (1.2)$$

where hν is the energy of the incident photon, m_e is the static mass of the electron, and θ is the angle between the incident photon and scattered photon. Since the electron is bound to the nucleus, a minimum energy which equals to the binding energy has to be absorbed by the electron to get the electron out of the shell. So the energy transferred to the electron can vary from the binding energy to a substantial fraction of the photon energy, and the angle of scattering varies from a small angle to 180 degree.

Compton scattering offers little information for the *in vivo* XRF analysis of tissues, yet is often a dominant spectral feature. Geometry, source energy, and electronics considerations are important in order to minimize the Compton scattering contribution in XRF analysis.

c) Pair production

If the energy of the incident photon exceeds twice that of the rest-mass energy of an electron (1.022 MeV), the process of pair production is energetically possible. In the

interaction, the photon disappears and is replaced by an electron – positron pair. The source energies we used in the bone lead measurement systems, which we are going to discuss in this thesis, are much less than 1.022 MeV, so there will be no pair production phenomenon in these processes.

d) Coherent scattering

In addition to Compton scattering, another type of scattering can occur in which the photon interacts coherently with all the electrons of an absorber atom. The probability of coherent scattering is significant for low photon energies and is most prominent in high-Z materials and at small angles with respect to the incident photon direction. The probability of coherent scattering can be described as:

$$d\sigma = \frac{1}{2} r^2 (1 + \cos^2 \theta) \left| F(K)^2 \right|^2 d\Omega \quad \ldots\ldots\ldots\ldots \quad (1.3)$$

where r is the classical electron radius, θ is the angle of scatter, and F(K) is the atomic form factor, which is a function of atomic number, Z, photon energy, E, and θ. At very small angles the cross section varies as Z^2. This dependence on atomic number increases at large scattering angles (120°-180°), for which the cross section varies by Z^5 or Z^6 in the energy range of the order of keV. For this reason the major source of coherently scattered photons at large scattering angles are the high Z elements, which will be bone minerals (Ca, P) in the case of bone measurement. This is a very important factor in the normalization procedure for determining lead concentration in the bone, which will be illustrated in detail in section 1.5.3.

1.5.2 In vivo XRF bone lead measurement systems

Both K- and L-x-rays are suitable for the analysis of lead in bone. To induce K-x-ray fluorescence, the incident radiation has to be above the 88.001 keV K-absorption edge (Lederer et al. 1978). The sources used in K-XRF bone lead measurement system include ^{57}Co and ^{109}Cd. The lead L-absorption edge is 15.870 keV, and the sources used in L-XRF bone lead measurement system include ^{109}Cd and ^{125}I, as ^{109}Cd produces both 88.035 keV γ-ray and silver x-rays (22 keV and 25 keV). There are also some studies about X-ray tube source-based L-XRF lead measurement system. The x-ray tube based K-XRF *in vivo* bone lead measurement system has never had a chance to be explored because of the successful use of the source based K-XRF system.

1.5.2.1 In vivo L XRF bone lead measurement systems

The feasibility study for the *in vivo* measurement of lead in bone using L-x ray fluorescence was first investigated by Wielopolski et al. (1981). It was concluded that ^{109}Cd and ^{125}I could be used to detect bone lead by inducing lead L x-rays. In 1982, Wielopolski conducted a postmortem study to measure bone lead by using an ^{125}I source (1983). The minimum detection limit (MDL) for this system was calculated to be about 40 μg Pb/g bone mineral, for a skin dose of 10 mGy. The first *in vivo* study using L XRF estimated bone Pb values in 45 workers (Wielopolski et al. 1986). In this study, a ^{109}Cd source was utilized, and the MDL was estimated to be about 36 μg Pb/g bone mineral. Later, an x-ray tube source based L-XRF system was designed for potential use in children (Wielopolski et al. 1987, Wielopolski et al. 1989). This system utilizes polarized

x rays and hence greatly reduced the intensity of the scattering background. The MDL for this system is approximately 12 μg Pb/g bone mineral. Another system development was investigated by Todd (2002a). In this study, a secondary target, as well as partially polarized x-ray, was considered in the system. The best signal-to-background ratio was obtained by polarizer + secondary target design. Some other aspects of L XRF measurement of lead in bone were also discussed (Todd 2002b, Todd et al. 2002c). The polarization of a ^{109}Cd source to induce lead L x-rays was discussed in Ao et al.'s work (1997). This study is conducted by Monte Carlo simulation and it investigated the effects of source polarization and source-bone-detector geometry modification on reducing the scattering background. Recent research related with L XRF *in vivo* bone lead measurement include a study to combine K and L XRF method for the tibia bone (Lee et al. 2001) and a preliminary study on K and L coincidence spectroscopy (Guo et al. 2004). The former work suggests that more information about bone lead can be obtained by combining K and L XRF. Due to the low energy of lead L-series x-rays, L XRF is believed to only measure the lead concentration of superficial bone tissue. The results from bone K and L line can be used to determine if the superficial bone lead concentration can represent the whole bone lead concentration. If it is, then the analysis from bone K and L line can be combined to get a more precise result. The latter work presents an optimal configuration for coincidence spectroscopy of K and L X-rays and further optimization and development were proposed.

There are some advantages of using the L XRF system. Because of the much lower energy of the source, the dose to the bone marrow is lowered significantly. This is

a big advantage for measuring bone lead in children, since most of the dose for a child's bone lead measurement comes from bone marrow. If it is an x-ray tube based system, the L x-ray system has an advantage in that it only needs an x-ray system with relatively low voltage, which is more generally used due to its low dose and simplicity. In addition, low energy x-rays are more easily polarized, and polarization of the x-rays can improve the detection limits and at the same time lower the dose. But the L XRF system has major disadvantages in that the detection limit depends largely on the thickness of the overlying tissue and the low energy x-rays can only sample the surface of the bone. In addition, it is hard to correct tissue attenuation for the x-rays.

1.5.2.2 In vivo K XRF bone lead measurement systems

The first *in vivo* measurements of bone lead was reported by Ahlgren et al. (1976). In this study, γ-rays from ^{57}Co were used to excite the K series x-rays of lead in finger bone with a 90-degree geometry. The minimum detectable limit (MDL) for this system is about 50-60 μg/g bone mineral. Later, ^{109}Cd was found to have significant advantages (Somervaille et al. 1983, 1985). The initial ^{109}Cd XRF bone lead measurement system is shown in figure 1-3. In this system, a HPGe detector with 16 mm diameter was applied and an annular ^{109}Cd source was mounted in front of the detector. This system measures bone lead in tibia and calcaneus. The MDL for this system is about 16-20 μg/g bone mineral for tibia measurement. This system was improved by Gordon et al. (1993). The improved system is based on a larger area HPGe detector with a diameter of 51 mm, and a point ^{109}Cd source. The ^{109}Cd source is mounted coaxially in front of the detector. The

bigger detector and the point source decreased MDL to about 6-10 μg/g bone mineral for tibia measurement. The conventional system that is currently used in Medical Physics group in McMaster University is based on this system.

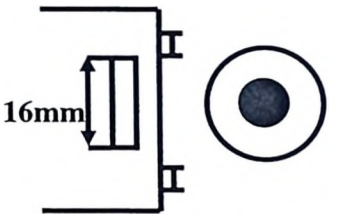

Figure 1-3 Initial ^{109}Cd XRF bone lead measurement system

1.5.3 ^{109}Cd γ-ray induced KXRF bone lead measurement

The principle of ^{109}Cd γ-ray induced KXRF bone lead measurement is to irradiate human tibia or calcaneus or other bone sites to get lead K x rays from the irradiated bone and then deduce bone lead concentrations from the counts of the lead K x rays. The lead K edge is 88.001 keV. ^{109}Cd source emits γ rays of 88.035 keV with 3.6% intensity (Lederer et al. 1978). The energy of these gamma rays is just above the energy threshold for the K shell absorption edge in lead and thus maximizes the photoelectric cross section and hence the x-ray fluorescence yield. The γ rays can interact with a K shell electron in lead and eject it. There will be a vacancy in the K shell which the electrons from the outer shells can fill. The energy is released as K_α or K_β x-rays with 96% intensity or Auger electrons with around 4% intensity. Table 1-1 shows the energies of lead K x-rays and their characteristics.

Line	Transition	Energy (keV)	Intensity (%)
$K_{\alpha 1}$	L_{III} to K	74.969	49.19
$K_{\alpha 2}$	L_{II} to K	72.804	29.17
$K_{\beta 1,3}$	M_{II}/M_{III} to K	84.936/84.450	10.92/5.7
$K_{\beta 2}$	N_{II}/N_{III} to K	87.300	5.02

Table 1-1 Energies of lead K x-rays and their characteristics

Other than the K x-rays, there are also elastic (or coherent) scattered γ rays with energy 88.035 keV and Compton scattered γ rays with energy range from 65.47 keV (180°) to (88.035 keV – binding energy for the scattered electron) (~ 0°). In the backscattered system with a point ^{109}Cd source mounted in front of the detector, the backscatter geometry is about 140-170 degrees and γ rays scattering through angles smaller than 140° or greater than 170° do not reach to the detector. In this case, the Compton scattered photons have a peak at energy around 66 keV according to formula (1.2).

Figure 1-4 shows the spectrum of ^{109}Cd K XRF lead measurement of a phantom with a lead concentration of 200 ppm and live counting time of 30 minutes. The names and the energies of the peaks used for the analysis are listed in the spectrum.

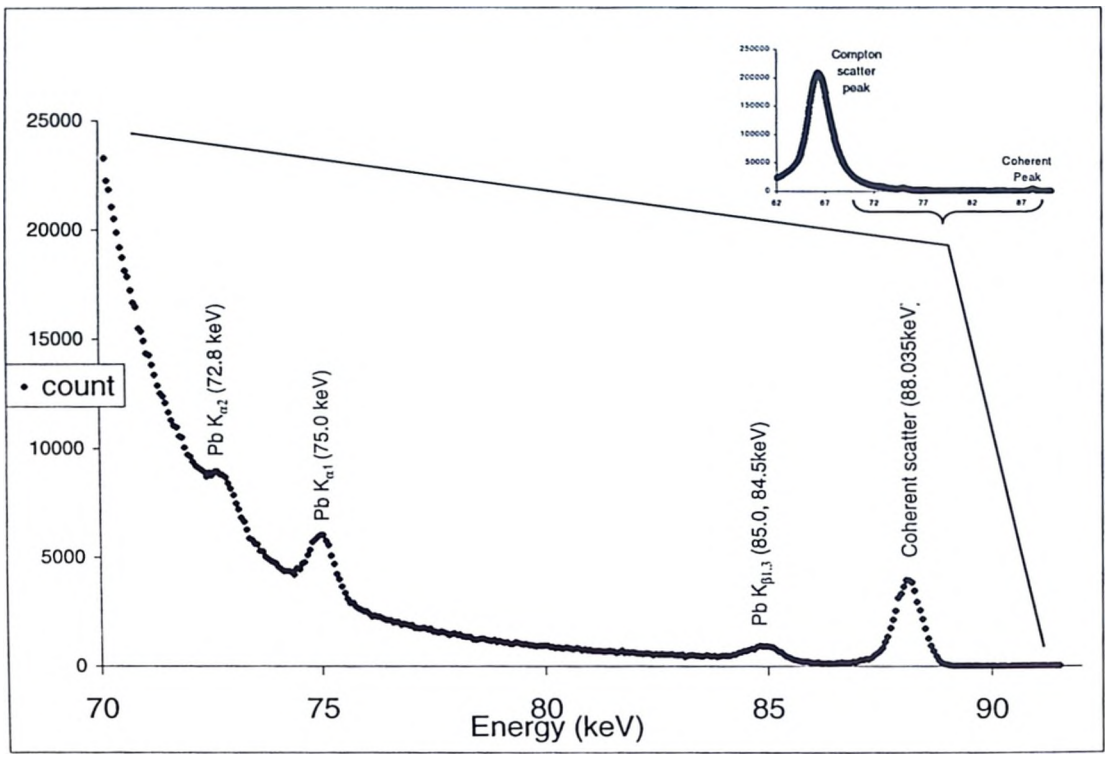

Figure 1-4 Spectrum for ^{109}Cd KXRF lead measurement

The spectrum shows that there is a broadening for the Compton scattering peak. It is a Doppler broadening due to the momentum distribution of bound electrons involved in Compton scattering. The broadened peak gives rise to a big background for the $K_{\alpha 1}$ and $K_{\alpha 2}$ peaks, which greatly affects the uncertainty of the analysis. The background for the $K_{\beta 1}$ and $K_{\beta 3}$ peaks is small, but their intensities are also relatively small. Since the uncertainty of the analysis is proportional to the square root of the background and inversely proportional to the peak amplitude, both α peaks and β peaks have their

advantage and disadvantage for the analysis. In practice, both peaks are used in the analysis.

A unique feature by using ^{109}Cd source and backscattering geometry is that both α peaks and β peaks can be normalized to the coherent peak, hence it is not necessary to correct for tissue attenuation. As mentioned before, for relatively low incident γ energy (in this case 88.035 keV), at large scattering angles (~160°), the cross section of the coherent scattering varies approximately as Z^5 for $Z \leq 20$ (Chettle et al. 1991). As a result, 98 to 99% of the elastic scatter signal arises from the bone mineral, rather than other tissue components. Two further factors are also pertinent to the normalization process. Firstly, the lead X-ray signal also arises from the bone as bone is the principal storage site and there is little lead X-ray signal coming from the soft tissue surrounding the bone. Secondly, the lead X-ray signals are the result of the interactions of photons with energy greater than the K edge 88.001 keV. These photons consist of photons emitted from source and those undergo Compton scattering through less than 3.6° scattering angle. Since the fraction of the latter is negligibly small (Somervaille et al. 1985), we can consider that lead x-ray signals were totally created from the interaction of the lead with the uncollided γ-rays from the source. So both of the coherent peak and the lead K x-ray peaks comes from the same photon fluence, which means the ratio of the lead K x-ray signals to the coherent scatter signals is proportional to the lead concentration in terms of lead/bone mineral.

A calibration process is necessary before the analysis of the *in vivo* measurements. Ten phantoms made of plaster of Paris (similar to the composition of bone) with known

concentrations (μg Pb/g plaster of Paris) are measured and the ratio of both ($K_{\alpha 1}$ peak) /(coherent peak) and ($K_{\beta 1}$ peak)/(coherent peak) are calculated from the spectra by using a peak fitting program (Nie 2001, and Appendix III). The two calibration lines (α calibration line and β calibration line) are the lines of the ratios versus the Pb concentrations. The concentration of Pb in bone for *in vivo* measurement can then be calculated from these calibration lines. The final value is an inversely weighted value from both α calibration and β calibration.

1.6 Brief introduction of the thesis

This dissertation includes the description of one major project and two minor projects. The major project is about the design, set up, test, and application of a new ^{109}Cd γ-ray induced KXRF bone lead measurement system. Two new systems have been purchased in our group based on the work of my Master's program. Several sets of electronics were tested and the best set was chosen for the new systems. The systems were installed and the initial experimental results showed the expected improvement. A thorough dosimetry study has been performed and the study shows that the dose is acceptable even for children. The *in vivo* experiments were also performed on volunteers by using both the new system and the conventional system. The result of the *in vivo* experiments is consistent with that of the simulations. At least two large population surveys are expected to follow. Two minor projects are about the study of a lead metabolism model and a statistical approach of the analysis for the bone lead measurement data. One of the well established lead metabolism models – Leggett's

model has been studied. This model showed that the simulated bone lead is quite different from the measured bone lead for the investigated groups. The bone lead data obtained by our group, as well as the blood lead history data, from several repeated surveys for large occupationally exposed populations, provide a possibility to investigate this problem. A simple model was designed to estimate the transfer parameters of different age groups for one of the lead metabolism models by using the data from these surveys. The simulation result was greatly improved when these calculated parameters were put into Leggett's model. For the other minor project, the statistical method used in the analysis for bone lead measurement data is called left censoring, which is widely used in life science. In the project, left-censoring is adopted for the analysis of the lead measurement data and it is shown to be a good approach from several aspects.

The thesis consists of six chapters. Chapter 1 is a brief introduction of some background knowledge related with the projects and the techniques used in the projects. This chapter consists of two major parts. One part summarizes the impact of lead on human health, and the other part emphasizes on the principles and experimental aspects of the XRF technique. Chapter 2 describes the design, performance, and test of the new system. Chapter 3 describes the methods and the results for the dose estimation for the system for three age groups. Chapter 4 is about the *in vivo* experiments of the new system. Twenty volunteers were recruited and measured by both the new system and the conventional system. The data analysis shows that the improvement of the MDL of the new system is as predicted by simulations. Chapter 5 describes a new model to estimate the kinetic parameters for lead metabolism by using the bone lead measurement data and

how these new parameters improve the current lead metabolism models. Chapter 6 introduces a new statistical approach, left-censoring, for XRF bone lead data analysis. The principle and process of left-censoring analysis is described in detail.

1.7 Purpose of the projects

The toxicity and health effects of lead have been investigated for a long time. Recent studies show that many aspects of lead toxicity require further investigation, especially for low level exposure. There are increasing concerns about the low level exposure for children, about the relationships between lead exposure and certain disease (such as high blood pressure, Parkinson's disease, bone disease etc.), and about the lead metabolism in human body. All these studies require more sensitive analysis techniques. The purpose of the first project is to reduce the MDL for the conventional XRF *in vivo* bone lead measurement system. The low MDL of the new system will open a door for the lead measurement for non-occupationally exposed populations, especially children, for whom even low exposures may exert severe effects. For the occupationally exposed workers, higher precision of the result means a higher precision of data analysis, which leads to a better understanding of the lead transfer and metabolism.

The purpose for the lead metabolism project is to show that there are problems with current lead metabolism models, and that the data obtained from the bone lead measurement can be used to investigate and maybe solve these problems.

In the bone lead measurement, the bone lead concentrations of some people are so low that they are below the detection limit of the measurement system. In this case, the value is called a censored value, i.e. a value that does not contain the full information for

the subject. So some information will be lost if we use the general analysis method to analyze censored dataset. Left-censoring is a statistical method used to analyze a censored data. The purpose of this project is to prove that left-censoring analysis is a good approach to analyze the censored bone lead data.

Chapter 2

DESIGN, PERFORMANCE, AND TESTS OF THE NEW SYSTEM

2.1 Conventional system and new system

2.1.1 ^{109}Cd γray induced XRF bone lead measurement system – conventional system

The conventional system here means the system that has been used in the Medical Physics Department in McMaster University. The new system has evolved from that introduced in Gordon et al.'s paper (1993). Figure 2-1 shows a schematic diagram of the system setup.

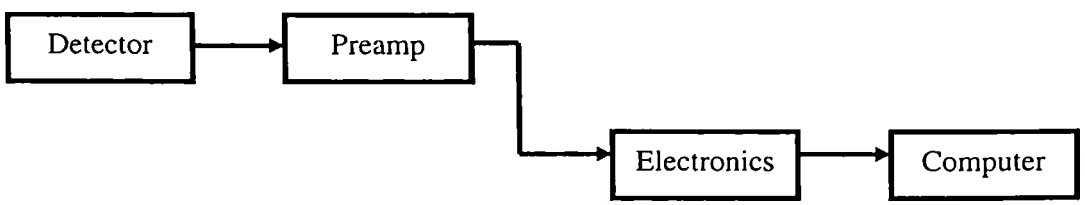

Figure 2-1 System setup

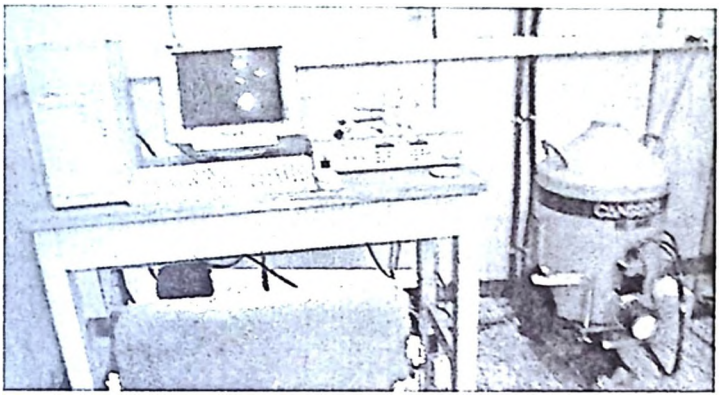

Figure 2-2 Conventional system setup

Figure 2-3 System setup for Tibia measurement

The detector is a 51 mm diameter Canberra HPGe detector (Canberra, Meriden, Connecticut). The analog electronics were used to collect and analyze the signals before the digital system was introduced. Then the integrated Canberra digital signal analyzer DSA-2000 was used as the electronics system. The signals are collected by the detector, adjusted and analyzed by the preamp and DSA-2000, and then regulated in the computer and displayed on the screen as a spectrum. Figure 2-2 shows a picture of this system and figure 2-3 shows the setup for the tibia lead measurement. From figure 2-3, ^{109}Cd source is mounted coaxially in front of the detector. The 88.035 keV γ-ray emitted from the source interacts with the bone as well as the trace lead in bone and emits lead characteristic x-rays, which are detected by the detector. The software used in the computer to process the signals is Genie 2000 (Canberra).

2.1.2 ^{109}Cd source

Figure 2-4 shows the decay scheme for the ^{109}Cd source (Lederer et al. 1978).

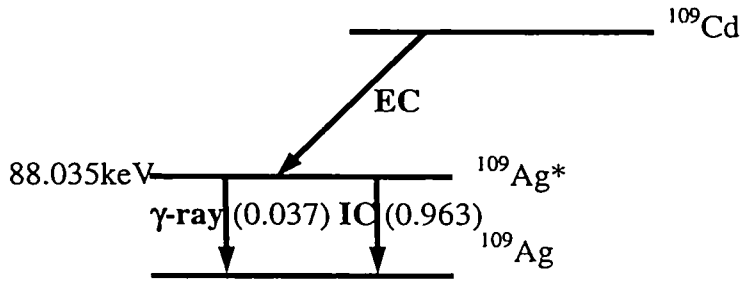

Figure 2-4 Decay scheme of ^{109}Cd source

^{109}Cd decays to the 88.035 keV first excited state of ^{109}Ag. Each decay produces a vacancy in an atomic electron shell of Ag and hence produces characteristic Ag x-rays. ^{109}Ag* de-excites to ^{109}Ag through γ-ray emission with 3.7% intensity and internal conversion with 96.3% intensity. The internal conversion also produces vacancies in atomic electron shells and hence produces characteristic Ag x-rays. So the ^{109}Cd emits 88.035 keV γ-rays with 3.7% intensity (or probability per disintegration), 22 keV and 25 keV Ag K x-rays with intensity 84% and 18% respectively. The source produces Ag L x-rays and Auger electrons as well. Figure 2-5 shows the size of the source holder. The backing behind the source is made of tungsten, which is used to prevent the 88.035 keV γ-rays from going directly to the detector from the source. The function of the copper filter in front of the container is to attenuate the Ag K x-rays and hence to reduce the dose to the person and to reduce the useless signals to the detector and electronics. The attenuation of the photons through different thicknesses of Cu filter can be calculated as:

$$attenuation = e^{-\mu_E x} \quad \ldots\ldots\ldots\ldots \quad (2.1)$$

where μ_E is the attenuation coefficient of Cu for photons with energy E, x is the Cu thickness. Table 2-1 lists the attenuation factors for 88, 25, and 22 keV photons through 0.7mm Cu filter. From the table we can see that 0.7mm Cu filter attenuates nearly all the photons with energies 22keV and 25keV, while the attenuation factor for 88keV is 0.67 (NIST: http://physics.nist.gov/PhysRefData/XrayMassCoef/tab4.html).

photon energy	μ (cm^{-1})	$e^{-\mu x}$
88keV	5.70	0.67
25keV	199	8.9e-7
22keV	260	1.2e-8

Table 2-1 Attenuation factors for 88, 25, and 22 keV photons through 0.7mm Cu filter

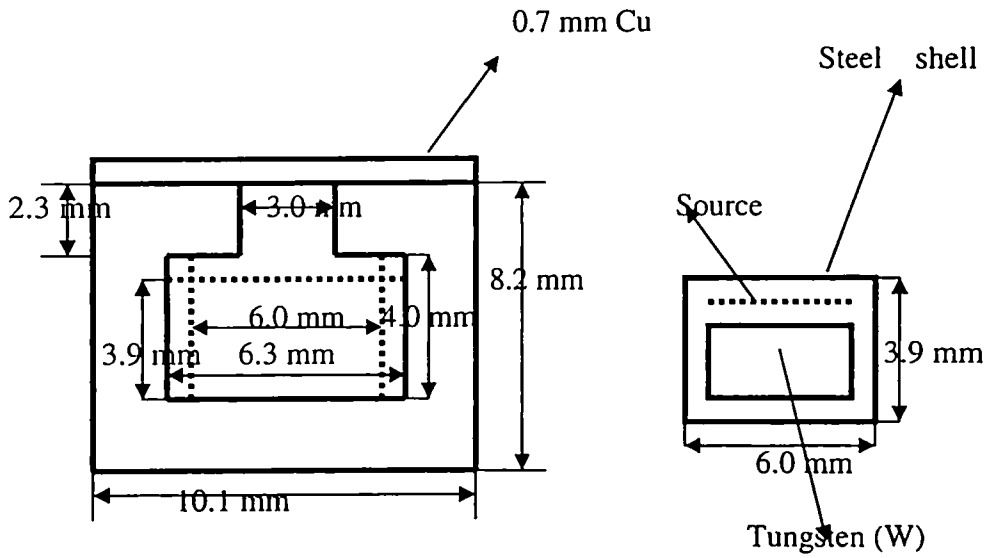

Figure 2-5 Size of the source holder for the conventional system

2.1.3 New system set up

The new system consists of four 16 mm diameter detectors. Hence four sets of electronics are required to collect the signals from the four detectors. The software used to process these four sets of signals is a new version of Genie2000, which can handle four channels of signals. Figure 2-6 is a schematic diagram for the four detectors. Figure 2-7 shows the experimental design of the new system.

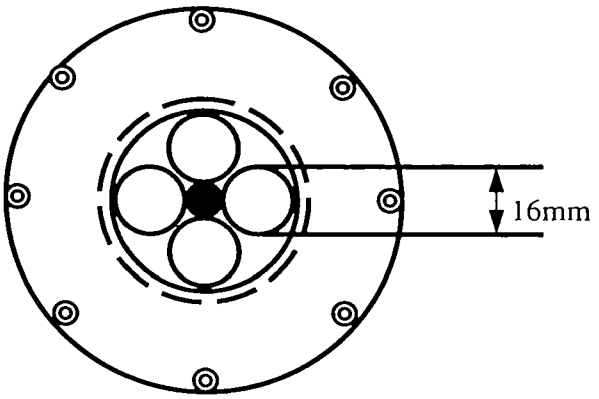

Figure 2-6 Schematic diagram for the four detectors

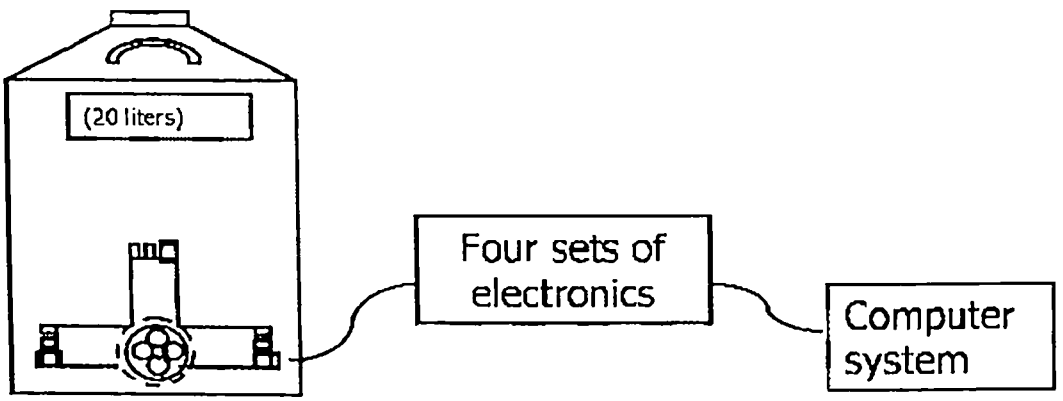

Figure 2-7 Experimental design for the new system

2.2 Electronics

In order to optimize the system, several sets of electronics were compared to decide the best set for the system. Sandra N. Bateman has performed some comparisons between the conventional analogue system with the PerkinElmer DSPECplus (Ortec, Oak Ridge, Illinois) and Canberra DSA (Digital Spectrum Analyzer) -2000 digital system in her Master program in McMaster University (Bateman SN, 2000). She concludes that the difference between the digital systems (DSPECplus and DSA-2000) is small although the DSA did perform better. Compared to the conventional analogue system, the digital systems offer higher throughput without major losses in resolution, and hence provide better precision and reduced detection limits for x-ray fluorescence measurements. In this study, we compared three digital systems to decide which one is the optimal choice. The three systems are Canberra's DSA-2000, DSA-1000, and X-ray Instrumentation Associates (XIA)'s Polaris system (XIA, Newark, California). All three systems are fully integrated Multichannel Analyzers based on digital signal processing techniques and all have superior count rate throughputs and resolution performances. Polaris system is believed to have a better pile up inspection than the DSA series, while the DSA series are believed to have a better energy resolution and true pulse throughput. There are three major differences between DSA-2000 and DSA-1000: DSA-2000 can be used in a network while DSA-1000 is built for single input application; DSA-2000 (40.6 cm x 42.5 cm x 8.9 cm) is bigger than DSA-1000 (18.5 cm x 22 cm x 6.5 cm); DSA-1000 is much cheaper than DSA-2000.

2.2.1 Comparison of Canberra DSA-2000 and XIA Polaris

2.2.1.1 Experimental design

Phantoms made of plaster of Paris with known added lead were used to simulate bone. Soft tissue was simulated either by a tissue equivalent plastic cylinder or by a wax cylinder with a hole to insert the bone phantom. The *in vivo* leg measurement was simulated by inserting the bone phantom into the soft tissue phantom. ^{109}Cd was placed co-axially in front of the 51 mm.diameter HpGe detector. Ag x-rays were removed by a copper filter placed in front of the source. During the experiments, two people from XIA worked with us and made minor adjustments to their instrument to optimize its performance.

Both instruments were used to process pulses from the same detector and pre-amplifier. Spectra were collected simultaneously on the DSA-2000 and Polaris using the energy and timing outputs of the pre-amplifier. Six different pairs of spectra were collected. The distance between the source and the sample (SSD) was varied between the first three sets of spectra, all of which used soft tissue equivalent plastic as soft tissue. The fourth to sixth sets of spectra used wax instead of the plastic, with two different lead concentrations in the plaster of Paris. These six sets of spectra are summarized in table 2-2.

Spectra #	SSD (mm)	Pb in plaster (ppm)	Soft tissue phantom
1	44	200	plastic
2	23	200	plastic
3	34	200	plastic
4	23	200	wax
5	23	9	wax
6	22	200	wax

Table 2-2 Summary of six sets of spectra

Table 2-3 lists the rise time, flat top, dead time, total counts, input count rate (ICR), and output count rate (OCR) for both DSA-2000 and Polaris. The real measurement time is 1800s. The ICR and OCR are calculated by the following formulae:

$$ICR = \frac{\text{Total Counts}}{(\text{Real Time}) * (1 - \text{dead time})} \quad \ldots\ldots\ldots\ldots (2.2)$$

$$\text{OCR} = \frac{\text{Total Counts}}{\text{Real Time}} \quad \ldots\ldots\ldots\ldots (2.3)$$

spectrum#	rise time	flat top	ICR	OCR	dead time	total counts
Dsa-1	1.2	0.7	48635	37493	22.91%	67486416
Dsa-2	1.2	0.7	104128	67745	34.94%	121941784
Dsa-3	1.2	0.7	67935	50945	25.01%	91700156
Dsa-4	1.2	0.7	103130	67354	34.69%	121237472
Dsa-5	1.2	0.7	103461	67488	34.77%	121478161
Dsa-6	1.2	0.7	102316	67038	34.48%	120667834
Polaris-1	1.2	0.7	45859	35093	n/a	n/a
Polaris -2	1.2	0.7	94736	60256	n/a	n/a
Polaris -3	1.2	0.7	63597	46570	n/a	n/a
Polaris -4	1.2	0.7	93776	59814	n/a	n/a
Polaris -5	1.2	0.7	94067	59829	n/a	n/a
Polaris -6	1.2	0.7	93102	58036	n/a	n/a

Table 2-3 Parameter setup and some characteristics of the spectra for DSA-2000 and Polaris

The tissue equivalent plastic contained antimony as an additive. This produced a spectral artifact. Random summing between Sb K x-rays (26.1-26.4 keV) and Compton scattered γ-rays (65.5-66.0 keV) results in a feature at about 92-93 keV. This results in a larger than usual background under the coherent peak. This peak conferred a somewhat exaggerated advantage on the system with the better pile up rejection (Polaris) because this peak is not present in the spectrum from a person. This is why wax was used instead of plastic for the later spectra.

2.2.1.2 Results

All six spectra were fitted with a Marquardt non linear least squares algorithm (Bevington PR 1969) to extract peak amplitudes and uncertainties. The following formulae are applied for the calculation of MDLs from K_α and K_β peaks.

$$MDL_\alpha = 2\times\sigma_\alpha = 2\times\frac{\sigma(\frac{\alpha}{coh})}{slope_\alpha} \quad \ldots\ldots\ldots\ldots (2.4)$$

$$MDL_\beta = 2\times\sigma_\beta = 2\times\frac{\sigma(\frac{\beta}{coh})}{slope_\beta} \quad \ldots\ldots\ldots\ldots (2.5)$$

where $slope_\alpha$ and $slope_\beta$ are the slopes for the alpha and beta calibration lines. Table 2-4 shows the calculated MDLs from alpha fitting and beta fitting for DSA-2000 and Polaris. Table 2-5 shows the ratio of MDLs (DSA-2000/Polaris) for K_α, for K_β, and for the weighted estimate.

Spectrum#	DSA-2000			Polaris		
	MDL_α	MDL_β	$MDL_{weighted}$	MDL_α	MDL_β	$MDL_{weighted}$
1	9.22	13.35	7.59	9.50	12.26	7.51
2	7.01	13.67	6.24	7.51	11.06	6.21
3	8.35	14.98	7.29	8.86	12.44	7.22
4	8.28	15.00	7.25	9.49	13.24	7.71
5	7.13	12.16	6.15	8.01	9.82	6.21
6	8.42	12.97	7.06	9.34	12.35	7.45

Table 2-4 Calculated MDLs for DSA-2000 and Polaris

Spectra #	MDL ratios (DSA-2000/Polaris)		
	K_α	K_β	weighted
1	0.971	1.089	1.010
2	0.934	1.236	1.004
3	0.942	1.205	1.011
4	0.873	1.133	0.940
5	0.890	1.238	0.991
6	0.901	1.050	0.948

Table 2-5 Ratio of MDLs (DSA-2000/Polaris) for K_α, K_β, and the weighted estimate

The result showed that DSA-2000 always gave a lower MDL for the K_α; the Polaris always gave a lower MDL for K_β; the MDLs for the weighted estimates were always similar. It seems that the better pulse pile up rejection obtained using the Polaris is almost exactly offset by somewhat better energy resolution and true throughput obtained by DSA-2000. The reason that Polaris performs better with plastic as soft tissue is described before. Since there is no significant difference between the performance of DSA-2000 and Polaris, and we used DSA-2000 for a long time, there is no need to change DSA-2000 to Polaris.

2.2.2 Comparison of DSA-2000 and DSA-1000

2.2.2.1 Experimental design

Again, the bone was simulated by phantoms made of plaster of Paris with known added lead. Soft tissue was simulated by a wax cylinder. ^{109}Cd was placed co-axially in

front of the 51 mm diameter HPGe detector. Ag x-rays were removed by a copper filter placed in front of the source.

Both instruments were used to process pulses from the same detector and pre-amplifier. Spectra were collected simultaneously on the DSA-2000 and DSA-1000 using the energy and timing outputs of the pre-amplifier. Three different pairs of spectra were collected. We were told by the Canberra technicians that the performance differences between these two systems, if there were any, would be in the pileup rejection function. So the pileup rejection (PUR) parameter was varied between the first two sets of spectra. The source sample distance (SSD) was varied between the second and the third sets of spectra. These three sets of spectra are summarized in table 2-6.

Spectra #	SSD (mm)	PUR	Pb (ppm)	Tissue phantom
1	25	1.7	200	wax
2	25	1.1	200	wax
3	55	1.1	200	wax

Table 2-6 Summary of three sets of spectra

Table 2-7 lists the rise time, flat top, dead time, total counts, input count rate (ICR), and output count rate (OCR) for DSA-1000 and DSA-2000.

spectrum#	rise time	flat top	ICR	OCR	dead time	total counts
Dsa1-1	1.6	0.6	97436	57029	41.47%	102652386
Dsa1-2	1.6	0.6	98627	63240	35.88%	113831824
Dsa1-3	1.6	0.6	23070	20652	10.48%	37174076
Dsa2-1	1.6	0.6	102033	56557	44.57%	101802636
Dsa2-2	1.6	0.6	106295	61980	41.69%	111564753
Dsa2-3	1.6	0.6	23751	20920	11.92%	37655491

Table 2-7 Parameter setup and some characteristics of the spectra for DSA-1000 and DSA-2000

2.2.2.2 Results

The spectra were analyzed and the MDLs were calculated. Table 2-8 shows the MDLs from the alpha fitting, beta fitting, and the weighted MDLs for the DSA-1000 and DSA-2000. Table 2-9 shows the ratio of MDLs (DSA-1000/DSA-2000) for K_α, for K_β, and for the weighted estimate for the three sets of spectra.

Spectrum#	DSA-1000			DSA-2000		
	MDL_α	MDL_β	$MDL_{weighted}$	MDL_α	MDL_β	$MDL_{weighted}$
1	6.77	4.58	3.79	6.79	4.67	3.85
2	6.18	4.05	3.39	6.17	4.07	3.40
3	12.81	8.97	7.35	12.98	8.42	7.06

Table 2-8 Calculated MDLs for DSA-1000 and DSA-2000

Spectra #	MDLs ratio (DSA-1000/DSA-2000)		
	K_α	K_β	weighted
1	0.997	0.981	0.984
2	1.002	0.995	0.997
3	0.987	1.065	1.041

Table 2-9 Ratios of MDLs (DSA-1000/DSA-2000)

DSA-1000 shows a marginally better performance than DSA-2000. Given the fact that DSA-1000 is much cheaper and more portable, it is a better choice than DSA-2000.

2.3 New system

Figure 2-8 shows the picture for the new system.

Figure 2-8 New system setup

The system consists of four detectors, four pre-amps, a liquid nitrogen Dewar, four DSA-1000s, and a computer. All four detectors have an active diameter of 16 mm (active area 200 mm^2), and with a thickness of 10 mm. The window for the detector is made of 0.5 mm thick aluminum. The distance between the detector surface and the window is 5 mm. The capacity of the Dewar is 30 liters. The operating bias voltage for the system and hence for each detector is -500 volts. Four DSA-1000s are used for data acquisition. Each DSA-1000 provides power to one preamp. One of the DSA-1000s also provides power to the HV Inhibit box. One of the DSA-1000s provides the HV Bias for all four detector elements, and this one is connected to the HV Inhibit circuit to protect the preamplifiers against the effects of warm up with bias voltage applied. A four port USB hub is applied to transit the four channels of signals to the computer. Genie 2000 is installed in the computer to collect the signals. The four channels of signals are displayed in four separate interfaces.

2.3.1 Throughputs and resolutions

The preamplifiers used in this system are resistive feedback type. The feedback resistor was adjusted to give a higher throughput. The energy rate of this kind of preamplifier is around 15000 MeV/second. The ^{109}Cd was placed in front of and facing the detectors to measure the maximum throughput for different rise time/flat top settings. The source was put in a distance where the amplifier was just about to paralyze, which means the throughput is the maximum throughput the amplifier can handle. Five settings were tested for detector #1 and the average maximum throughput is 178k counts per

second (CPS). The expected maximum throughput is around 170k CPS (15000MeV/88keV).

Table 2-10, 2-11, 2-12, 2-13 show the energy resolution at 88 keV for four detectors with low and high input count rate (ICR). There is no specific pattern for the performance of resolution with the change of shaping time from 0.5 to 4 μSec. So there is no need to change this parameter that has been optimized by the conventional system.

Rise Time/Flat Top (μSec)	Equivalent Shaping Time (μSec)	Input Count Rate	
		~2k CPS FWHM	50-100k CPS FWHM
1.2/0.4	0.5	535	637
2.8/0.6	1	521	619
12/0.8	4	562	
36/2.4	12	535	

Table 2-10 Energy resolution for detector #1 with low and high ICR

Rise Time/Flat Top (μSec)	Equivalent Shaping Time (μSec)	Input Count Rate	
		~2k CPS FWHM	50-100k CPS FWHM
1.2/0.4	0.5	547	594
2.8/0.6	1	527	608
12/0.8	4	510	
36/2.4	12	613	

Table 2-11 Energy resolution for detector #2 with low and high ICR

Rise Time/Flat Top (μSec)	Equivalent Shaping Time (μSec)	Input Count Rate	
		~2k CPS FWHM	50-100k CPS FWHM
1.2/0.4	0.5	531	611
2.8/0.6	1	523	697
12/0.8	4	560	
36/2.4	12	603	

Table 2-12 Energy resolution for detector #3 with low and high ICR

Rise Time/Flat Top (μSec)	Equivalent Shaping Time (μSec)	Input Count Rate	
		~2k CPS FWHM	50-100k CPS FWHM
1.2/0.4	0.5	566	600
2.8/0.6	1	530	586
12/0.8	4	440	
36/2.4	12	539	

Table 2-13 Energy resolution for detector #4 with low and high ICR

The average resolution for a practical count rate is around 550eV, which is what we expected. So the initial test shows that the performance of the new system is what we predicted.

The purpose of this project is to improve the MDL of the conventional system. The following section will describe some experiments to estimate the MDLs for the new system. But before that, some study has been performed to predict the MDL improvement of the new system before it was purchased. The detail of this previous work can be found in my Master's thesis (Nie H 2001). The main points of the previous work are summarized below in section 2.3.2.

2.3.2 Summary of the predicting approaches and results

Three approaches were applied to predict the improvement of the MDL of the new system. These three approaches include crude calculations, Monte Carlo (MC) simulations, and single-detector experiments.

2.3.2.1 Calculations

The following is a formula for the MDL from K_α peak.

$$MDL_\alpha = 2\times\sigma\left(\frac{\alpha}{coh}\right)\times c = 2\times\frac{\alpha}{coh}\times\sqrt{\frac{\sigma_\alpha^{\,2}}{\alpha^2}+\frac{\sigma_{coh}^{\,2}}{coh^2}}\times c \quad \ldots\ldots\ldots\ldots (2.6)$$

where c is the slope of the alpha calibration line.

$$\frac{\sigma_\alpha^{\,2}}{\alpha^2} >> \frac{\sigma_{coh}^{\,2}}{coh^2}, \qquad \sqrt{\frac{\sigma_\alpha^{\,2}}{\alpha^2}+\frac{\sigma_{coh}^{\,2}}{coh^2}} \approx \frac{\sigma_\alpha}{\alpha}$$

so

$$MDL_\alpha \approx 2\times\frac{\sigma_\alpha}{coh}\times c \propto \frac{\sqrt{(background)_\alpha}}{coh}$$

Background is proportional to the throughput and proportional to the resolution of the detector, and the coherent peak is proportional to the throughput. There are four detectors for the new system, so the throughput for the new system is 4 times that of the old system, given a stronger source. This give rise to a factor of $(\sqrt{4}/4)/(1/1)$, which is 0.5. The resolutions of the new system and the old system are around 550eV and 750eV. This give rise to another factor of $\sqrt{550}/\sqrt{750}$. So the total improvement will be $0.5\times(\sqrt{550}/\sqrt{750})$, which is 0.428.

2.3.2.2 MC simulations

MC simulations were performed for both conventional system and new clover-leaf system at four geometries with detector sample distance (DSD) 30 mm, 25 mm, 22 mm, 20 mm, and source sample distance (SSD) 14 mm, 9 mm, 6 mm, 4 mm. Two kinds of samples were used. One is the bare phantom made of plaster of Paris to simulate bare bone measurement; the other is the bare phantom in a soft tissue equivalent plastic phantom to simulate the *in vivo* leg measurement. The MDLs for these geometries are compared with the MDL for the standard geometry with DSD 38 mm and SSD 24 mm. Three plaster phantoms with Pb concentrations 16 ppm, 63 ppm, and 210 ppm are simulated for the bare bone simulation. Three plaster phantoms with Pb concentrations 9 ppm, 69 ppm, 200 ppm in a plastic phantom are simulated for the *in vivo* simulation. The MDL is the average MDL of the three. The results are shown together with the results for the single-detector experiments in Table 2-14.

2.3.2.3 Single-detector experiments

A single detector with diameter 24 mm was set up to simulate one of the detectors of the clover-leaf system. Figure 2-9 shows the schematic diagram for the detector setup.

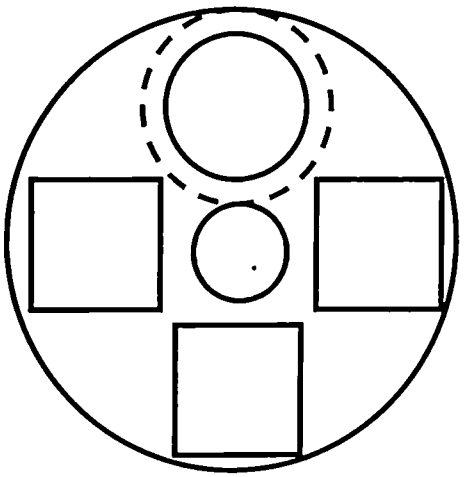

Figure 2-9 Single-detector setup

The detector is covered by a tin ring with an inner diameter of 16 mm to simulate the 16 mm detector. Three iron blocks are placed side by side to simulate the scatter effect from the other three detectors. The geometries and samples applied in the experiments are the same as those in MC simulations. Table 2-14 shows the MDL ratios of the new system and the old system by MC simulations and single-detector experiments.

Result for *in vitro* (bare phantom)			
DSD	SSD	MC simulation	Single-D experiment
30mm	14mm	0.40	0.39±0.01
25mm	9mm	0.36	0.35±0.01
22mm	6mm	0.35	0.34±0.01
20mm	4mm	0.34	0.34±0.01
Result for *in vivo* (bare phantom in soft tissue equivalent phantom)			
30mm	14mm	0.36	0.36±0.02
25mm	9mm	0.31	0.31±0.02
22mm	6mm	0.28	0.28±0.02
20mm	4mm	0.27	0.28±0.02

Table 2-14 MDL_{new}/MDL_{old} ratios by MC simulations and single-detector experiments

The MDL can be improved by a factor of 3.6 (1/0.28) for an optimal geometry with a stronger source.

2.4 New system experiments and results

The prerequisite for the MDL improvement of the new system is that it has four times throughput of the conventional system. This means each small detector of the new system has to collect the same amount of signals as the larger detector of the conventional system. That is why a stronger source is required. The active surface of the

16 mm diameter detector is 200 mm^2 and the active surface of the 51 mm diameter detector is 2000 mm^2. In order for the smaller detector to get the same amount of signals as the larger detector, the source strength has to be increased by a factor of 10. For the conventional system, the source activity is about 1 GBq. So the activity of the new source has to be 10 GBq. A 5 GBq source is purchased instead for the experiments.

The following formulae are used to calculate the MDL for the new system.

$$\sigma_\alpha = \frac{\frac{\alpha}{coh} \times \sqrt{\frac{\sigma_\alpha^{\,2}}{\alpha^2} + \frac{\sigma_{coh}^{\,2}}{coh^2}}}{(slope)_\alpha} \quad \text{..... (2.7)}$$

$$\sigma_\beta = \frac{\frac{\beta}{coh} \times \sqrt{\frac{\sigma_\beta^{\,2}}{\beta^2} + \frac{\sigma_{coh}^{\,2}}{coh^2}}}{(slope)_\beta} \quad \text{..... (2.8)}$$

$$\sigma_\alpha' = \frac{1}{\sqrt{\frac{1}{(\sigma_\alpha)_1^{\,2}} + \frac{1}{(\sigma_\alpha)_2^{\,2}} + \frac{1}{(\sigma_\alpha)_3^{\,2}} + \frac{1}{(\sigma_\alpha)_4^{\,2}}}} \quad \text{..... (2.9)}$$

$$\sigma_\beta' = \frac{1}{\sqrt{\frac{1}{(\sigma_\beta)_1^{\,2}} + \frac{1}{(\sigma_\beta)_2^{\,2}} + \frac{1}{(\sigma_\beta)_3^{\,2}} + \frac{1}{(\sigma_\beta)_4^{\,2}}}} \quad \text{..... (2.10)}$$

$$MDL = 2 \times \sigma = \frac{2}{\sqrt{\frac{1}{(\sigma_\alpha')^2} + \frac{1}{(\sigma_\beta')^2}}} \quad \text{..... (2.11)}$$

The calculated MDLs (ppm) for the new system are listed in Table 2-15.

For the new phantom				For the old phantoms in leg phantom			
Geometry	MDLclov			Geometry	MDLclov		
	16ppm	63ppm	210ppm		9ppm	69ppm	200ppm
(30,14)	1.046	1.265	1.659	(30,14)	2.004	2.189	2.74
(25,9)	1.011	1.215	1.581	(25,9)	1.828	1.954	2.438
(22,6)	1.012	1.224	1.567	(22,6)	1.713	1.86	2.295
(20,4)	1.032	1.273	1.61	(20,4)	1.649	1.789	2.241

Table 2-15 Calculated MDLs for the new system

Result for *in vitro* (bare phantom)					
DSD	SSD	MC	Single-D	New system (5GBq)	New System (10GBq)
30 mm	14 mm	0.40	0.39 ± 0.01	0.58 ± 0.03	0.40 ± 0.02
25 mm	9 mm	0.36	0.35 ± 0.01	0.54 ± 0.03	0.38 ± 0.02
22 mm	6 mm	0.35	0.34 ± 0.01	0.54 ± 0.03	0.38 ± 0.02
20 mm	4 mm	0.34	0.34 ± 0.01	0.56 ± 0.03	0.40 ± 0.02
Result for *in vivo* (bare phantom in tissue equivalent phantom)					
30 mm	14 mm	0.36	0.36 ± 0.02	0.39 ± 0.01	0.28 ± 0.01
25 mm	9 mm	0.31	0.31 ± 0.02	0.35 ± 0.01	0.25 ± 0.01
22 mm	6 mm	0.28	0.28 ± 0.02	0.33 ± 0.01	0.23 ± 0.01
20 mm	4 mm	0.27	0.28 ± 0.02	0.32 ± 0.01	0.23 ± 0.01

Table 2-16 Ratios of the MDLs of the new system and the old system

Table 2-16 shows the ratios of the MDLs of the new system and the conventional system, by MC simulation, by single-detector experiments, and by the experiments with the new system. The experiments were performed with a 5 GBq source, so the extrapolated ratios for a 10GBq source are also listed in the table.

2.5 Discussion

We have already discussed the importance of measuring bone lead in human body in the first chapter. Improving the MDL of the bone lead measurement system is one of the essential issues to help understand the role that lead played and is still playing in affecting human health. Table 2-16 shows that the new bone lead measurement system can reduce the MDL by a factor of ~2.5 for *in vitro* measurement and a factor of ~4 for *in vivo* measurement compared to the most advanced previous system. This is a huge advance, especially for the *in vivo* measurement because the MDL for measuring lead *in vivo* is what we are most concerned about. The results from the experiments seem better than those from the MC simulations and Single-detector experiments for the in vivo part. This may due to three factors. Firstly, the new source has a smaller radius and a smaller collimator, so for the same source intensity, less soft tissue will be covered and hence less Compton scattering background will be present for the spectrum analysis. Less Compton background means a smaller uncertainty for the useful signal and a reduced MDL. Secondly, the resistive feedback type preamplifier in the new system allows for a larger throughput, which means more signals for the same source strength and hence a better MDL. Thirdly, the resolutions for the detectors are smaller than expected for the

experiment, which gives rise to a reduced MDL. In summary, the improvement of the new system comes from the factors listed below in Table 2-17.

	conv. system	new system	reason for the improvement	improvement factor
detector number	1	4	4 times signals	2
detector resolution	~750ev at 88 keV	~500ev at 88 keV	less background	1.225
source diameter	3 mm	<1.5 mm	less background	N/A
source holder shielding	with	without	more signals	N/A
max preamp throughput	~100kcps	~170kcps	more signals	1.3, if not count for the resolution loss

Table 2-17 Factors that affect the improvement of the new system

The MDL for the previous system to measure bone lead *in vivo* is about 6-10 μg/(g bone mineral) and the MDL for the new system is reduced to about 1.5-2.5 μg/(g bone mineral). For those people who are heavily exposed to lead for a long time, the previous system can measure their bone lead with a relatively high precision. Even in that case, a smaller uncertainty for the data by using the new system will provide a better way

to analyze and understand the result. For people who are moderately or lightly exposed to lead, or acutely exposed to lead by accident, the bone lead concentration will be relatively low, which means the previous system sometimes can only give a detection limit instead of an actual measured value. In this case, the new system has a much greater advantage. Recently low-level lead exposure, especially childhood low-level exposure, has been emphasized. The new system provides a very valuable measure to look into these issues.

Chapter 3

Dosimetry study

3.1 Introduction

The dose delivery involved in the *in vivo* XRF bone lead measurement system is always considered negligibly small. The effective dose delivered by the finger lead measurement system using two ^{57}Co sources at the 90 degree geometry was estimated to be approximately 0.1 μSv (Ahlgren et al. 1980, Somervaille et al. 1989). Todd et al. did a dosimetry study for the ^{109}Cd KXRF tibia and calcaneus lead measurement system and the effective dose for an *in vivo* measurement of tibia lead concentration in 1-, 5-, and 10-year old and adult subjects was calculated to be 1100, 420, 190, and 34/38 (male/female) nSv for a 30-min measurement (Todd et al. 1992).

The new clover-leaf system improved the MDL of the measurement by a factor of around four. Since it requires a stronger source, the dose delivered will be greater than the previous systems. Low-level lead exposure for children is a big concern, so this system is very suitable for the lead measurement for children due to its low MDL. On the one hand, children are sensitive to lead; on the other hand, children are also sensitive to radiation. Furthermore, the dose delivered to children will be much higher than for the adults, because of the active bone marrow in a child's leg where the measurement is taken. Due to the above reasons, the dose study for this system is necessary, especially for the children.

3.2 Materials and methods

The source is ^{109}Cd, and the provided activity for the source is 137 mCi (or 5.07 GBq) in Nov.18, 2003 with half-life 464 days (Techsnabexport, Moscow, Rssia). The diameter of the source is less than 1.5mm, and the thickness is 0.06mm. The source was recalibrated on May.19, 2004 and the detected numbers of 88.035 keV photons are 1.385e8/sec without source container and 1.059e8/sec with source container (due to the attenuation of the Cu filter), compared with 1.427e8/sec without container derived from the provided value. Figure 3-1 shows the size of the new source holder.

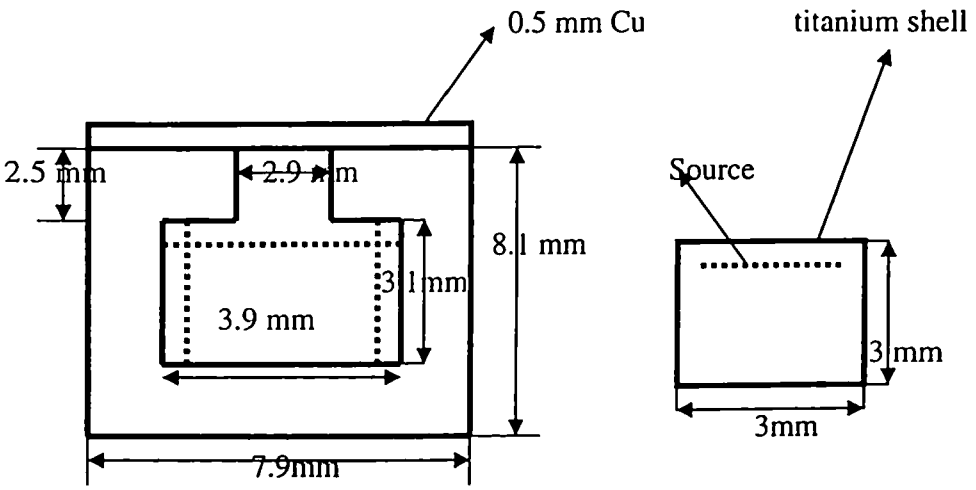

Figure 3-1 New source holder

Calculations, MC simulations, and experiments were performed to estimate the dose delivered by this system. For the experiments, three sets of human phantoms, simulating 5-years old, 10-years old, and adults, were set up to measure the dose. The simulated torsos were made of two rice packs. The upper thighs were made of wax with 305 mm x 305 mm x 152 mm dimension. The lower legs were also made of wax, with

bone phantoms inserted inside. The bone phantoms were made of plaster of Paris, with a cavity filled with rice to represent bone marrow. The sizes of the lower legs of the three sets of the phantoms are listed in Table 3-1.

	Leg radius	Tissue overlay	Bone radius	Bone cavity radius
5	35	5	12	9
10	50	5	12	6
adult	50	5	17	9

(Unit: mm)

Table 3-1 The sizes of the lower legs for the three sets of human phantoms

The dosimeters used for the dose measurement are Panasonic UD-803AS TLDs (Panasonic Corp. Secaucus, New Jersy). Figure 3-2 shows the back side of the TLD without the holder. It consists of four elements, with two elements of $Li_2B_4O_7$ as the phosphor and two empty elements and is a simple dosimeter to measure beta particles and photons. Table 3-2 shows the characteristic of this TLD series.

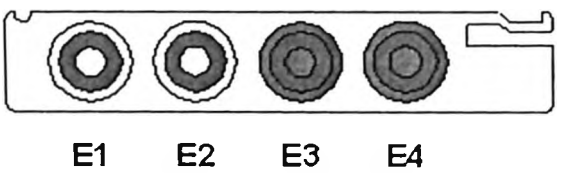

Figure 3-2 Back side of the Panasonic UD-803AS TLD

	Element1	Element 2	Element 3	Element 4
Phosphor	$Li_2B_4O_7$	$Li_2B_4O_7$	None	None
Front filtration	Plastic- 14mg/cm^2	Plastic- 160mg/cm^2	Plastic- 160mg/cm^2	Plastic- 160mg/cm^2
Rear filtration	Plastic- 14mg/cm^2	Plastic- 160mg/cm^2	Plastic- 160mg/cm^2	Plastic- 160mg/cm^2

Table 3-2 Characteristic of Panasonic UD-803AS TLD

The calibration source for the TLDs is an Am-241 source with an emission of 7.14e6 photons per second per steradian for the 60 keV photons measured on Dec.08, 1981.

3.2.1 Experiments

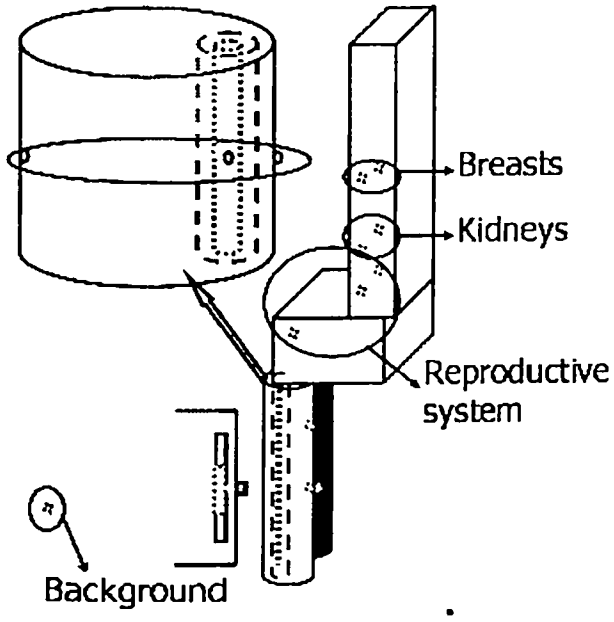

Figure 3-3 TLD setup for the experiments

Figure 3-3 shows the detector, source, phantom, and TLD setup for the experiments. The TLDs were fixed at the locations where the critical organs (such as breasts, kidneys, reproductive systems) are located. There are also several TLDs placed at the lower leg phantom. Three were placed aligned with the source: one is on the skin surface, one is in the bone marrow, and

one is on the midcalf. Another two were placed unaligned with the source in the bone marrow, one is above the source, and one is beneath the source. Three TLDs were placed in the lab room several meters away from the source to represent the background dose. The measurements were first performed with the leg 5 mm away from the source surface. This results in an inaccurate skin and bone marrow dose in front of the source due to the small collimator and the finite size of the TLD sensor. These experiments lasted for about 60 hours. The skin dose and bone marrow dose of the targeted lower leg were collected separately later by setting the leg 50 mm away from the source surface.

3.2.2 MC simulation

The MC simulation program is designed specifically to model source-excited *in vivo* x-ray fluorescence. It is loosely based on the code originally reported by Todd et al. (Todd et al. 1991) and was extensively revised by O'Meara (O'Meara 1999). The dose is only simulated for the lower leg. In order to simulate the dose distribution, the lower leg was divided into 1 cm layers. Each layer was broken into 32 pieces as shown in figure 3-4.

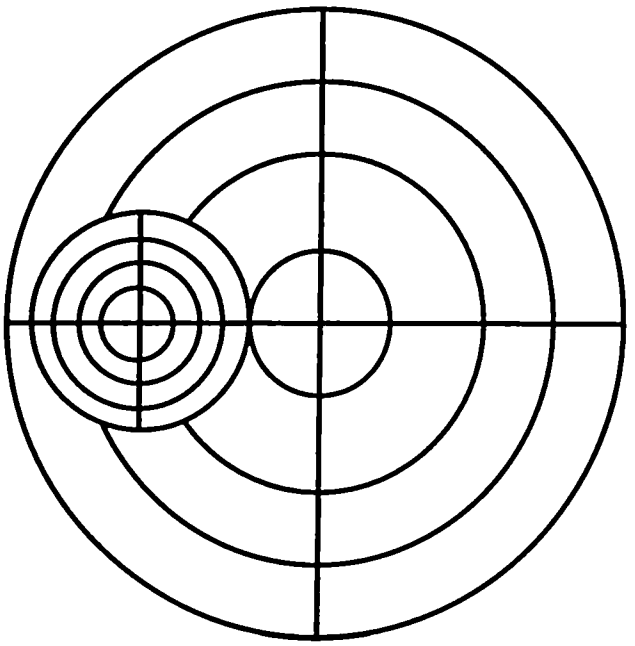

Figure 3-4 The cross section of the lower leg for the dose distribution

Dose of each piece is obtained by

$$dose = \frac{energy}{mass} \quad \text{..... (3.1)}$$

where energy is the energy deposited in that piece and mass is the mass for that piece.

3.2.3 Calculation

The following formula is used for the skin surface exposure rate (Turner JE 1995)

$$\dot{X}_s = \frac{e}{4\pi\omega_{air}} \times \frac{N\lambda}{r^2} \times \sum P_i(E) E_i \left(\frac{\mu_{en}(E_i)}{\rho} \right)_{air} \quad \text{..... (3.2)}$$

where e is the charge of an electron, ω_{air} is the energy required to produce an ion-pair in the air, N is the atomic number of the radioactive atoms, λ is the decay probability, $N\lambda$ is

the source activity, r is the distance from the source to the skin surface, $P_i(E)$ is the intensity of the photon with energy E_i, E_i is the energy of the photon, $(\mu_{en}(E)/\rho)_{air}$ is the mass energy absorption coefficient of the photon with energy E_i in the air.

The exposure rate in the medium depends on the depth of the medium and several other medium related parameters. Figure 3-5 shows the geometry of the source and the thickness of the media.

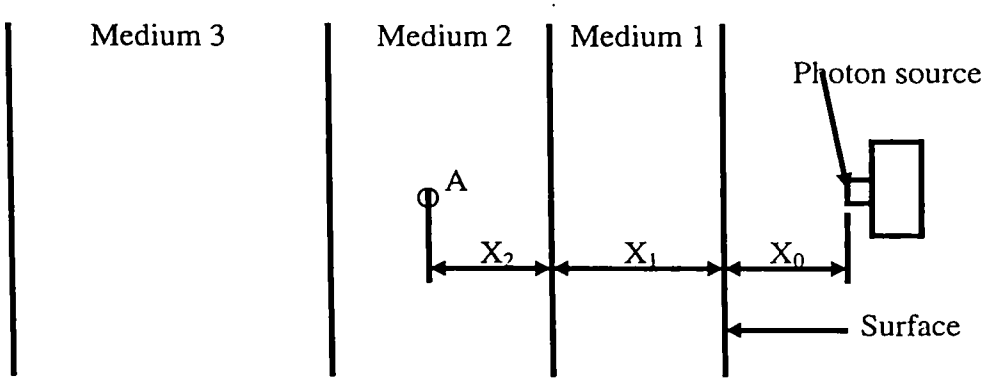

Figure 3-5 Geometries to calculate exposure rate at point A

Assume the exposure rate for the surface is $\dot{X}_s$, then the exposure rate at point A in medium 2 can be expressed as

$$\dot{X} = \dot{X}_s \times e^{-\mu_{m1} \times X_1 - \mu_{m2} \times X_2} \times B \times \frac{X_0 \times X_0}{(X_0 + X_1 + X_2) \times (X_0 + X_1 + X_2)} \quad \text{..... (3.3)}$$

where μ_{m1} is the attenuation coefficient for medium 1, μ_{m2} is the attenuation coefficient for medium 2, and B is the buildup factor.

$$B = B_1 \times B_2 \quad \text{..... (3.4)}$$

where B_1 and B_2 are the buildup factors for medium 1 and medium 2. The buildup factors are derived from the tables in Shimizu et al.'s paper (2004).

The exposure rate can be converted to dose rate by the following formula

$$\dot{D} = f_x \times \dot{X} = \left(\frac{\omega_{\text{air}}}{\text{e}}\right) \times \frac{(\mu_{en}/\rho)_m}{(\mu_{en}/\rho)_a} \times \dot{X} \quad \ldots\ldots\ldots\ldots (3.5)$$

where (ω_{air}/e) is the average energy required to produce one unit of ion charge (J/C), $(\mu_{en}/\rho)_m$ is the mass energy absorption coefficient in the medium for the concerned energy, and $(\mu_{en}/\rho)_a$ is the mass energy absorption coefficient in the air for the same energy. When the unit of the exposure rate is R* (roentgen), the converting factor f_x is:

$$f_x = 100 \times 2.58 \times 10^{-4} \times \left(\frac{\omega_{air}}{e}\right) \times \frac{(\mu_{en}/\rho)_m}{(\mu_{en}/\rho)_a} = 0.873 \times \frac{(\mu_{en}/\rho)_m}{(\mu_{en}/\rho)_a} (rad/R) \quad \ldots\ldots\ldots\ldots (3.6)$$

For a chemical compound or a mixture, its mass attenuation coefficient (μ/ρ) can be approximately evaluated from the coefficients (μ_i/ρ_i) for the constituent elements (U.S. Department of Commerce, 1969).

$$\frac{\mu}{\rho} = \sum_i \omega_i \times \frac{\mu_i}{\rho_i} \quad \ldots\ldots\ldots\ldots (3.7)$$

where ω_i is the proportion of the elements by mass.

For some materials or tissues that can be found from the ICRU website (ICRU, http://physics.nist.gov/PhysRefData/XrayMassCoef/tab4.html), the parameters from the website were used in these calculations. For those that could not be looked up, the above formula (3.7) was applied to estimate the parameters approximately.

*: Although Roentgen is not officially an SI unit, there is not an explicit SI unit and the Roentgen is now defined as $2.58*10^{-4}Ckg^{-1}$.

Table 3-3 shows proportion of the elements in some materials and tissues and the densities of these materials.

Z	Symbol	H_2O	Air	C-bone*	Muscle	Plaster**	Wax
1	H	0.1119		0.064	0.102	0.01	0.1437
6	C			0.278	0.123	0.06	0.8563
7	N		0.755	0.027	0.035		
8	O	0.8881	0.232	0.410	0.729	0.519	
11	Na				0.0008		
12	Mg			0.002	0.0002		
13	Al						
14	Si					0.004	
15	P			0.070	0.002		
16	S			0.002	0.005	0.090	
19	K				0.003		
20	Ca			0.147	0.00007	0.317	
26	Fe						
Density (g/cm^3)		1.001	0.001205	1.85	1	1.35	1.3

*: Compact bone.

**: Plaster of Paris.

Table 3-3 Proportion of the elements in H_2O, Air, Compact bone, Muscle, plaster of Paris, and Wax

The mass energy attenuation coefficient for these elements can be looked up in the book (U.S. Department of Commerce, 1969).

3.3 Results

In the experiments, in order to put the TLDs into the small bone marrow cavities, the TLDs were taken out from the holders, and this gives rise to a relatively high background dose probably due to the dosimeter's sensitivity to the visible light. The measured background is: 0.43±0.14 mR/hr.

As mentioned before, the measurements were firstly performed with the leg 5 mm away from the source surface. Table 3-4 shows the exposure rate of some organs with the leg 5 mm away from the source without subtracting background.

	5	10	adult
Testes	0.91±0.22	0.48±0.08	0.39±0.03
Ovary	0.54±0.09	0.70±0.31	0.30±0.13
Kidney	0.20±0.04	0.26±0.01	0.15±0.08
Breast	0.52±0.03	0.39±0.11	0.32±0.03
The other leg*, skin	3.70±0.61	0.66±0.09	0.38±0.05
The other leg, bone marrow	0.76±0.05	0.17±0.09	0.13±0.16

(Unit: mR/hr)

*: the other leg means the one that not targeted by the source.

Table 3-4 Exposure rate of some key organs for the three sets of human phantoms

The exposure rates for all the organs were comparable to background exposure rate except for the 5-year old's testes, skin of the other leg, and bone marrow of the other leg. Compared to the skin exposure rate and bone marrow exposure rate measured and calculated later for the target leg, the skin exposure rate and bone marrow exposure rate of the other leg for the 5-year old can be neglected. The testes exposure rate for the 5-year old is 0.48±0.26 mR/hr after accounting for the background exposure. Given an organ weighting factor of 0.2, a radiation weighting factor of 1, and an exposure/dose converting factor of 0.96 cGy/R, the contribution to effective dose for 5-year old male gonads is 0.92±0.50 μSv for a one hour exposure from the 5GBq source at 5 mm from the skin.

Now that we know the dose to the other organs are the same as background dose within the error, the dose evaluation for the whole body can be converted to the dose evaluation for the targeted lower leg. The following paragraphs will show that the measured dose rates for the skin, bone surface, bone marrow, and midcalf are consistent with the calculated ones, and the calculated bone marrow dose rates are consistent with the simulated ones. The dose to the whole leg will be calculated from the MC simulation because firstly it is proved to be reliable, and secondly, numerous TLDs and calculations will be required to get an accurate value by experiments.

Table 3-5 lists the skin, bone surface, bone marrow, and midcalf exposure rate for the 5-year old with the lower leg 50 mm away from the source, by measurement and calculation respectively.

	Measured*	Calculated**
Skin	47.96±1.07	47.74
Bone surface	N/A	56.35
Bone marrow	25.59±0.35	30.93
Midcalf	5.14±0.15	8.72

(Unit: mR/hr)

Table 3-5 Skin, bone surface, bone marrow, and the midcalf exposure rate for 5-year old

*: Wax as leg, plaster as bone, and rice as bone marrow.

**: Wax as leg, plaster as bone, and water as bone marrow.

The measured values are close to the calculated values and the differences may be due to the different materials used for the bone marrow.

Since it is difficult to measure the skin, bone surface, and bone marrow dose at 5 mm away and the above results show that the calculation is only a slight overestimation, we will get these doses by calculation. Table 3-6 shows the calculated skin, bone surface, bone marrow, and the midcalf exposure rate and dose for 5-year old, 10-year old, and adult for source 5mm away from the skin. These calculations were done by using the parameters for muscle, bone, and soft tissue, instead of the parameters for wax, plaster, and rice.

	Exposure rate (mR/hr)			Dose rate (mSv/hr)		
	5	10	adult	5	10	adult
Skin	4774	4774	4774	45.83	45.83	45.83
Bone surface	1347	1347	1347	29.63	29.63	29.63
Bone marrow	518.72	516.16	327.35	4.98	4.96	3.14
Midcalf	36.29	30.17	33.63	0.35	0.29	0.32

Table 3-6 Calculated skin, bone surface, bone marrow, and the midcalf exposure rate and dose for 5-year old, 10-year old, and adult

MC simulation dose evaluation was performed for three groups. The bone marrow dose were calculated as the average of the dose rate for the 8 center sections of the bone marrow (as shown in figure 3-6).

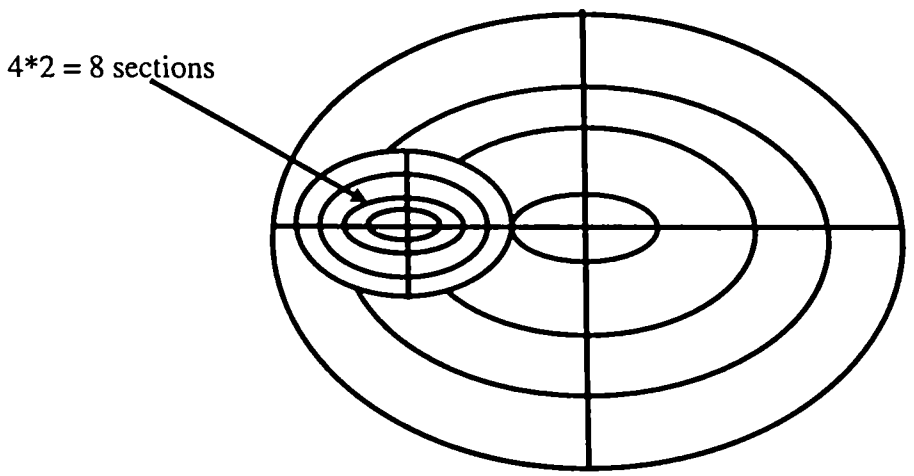

Figure 3-6 MC simulation for the bone marrow dose

Table 3-7 shows the comparison of the bone marrow dose rate from the calculation and from MC simulation.

	5-year old	10-year old	adult
Calculation	4.98	4.96	3.14
MC simulation	4.55±0.62	4.56±0.62	2.90±0.48

(Unit: mSv/hr)

Table 3-7 The comparison of the bone marrow dose rate from calculation and from the MC simulation

The values agree with each other within the error range. Also, although the MC simulation is numerically lower than the calculation, it was shown previously that the calculation was numerically higher than the measurement (Table 3-5). So MC simulation is performed to get the dose rate for the lower leg (bone, bone marrow, and tissue). Table 3-8 shows the equivalent bone dose, bone marrow dose, and tissue dose for the target lower leg for the three age groups by MC simulation, for 1 hr bone lead measurement by using a 5 GBq ^{109}Cd source with the source 5 mm away from the leg surface.

	5-year old	10-year old	adult
Bone	965	1047	714
Bone marrow	2210	2300	1710
Muscle	95	64	51

(Unit: μSv)

Table 3-8 The equivalent bone dose, bone marrow dose, and tissue dose for the three age groups by MC simulation for 1 hour lead measurement

The effective dose can be calculated by the following formula

$$Dose_{eff} = Dose_{equi} \times W_T \times F \quad \ldots\ldots\ldots\ldots (3.8)$$

where $Dose_{equi}$ represents the equivalent dose, W_T is the tissue weighting factor, and F is the fraction of each of the tissues. W_T is 0.01 for bone, 0.12 for bone marrow, and ~0 for muscle. F is the proportion of the tissue (bone, active bone marrow, and muscle) in the lower leg over the tissue in the whole body. It is worth to mention that the active bone marrow in lower leg is about 9% for the 5-year old, 5.5% for the 10-year old, and ~0 for the adult (Cristy 1981). Table 3-9 shows the effective bone dose, bone marrow dose for 1hr bone lead measurement with source 5 mm away.

Age group	5-year old	10-year old	adult
Bone	0.363	0.338	0.231
Bone marrow	7.96	3.80	~0

(Unit: μSv)

Table 3-9 Effective bone dose and bone marrow dose for 1hr bone lead measurement

The skin dose can be calculated with equation (3.8). The tissue weighting factor for skin is 0.01. Figure 3-7 shows the irradiated skin area. The area is calculated as 1.24cm^2 from the figure. Assume the skin surfaces for the adult, 10-year old and 5-year old are 18000 cm^2, 9000 cm^2, and 4500 cm^2, then the skin doses for adult, 10-year old, and 5-year old are 0.032, 0.063, and 0.126 μSv for 1 hr bone lead measurement 5 mm away from the source.

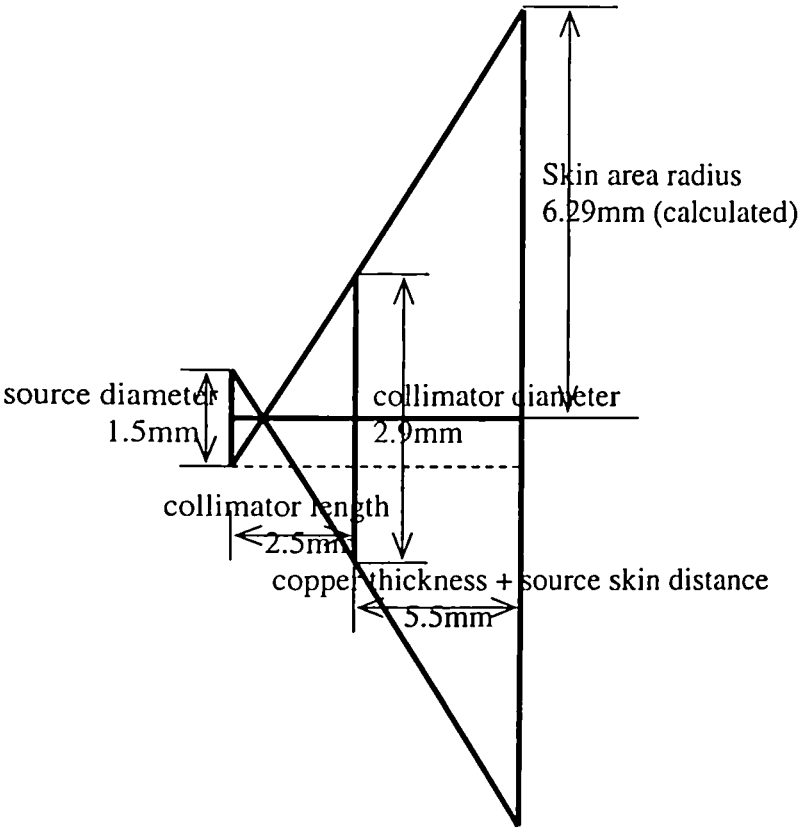

Figure 3.7 Irradiated skin area

Table 3-10 shows the whole body dose for the three age groups for 1 hr bone lead measurement.

Age group	5-year old	10-year old	adult
Whole body dose	8.45*/9.37**	4.20	0.26

(Unit: μSv)

*: for female.

**: for male.

Table 3-10 Whole body dose for the three age groups

The doses estimated here are for a 5 GBq ^{109}Cd source and a one hour measurement. The measurement generally lasts for half an hour. So the actual doses by using a 10 GBq source will be the same as listed in table 3-10.

3.4 Discussion

The maximum annual effective dose limit to public is 1 mSv and to any single organ is 50 mSv. The dose for a typical chest x-ray is about 0.1 mSv. The dose to a child for a DEXA scan is about 10 μSv to 100 μSv. Compared to these values, dose involved in the bone lead measurement, even for a child, is acceptable.

Chapter 4

In vivo bone lead measurement using the new system

4.1 System setup

Both the conventional system and the new system were set up to compare the performance of the systems and to test the improvement of the new system. The conventional system was setup as described in section 2.1.1. The new system was setup as described in section 2.3. The critical parameters selected for the two systems are listed in Table 4-1.

parameters	conv. system	new det#1	new det#2	new det#3	new det#4
voltage	-2500V	-500V	-500V	-500V	-500V
rise time	1.6μs	5.6μs	5.6μs	5.6μs	5.6μs
flat top	0.6μs	0.8μs	0.8μs	0.8μs	0.8μs
P/Z	3168	3447	3316	3400	3364

Table 4-1 Setup parameters selected for the conventional system and the new system

The rise up times for the conventional system and the new system were set as 1.6μs and 5.6μs. The surface area of the detectors for the new system is 10 times smaller than that of the detector for the conventional system, so the count rate throughput, and hence the dead time, will be smaller for the same source strength. The source strength for the new system at the time of the measurement was about 2.45 GBq, and 5.6μs of rise up

time will give a better performance with this source strength. If the source is stronger, the rise up time can be set lower to give rise to a higher throughput.

It is worth mentioning that the Pole/Zero (P/Z) adjustment is critical for the performance of the system. A digital oscilloscope is built inside the DSA-1000 to adjust the pulses to get the best pulse shape hence the best P/Z parameter. The adjustment of (flat top)/(rise time) is also very important to allow the best combination of throughput and pulse shape.

The dosimetry study described in Chapter 3 showed that the dose delivered by the system is acceptable. So the permission (license) to operate this system on human was obtained from the Research Ethics Board of Hamilton Health Sciences and the system is ready for the *in vivo* experiments.

4.2 Experiments

Twenty volunteers, 10 male, 10 female, aged from 24 to 57, were recruited for this study. Table 4-2 shows the age and sex of the volunteers. These people do not have known lead exposure history. The purpose of the *in vivo* study is to test the results obtained from the simulations and previous experiments, i.e. the new system improves the MDL by a factor of ~4 for *in vivo* measurement. The volunteers were measured by both the conventional system and the new system.

The left lower leg of the volunteers is fixed in front of the source as shown in figure 2-3 in chapter 2. The skin in front of the source is cleaned by an alcohol wipe to remove the external contamination. Because the sources for both systems were purchased

more than 1 and half years ago, the legs were fixed at the closest optimized distance (~5mm) to get higher signals. All the volunteers were measured by both systems for 1800s clock time. The spectra were then saved for analysis.

number	age	sex
1	29	M
2	55	M
3	46	M
4	27	F
5	34	M
6	27	F
7	51	F
8	26	F
9	34	M
10	25	F
11	29	F
12	31	F
13	24	F
14	38	M
15	26	M
16	57	M
17	26	F
18	27	M
19	27	M
20	40	F

Table 4-2 Age and sex of the 20 volunteers

4.3 Results

The spectra for all the volunteers are collected by Genie2000 and are analyzed by the "Mqerfy" fitting program (The source code of this program is shown in Appendix IV). For the conventional system, there is only one detector, therefore only one spectrum for each individual. The new cloverleaf system contains four detectors; therefore four spectra were collected for each person. The concentrations from the alpha fitting and beta fitting for the conventional system are listed in Table 4-3. The concentrations from the alpha fitting and beta fitting for the four detectors of the new system are listed in Table 4-4,4-5,4-6, and 4-7. Also shown in the tables are Z values calculated as:

$$z = \frac{conc_{\alpha} - conc_{\beta}}{\sqrt{\sigma_{\alpha}^{2} + \sigma_{\beta}^{2}}} \quad \ldots\ldots\ldots\ldots (4.1)$$

where $conc_{\alpha}$ and $conc_{\beta}$ are the concentrations from alpha fitting and beta fitting, and σ_{α} and σ_{β} are the associated uncertainties. The means and standard deviations for z values for the conventional system and the four detectors of the new system are shown in Table 4-11. If there is no difference between the lead concentrations measured by the new system and the conventional system, then it is expected the individual z values will be distributed with a mean of 0 and standard deviation of 1. The χ^2 values are also listed in the table and it can be used to test the variance of the z value. The χ^2 value is calculated as:

$$\chi_{19}^{2} = \sum \frac{(X-\mu)^2}{\sigma^2} = \sum \frac{(Z-0)^2}{1^2} \quad \ldots\ldots\ldots\ldots (4.2)$$

subject#	alpha	sig(alp)	beta	sig(bet)	alp-bet	sig(α-β)	Z
1	-2.44	4.78	-6.11	4.19	3.67	6.36	0.58
2	-18.5	8.8	12.26	5.19	-30.76	10.22	-3.01
3	4.52	7.07	11.14	5.1	-6.62	8.72	-0.76
4	-2.34	6.64	6.75	4.84	-9.09	8.22	-1.11
5	-27.09	7	-2.24	5.4	-24.85	8.84	-2.81
6	4.02	14.43	9.65	10.95	-5.63	18.11	-0.31
7	2.83	6.52	5.74	6.14	-2.91	8.96	-0.32
8	-20.51	7.56	-1.54	5.9	-18.97	9.59	-1.98
9	7.85	4.86	14.96	4.03	-7.11	6.31	-1.13
10	13.01	7.99	-6.64	6.59	19.65	10.36	1.90
11	-9.53	7.67	-2.09	6.6	-7.44	10.12	-0.74
12	2.76	7.03	1.5	6.66	1.26	9.68	0.13
13	2.54	5.48	2.16	4.38	0.38	7.02	0.05
14	-14.09	5.74	-2.94	4.47	-11.15	7.28	-1.53
15	-3.3	7.34	6.52	6.82	-9.82	10.02	-0.98
16	8.08	5.56	11.53	5.21	-3.45	7.62	-0.45
17	4.27	7.35	5.86	6.44	-1.59	9.77	-0.16
18	-5.28	5.41	2.3	4.8	-7.58	7.23	-1.05
19	-13.92	5.75	1.28	4.47	-15.2	7.28	-2.09
20	-25.08	18.67	-20.64	12.29	-4.44	22.35	-0.20

Table 4-3 Concentrations from α and β fittings for the old system

subject#	alpha1	sig(alp1)	beta1	sig(bet1)	alp1-bet1	sig(α-β)	Z
1	-6.69	4.12	-2.6	4.46	-4.09	6.07	-0.67
2	11.48	4.54	18.36	5.08	-6.88	6.81	-1.01
3	1.09	4.29	-2.21	4.5	3.3	6.22	0.53
4	6.81	4.43	4.93	4.88	1.88	6.59	0.29
5	12.45	5.09	0.51	5.37	11.94	7.40	1.61
6	0.21	11.19	22.03	11.08	-21.82	15.75	-1.39
7	5.24	5.64	8.14	6.22	-2.9	8.40	-0.35
8	-4.01	5.16	9	5.48	-13.01	7.53	-1.73
9	0.97	3.77	6.82	4.17	-5.85	5.62	-1.04
10	3.58	6.23	-12.55	6.65	16.13	9.11	1.77
11	9.91	5.21	-3.43	5.66	13.34	7.69	1.73
12	7.92	7.39	0.01	8.02	7.91	10.91	0.73
13	4.45	4.08	4.41	4.56	0.04	6.12	0.01
14	13.94	4.73	11.98	4.95	1.96	6.85	0.29
15	8.23	4.78	0.32	4.84	7.91	6.80	1.16
16	21.95	5.11	11.21	5.62	10.74	7.60	1.41
17	-10.03	4.64	2.17	4.98	-12.2	6.81	-1.79
18	1.93	3.8	-4.31	3.87	6.24	5.42	1.15
19	6.86	4.62	10.41	4.88	-3.55	6.72	-0.53
20	-0.02	12.16	15.5	13.1	-15.52	17.87	-0.87

Table 4-4 Concentrations from α and β fittings for the new system, det#1

subject#	alpha2	sig(alp2)	beta2	sig(bet2)	alp2-bet2	sig(α-β)	Z
1	-5.2	4.93	3.97	5.04	-9.17	7.05	-1.30
2	7.61	4.89	9.48	5.3	-1.87	7.21	-0.26
3	3.12	4.47	4.57	4.52	-1.45	6.36	-0.23
4	4.26	5.00	4.14	5.22	0.12	7.23	0.02
5	-1.00	4.98	5.78	5.39	-6.78	7.34	-0.92
6	2.66	9.71	20.6	9.73	-17.94	13.75	-1.31
7	-1.45	6.42	4.13	6.94	-5.58	9.45	-0.59
8	7.91	5.37	-4.89	5.71	12.8	7.84	1.63
9	1.16	4.06	8.06	4.35	-6.9	5.95	-1.16
10	-14.42	6.87	-4.91	7.30	-9.51	10.02	-0.95
11	-4.13	4.57	8.56	5.02	-12.69	6.79	-1.87
12	5.17	7.92	6.97	8.29	-1.8	11.47	-0.16
13	-7.11	4.06	4.37	4.35	-11.48	5.95	-1.93
14	4.04	4.57	1.45	4.88	2.59	6.69	0.39
15	5.64	5.27	7.93	5.46	-2.29	7.59	-0.30
16	10.87	5.31	15.82	5.89	-4.95	7.93	-0.62
17	0.94	5.61	5.03	6.09	-4.09	8.28	-0.49
18	6.58	4.51	9.43	4.69	-2.85	6.51	-0.44
19	3.92	4.90	10.24	5.07	-6.32	7.05	-0.90
20	-32.08	13.53	12.99	13.11	-45.07	18.84	-2.39

Table 4-5 Concentrations from α and β fittings for the new system, det#2

subject#	alpha3	sig(alp3)	beta3	sig(bet3)	alp3-bet3	sig(α-β)	Z
1	4.43	4.06	-0.79	4.76	5.22	6.26	0.83
2	7.93	4.39	11.43	5.19	-3.5	6.80	-0.51
3	1.77	4.05	8.82	4.58	-7.05	6.11	-1.15
4	3.73	4.50	2.79	5.13	0.94	6.82	0.14
5	-4.05	4.63	4.22	5.45	-8.27	7.15	-1.16
6	4.85	10.62	-3.56	10.95	8.41	15.25	0.55
7	6.69	5.16	15.46	6.24	-8.77	8.10	-1.08
8	0.93	4.79	-3.56	5.66	4.49	7.41	0.61
9	8.29	3.84	4.72	4.41	3.57	5.85	0.61
10	-5.97	5.69	-12.43	6.77	6.46	8.84	0.73
11	5.18	5.06	-7.79	5.54	12.97	7.50	1.73
12	-9.80	6.55	-1.65	7.69	-8.15	10.10	-0.81
13	3.63	3.87	2.62	4.6	1.01	6.01	0.17
14	14.23	4.34	-1.9	4.88	16.13	6.53	2.47
15	5.88	4.61	-1.13	4.98	7.01	6.79	1.03
16	13.08	4.67	23.66	5.68	-10.58	7.35	-1.44
17	-7.69	4.78	8.35	5.73	-16.04	7.46	-2.15
18	-6.44	4.10	7.93	4.68	-14.37	6.22	-2.31
19	7.28	4.58	8.35	5.4	-1.07	7.08	-0.15
20	5.92	10.95	-29.29	12.4	35.21	16.54	2.13

Table 4-6 Concentrations from α and β fittings for the new system, det#3

subject#	alpha4	sig(alp4)	beta4	sig(bet4)	alp4-bet4	sig(α-β)	Z
1	2.10	3.77	9.35	4.24	-7.25	5.67	-1.28
2	7.93	4.11	10.07	4.86	-2.14	6.36	-0.34
3	3.15	3.86	6.18	4.33	-3.03	5.80	-0.52
4	8.82	4.06	6.17	4.53	2.65	6.08	0.44
5	3.21	4.24	12.59	4.97	-9.38	6.53	-1.44
6	-11.00	12.56	-10.49	13.53	-0.51	18.46	-0.03
7	-3.66	5.17	12.79	5.70	-16.45	7.70	-2.14
8	2.25	4.89	6.13	5.29	-3.88	7.20	-0.54
9	4.50	3.79	7.70	4.24	-3.2	5.69	-0.56
10	-6.81	5.45	-0.83	6.09	-5.98	8.17	-0.73
11	-1.66	4.95	-9.35	5.61	7.69	7.48	1.03
12	4.42	6.30	-1.83	7.06	6.25	9.46	0.66
13	-5.47	3.80	2.61	4.38	-8.08	5.80	-1.39
14	4.41	4.80	4.20	4.97	0.21	6.91	0.03
15	12.07	4.23	8.45	4.54	3.62	6.21	0.58
16	13.73	4.00	23.09	4.82	-9.36	6.26	-1.49
17	-2.80	4.81	4.01	5.11	-6.81	7.02	-0.97
18	-3.34	3.98	5.42	4.42	-8.76	5.95	-1.47
19	3.87	4.78	-6.52	4.95	10.39	6.88	1.51
20	28.33	10.07	23.37	10.95	4.96	14.88	0.33

Table 4-7 Concentrations from α and β fittings for the new system, det#4

The bone lead concentrations measured by the four detectors of the new system are listed in Table 4-8.

Subject#	conc1	sig1	conc2	sig2	conc3	sig3	conc4	sig4
1	-4.81	3.03	-0.72	3.52	2.23	3.09	5.31	2.82
2	14.53	3.39	8.47	3.60	9.39	3.35	8.83	3.14
3	-0.47	3.11	3.84	3.18	4.86	3.03	4.49	2.88
4	5.96	3.28	4.20	3.61	3.32	3.39	7.64	3.02
5	6.80	3.70	2.13	3.66	-0.58	3.53	7.16	3.22
6	11.23	7.87	11.61	6.87	0.77	7.62	-10.76	9.21
7	6.55	4.18	1.12	4.71	10.25	3.98	3.76	3.83
8	2.10	3.76	1.91	3.91	-0.94	3.66	4.04	3.59
9	3.60	2.80	4.38	2.97	6.76	2.90	5.92	2.83
10	-3.96	4.54	-9.95	5.00	-8.65	4.36	-4.15	4.06
11	3.79	3.84	1.62	3.38	-0.72	3.74	-5.03	3.71
12	4.29	5.44	6.03	5.73	-6.38	4.98	1.65	4.70
13	4.44	3.04	-1.77	2.97	3.21	2.96	-2.00	2.87
14	13.00	3.42	2.83	3.34	7.12	3.24	4.30	3.45
15	4.33	3.40	6.75	3.79	2.65	3.38	10.39	3.10
16	17.09	3.78	13.09	3.94	17.35	3.61	17.55	3.08
17	-4.37	3.39	2.81	4.12	-1.12	3.67	0.39	3.50
18	-1.13	2.71	7.95	3.25	-0.20	3.08	0.58	2.95
19	8.54	3.36	6.97	3.52	7.72	3.49	-1.15	3.44
20	7.16	8.91	-8.84	9.42	-9.50	8.21	26.05	7.41

Table 4-8 Bone lead concentrations measured by the four detectors of the new system

The lead concentrations and the uncertainties from the conventional system and the new system are listed in Table 4-9. This time, the results for the new system combine the values from all the four detectors by using the following formulae:

$$Conc = \frac{\frac{conc1}{\sigma_1^2} + \frac{conc2}{\sigma_2^2} + \frac{conc3}{\sigma_3^2} + \frac{conc4}{\sigma_4^2}}{\frac{1}{\sigma_1^2} + \frac{1}{\sigma_2^2} + \frac{1}{\sigma_3^2} + \frac{1}{\sigma_4^2}} \quad \text{..... (4.3)}$$

$$\sigma_{conc} = \frac{1}{\sqrt{\frac{1}{\sigma_1^2} + \frac{1}{\sigma_2^2} + \frac{1}{\sigma_3^2} + \frac{1}{\sigma_4^2}}} \quad \text{..... (4.4)}$$

where conc and σ_{conc} are the inverse weighted concentration and uncertainty for the new system, conc1, conc2, conc3, and conc4 are the concentrations measured by the four detectors, σ_1, σ_2, σ_3, and σ_4 are the corresponding uncertainties. Also shown in Table 4-9 is the z-value calculated from the following equation:

$$z = \frac{conc_{new} - conc_{conv}}{\sqrt{\sigma_{new}^2 + \sigma_{conv}^2}} \quad \text{..... (4.5)}$$

Where $conc_{new}$ is the lead concentration measured from the new system and $conc_{conv}$ is the lead concentration from the conventional system, and σ_{new} and σ_{conv} are the associated uncertainties. The relation between σ_{new} and σ_{conv} is fitted by a linear curve, and the result shows that σ_{new} is strongly correlated with σ_{conv} (Figure4-1). The relation between σ_{new}^2 and σ_{conv}^2 can also be fitted as: $\sigma_{new}^2 = 0.173 \times \sigma_{old}^2 + 0.187$ with a R^2 of 0.946. Two other interesting and encouraging results were also discovered from this table. The first is that the censoring proportion for the measurements by the conventional system is 85%, and the censoring proportion for the measurements by the new system is 50% (please refer to Chapter 6 for the concept about censoring). The other is that the result from the new system shows a significant correlation between the lead concentration and age, while

the result from the conventional system does not. Table 4-10 show the regression results. These discoveries show that the new system does make a difference.

	Conventional system		new system		
subject #	conc.1 (ppm)	sig (ppm)	conc.2 (ppm)	sig (ppm)	Z
1	-4.52	3.15	0.76	1.54	-1.45
2	4.31	4.47	10.29	1.68	-1.25
3	8.87	4.14	3.25	1.52	1.27
4	3.60	3.91	5.47	1.65	-0.43
5	-11.52	4.28	4.01	1.76	-3.36
6	7.59	8.72	4.73	3.88	0.30
7	4.37	4.47	5.69	2.07	-0.27
8	-8.72	4.65	1.79	1.86	-2.10
9	12.07	3.10	5.16	1.44	2.02
10	1.31	5.08	-6.43	2.23	1.39
11	-5.25	5.01	-0.06	1.83	-0.97
12	2.10	4.83	0.97	2.58	0.21
13	2.31	3.42	0.88	1.48	0.38
14	-7.15	3.52	6.78	1.68	-3.57
15	1.97	5.00	6.21	1.70	-0.80
16	9.92	3.80	16.49	1.78	-1.57
17	5.17	4.85	-0.88	1.82	1.17
18	-1.04	3.59	1.43	1.49	-0.64
19	-4.45	3.53	5.52	1.73	-2.54
20	-21.98	10.27	5.69	4.19	-2.49

Table 4-9 Lead concentrations and uncertainties measured by both systems

subject	regression line and statistics
all subjects, new system	Pb concentration = 0.318*age – 6.901
	R^2 = 0.512, t = 4.35, p = 0.000
male subjects, new system	Pb concentration = 0.299*age – 5.18
	R^2 = 0.57, t = 3.26, p = 0.012
female subjects, new system	Pb concentration = 0.245*age – 5.71
	R^2 = 0.295, t = 1.83, p = 0.105
all subjects, old system	Pb concentration = 0.153*age – 5.26
	R^2 = 0.038, t = 0.84, p = 0.410
male subjects, old system	Pb concentration = 0.343*age – 11.9
	R^2 = 0.252, t = 1.64, p = 0.14
female subjects, old system	Pb concentration = -0.238*age + 6.3
	R^2 = 0.052, t = -0.66, p = 0.526

Table 4-10 Regression results between concentration and age for both systems

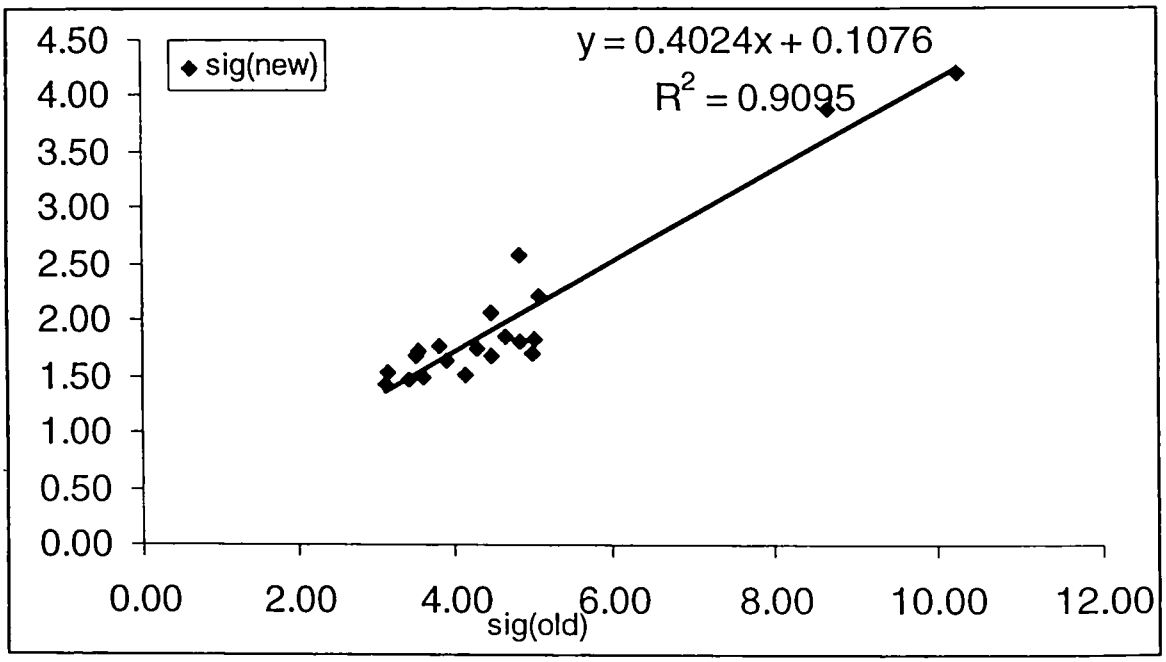

Figure 4-1 The relation between uncertainties for the new system and the old system

The mean and standard deviation for z values are listed in Table 4-11.

MDL is calculated as twice the uncertainty of the concentration. Table 4-12 shows the MDLs for both systems and the ratios of the MDLs. The original MDLs for both system and the normalized MDLs for the new system were calculated by the following formulae:

$$MDL = 2 \times \sigma_{ppm} \quad \ldots\ldots\ldots\ldots \quad (4.6)$$

Where σ_{ppm} is the lead concentration and uncertainties for the conventional system and new system; coh_{conv} and coh_{new} are the coherent area counts for the conventional system and the new system.

		$Z_{average}$	Z_{stdev}	X_{19}^2
old system	α-β	-0.80	1.15	37.68
new system	$\alpha 1$-$\beta 1$	0.07	1.17	26.22
	$\alpha 2$-$\beta 2$	-0.69	0.89	24.46
	$\alpha 3$-$\beta 3$	0.01	1.33	33.81
	$\alpha 4$-$\beta 4$	-0.42	0.97	21.49
	α-β	-0.26	1.13	105.98*
comparison	$Conc_{old}$-$conc_{new}$	-0.74	1.59	58.81

Table 4-11 Averages and standard deviations of Z values

*: degree of freedom is 76 instead of 19.

Subject #	MDL_{conv}	MDL_{new}	ratio1
1	6.30	3.09	0.49
2	8.94	3.36	0.38
3	8.28	3.04	0.37
4	7.84	3.30	0.42
5	8.56	3.51	0.41
6	17.44	7.76	0.45
7	8.94	4.14	0.46
8	9.30	3.72	0.40
9	6.20	2.87	0.46
10	10.16	4.45	0.44
11	10.02	3.65	0.36
12	9.66	5.17	0.53
13	6.84	2.96	0.43
14	7.04	3.36	0.48
15	10.00	3.39	0.34
16	7.60	3.55	0.47
17	9.70	3.64	0.38
18	7.18	2.98	0.41
19	7.06	3.45	0.49
20	20.54	8.38	0.41

Table 4-12 MDLs for the conventional system and the new system and their ratios

The original source strength for the new system was 5GBq. It has decayed to 2.45GBq. The source strength could go up to 10GBq. Table 4-13 shows the MDLs for the new system for a 2.45GBq source, and the extrapolated MDLs for a 10GBq source.

subject #	$MDL_{2.45GBq}$ (ppm)	MDL_{10GBq} (ppm)
1	3.09	1.53
2	3.36	1.66
3	3.04	1.51
4	3.30	1.64
5	3.51	1.74
6	7.76	3.85
7	4.14	2.05
8	3.72	1.84
9	2.87	1.42
10	4.45	2.21
11	3.65	1.81
12	5.17	2.56
13	2.96	1.47
14	3.36	1.66
15	3.39	1.68
16	3.55	1.76
17	3.64	1.80
18	2.98	1.47
19	3.45	1.71
20	8.38	4.15

Table 4-13 MDLs for the new system for 2.45GBq and 10GBq sources

4.4 Discussion

With 2.45GBq source, the median uncertainty for the concentrations of these 20 people is 1.74 ppm, so the median MDL is 3.48 ppm. The extrapolated median MDL for 10GBq source is 1.72 ppm. The median MDL by using the old system is 8.75 ppm. So

the actual ratio of the MDLs is 0.40 (3.48/8.75) and the extrapolated ratio is 0.20 (1.72/8.75). The extrapolated ratio may be higher than 0.20, since the straight extrapolation is not quite fair. As the source strength get higher, the dead time will be higher and the counts for the stronger source (10GBq) will be less than four times the counts for the weaker source (2.45GBq) in fixed clock time.

With a much lower MDL for the new system, many studies that can not be performed by the conventional system due to the relatively high MDL can now be carried out by the new system.

As mentioned in the first Chapter, low-level lead exposure is believed to cause many adverse health effects, especially for children. But the study of low-level lead exposure is limited by the sensitivity of the measurement system. With the new bone lead measurement system described in this thesis, big surveys for the low-level exposed population can be organized to get more precise data and to understand better about the health effects of low-level lead exposure.

The new system can also be used to distinguish small differences between the populations with different exposure categories, or the same population at different stages. For example, it is difficult to tell the difference between a population with low-level exposure and a population with environmental exposure by using the conventional system; however, it will be much easier to do it by using the new system. In chapter 6, a statistical method is described to distinguish populations with and without low-level lead exposure in their childhood decades ago. The controlled population has 268 young adults and the exposed population has 262 young adults. The measurements were performed by

using the conventional system. According to the results, the concentrations for 251 people out of 268 are censored (with concentration less than the detection limit) for the controlled group, and 194 out of 262 are censored for the exposed group. So the censored proportions are 94% and 74%. If these people were measured by using the new system, assuming a detection limit of 2.5 μg/g bone mineral, the censored proportion would be 62% and 40% for the controlled group and the exposed group respectively. This will greatly improve the analysis significance by using the traditional analysis method, and the study of left-censoring method would not be necessary. Also for the in-vivo measurement described in Chapter 4, among the 20 people, 85% of them have a censored lead concentration when measured by the old system, and the proportion dropped to 50% when measured by the new system.

There are some studies show that the current lead metabolism model cannot correctly reflect lead transfer in human in many circumstances. Brito et al. (2001) studied two data sets from four big lead surveys for the occupationally lead exposed factory workers, and the result showed that the lead transfer rate in human body depends on a person's age and on how heavy the exposure to lead has been. The problems with the lead metabolism models are also described in Chapter 5 in this thesis and in Fleming et al.'s work (1999). By using the more sensitive new system, these problems can be further investigated.

From the statistical point of view, the new system can reduce a survey population by a factor of ~9 to get the same statistical significance. Or with the same population, the conclusion for the study will be more significant.

4.5 Future work

There are three parts about the future work.

The first part is the future studies by using the new system. This includes surveys for occupational exposed and low-level exposed people. Two bone lead surveys have been performed to a group of active workers at Nova Pb, a battery recycling plant in Montreal, Québec, Canada, in 1993 and 1998. Another two surveys were performed at the Brunswick Mining and Smelting plant in Belledune, New Brunswick, Canada, in 1994 and 1999. The third surveys for both populations by using the new system are expected to start very soon. These data sets will produce very important information about the lead metabolism in human body, with bone lead data over a 10 year time period. The surveys for lead exposed children will also be organized soon.

The second part is the future studies that are induced by the improvement of the system sensitivity. One of the projects for my Master's program investigated the problem with the calibration lines by using a new set of phantoms with fixed lead concentrations. The problem with the new alpha and beta calibration lines is that the slopes and intercepts of the lines are different from those for the old phantoms. The reason for the discrepancy is that the composition of the phantom is not what it is supposed to be. By modifying the parameters related with the composition of the phantoms in the fitting program, the major problem is fixed. However, there is still a minor problem with the intercept, in that there are still intercepts with the calibration lines, which should be zero. Moreover, the intercept for the alpha line is different from that for the beta line. The intercept is at a range of 1-2 ppm. For the old system with an MDL of 6-10 ppm, the intercept is

acceptable. The new system has an MDL of 2 to 3 ppm, which means the intercept of 1-2 ppm will affect the result significantly. Further investigations with the intercepts should be carried out. In addition, the old version of the fitting program is based on the maximum channel of 4096. A maximum channel of 8192 or 16382 may give a better fitting, given sufficient count rate, which will improve the accuracy of the result. A new version of the fitting program is another topic for future work.

The third part is the future studies about the improvement of the new system. The main idea of improving the MDL for the system is to increase the useful signals and to decrease the background. The maximum count rate the detector can handle is ~700 kcps for 16 mm diameter detectors (the value comes from a private conversation between Sandra N. Bateman and Dr. David Chettle; in the experiment, the preamp was opened and adjusted to get a higher throughput than the detector), the maximum count rate the preamp can handle is ~180 kcps, the maximum count rate the DSA-1000 can handle is ~90kcps (~50% dead time with maximum preamp throughput). So if in someway, the preamp can sense the signal height, and drop some of the signals that are useless for the analysis (e.g. Compton scattering signals at energy lower than 68 keV), then we will get more useful signals at the right energy range and hence improve the MDL of the system. The X-ray optics can also be used to focus the x-ray beam to the critical location and hence increase the useful signals and reduce the background.

Chapter 5

Lead metabolism modeling

5.1 Lead metabolism models

Many models have been developed to assess lead metabolism in human body. Rabinowitz's model (Rabinowitz et al. 1976) predicts changes in blood lead concentrations in adult males in response to lead uptakes. The model consists of three compartments and two excretion paths. Transfer rates between the compartments and excretion paths were derived from data collected from five healthy subjects, who received oral doses of stable lead isotopes for various periods of time. Bert's model (Bert et al. 1989) is more complicated. It calculates the lead body burden associated with intakes to the gastrointestinal and respiratory tracts for adult males. This model has more compartments and it is an expansion of Rabinowitz's model. Stern developed two models to assess risks from exposures to lead in soil. The 1994 model (Stern 1994) estimates the residential child exposure from lead in soil and the 1996 model (Stern 1996) describes the relationship between soil lead and blood pressure changes for adults.

The two most investigated models are O'Flaherty's model (O'Flaherty 1993, O'Flaherty 1995) and Leggett's model (Leggett 1993a, Leggett et al. 1993b, Pounds and Leggett 1998). O'Flaherty's model is a physiologically-based biokinetic model which predicts the delivery of lead to tissues as a function of blood flow. Leggett's model was developed in the last 10 years at Oak Ridge National Laboratory and it is currently used

by the International Commission on Radiological Protection (ICRP) to predict internal radiation doses of radionuclides that have biokinetics similar to calcium. The whole model is based on a linear differential equation (Leggett et al. 1993b) with transfer rates between various compartments. Bone is divided into four compartments, which include cortical surface, cortical volume, trabecular surface, and trabecular volume. The cortical volume and trabecular volume each consist of an exchangeable and a non-exchangeable pool, and the slow kinetics of bone lead is attributed to the non-exchangeable pool. The transfer rates from non-exchangeable bone to blood applied in the model are bone resorption rates adopted from Frost's bone remodeling study (Frost 1969).

It has long been known that age and exposure level will affect the lead transfer rate from bone to blood. The effect of exposure level has been investigated previously by Brito (2000). In this work, we will study the effect of the age. A new simplified model is designed to investigate the bone and blood lead metabolism of different age groups of smelter workers. The idea of the model is adopted from Brito's work (2000), and details of the model will be described. Through this study, it is proposed that bone metabolism in occupationally exposed individuals is not accurately reflected in the current lead metabolism models, and that more study is required in this area. The availability of extensive data sets obtained by an *in vivo* x-ray fluorescence (XRF) bone lead measurement system provides a unique way to investigate this problem.

5.2 Method

5.2.1 Bone lead measurement and subject population

The first *in vivo* x-ray fluorescence (XRF) bone lead measurement system was installed by Ahlgren *et al* using a ^{57}Co source in a 90° geometry (Ahlgren et al. 1976). The technique used in our group is ^{109}Cd γ-ray induced K x-ray fluorescence in a back-scatter geometry, which was developed at the University of Birmingham (Laird et al. 1982). The system used for the survey is an enhanced system developed at McMaster University (Gordon et al. 1993), in which a ^{109}Cd source is mounted coaxially with, and in front of, the detector, resulting in a backscatter source-sample-detector geometry.

Two bone lead surveys have been performed at the Brunswick Mining and Smelting plant in Belledune, New Brunswick, Canada. In both surveys, ^{109}Cd γ-ray induced XRF bone lead measurements were made to determine the lead concentration in tibia and calcaneus for a large group of people. 539 workers were involved in these surveys; among them 327 had their tibia and calcaneus bone lead measured both in the year 1994 and in 1999. Regular monitoring of the blood lead concentration for the workers started in 1967 and provides a well documented history of blood lead data for these workers.

5.2.2 Lead metabolism simulation by Leggett's model

Leggett's model predicts lead transfer between various compartments from the first day of life. The initial lead content originates from maternal sources and is distributed proportionally in some organs (Leggett 1993a). Postnatally there will be

exposure to environmental lead. The model includes three routes of lead intake (μg/day): ingestion, inhalation, and direct input to blood. The lead input will then be transferred to all organs following first-order kinetics. The lead exposure history determines a person's lead intake.

In this study, the lead metabolism simulations for the New Brunswick workers were regulated by their blood lead history data. The main source of lead comes from occupational exposure for these workers. However, the background exposure before the date they were hired should also be considered. There are not enough data available to allow for an accurate background evaluation. Fortunately, the simulations by changing the background exposure within a range shows that this will not significantly (<5%) affect the model-predicted bone lead concentrations for these workers. Data from several sources were taken into consideration (The Royal Society of Canada 1986, Annest et al. 1983, Brody et al. 1994, Pirkle et al. 1994). The average blood lead for children and adults were set as 25μg/dl and 16μg/dl respectively before 1970, and 10μg/dl and 8μg/dl after 1970. Initial lead intakes at several time periods were estimated. The time periods were chosen in a way such that the blood lead in that period was relatively stable. The initial input file was estimated for the first calculation of the model, and then the predicted blood lead and the actual blood lead history were used to adjust the input file for the second run. After two or three iterations, the average predicted blood lead will be the same as the average blood lead history for all time periods. After adjusting the lead intake according to the blood lead history, the predicted and measured bone lead can be compared.

5.2.3 The new model

The new model consists of only three compartments, based on the availability of data for lead concentrations in tibia, calcaneus and blood. These data provide an opportunity to draw direct statistical inference for rate constants pertaining to these compartments. The three compartments are: the cortical bone (based on the tibia data), the trabecular bone (based on the calcaneus data), and the blood (Figure 5-1). Six parameters are set up for this model: λ_{CB}, λ_{TB}, λ_{BC}, λ_{BT}, λ_0, and I_0, where λ_{CB} is the transfer rate (/day) from cortical bone to blood, λ_{TB} is the transfer rate from trabecular bone to blood, λ_{BC} is the transfer rate from blood to cortical bone, λ_{BT} is the transfer rate from blood to trabecular bone, λ_0 is the transfer rate out of blood to all other organs, and I_0 is the lead input (μg/day). The method used for this model is the minimum least squares. The tibia bone lead and calcaneus bone lead were measured each in 1994 and 1999, so this model is applied to the bone lead and blood lead data between these two surveys.

The starting point of the model is the first survey, at this time:

$$\begin{aligned} B(0) &= B_0 \\ C(0) &= C_0 \quad \text{.....(5.1)} \\ T(0) &= T_0 \end{aligned}$$

where B(0), C(0), and T(0), or B_o, C_o, and T_o, are the total blood, cortical bone, and trabecular bone lead from the measurements at the time when the first survey was performed.

Now assuming a time step of Δt, then at time t:

$$B(t) = I_0\Delta t + C(t-\Delta t)\lambda_{CB}\Delta t + T(t-\Delta t)\lambda_{TB}\Delta t - B(t-\Delta t)\lambda_{BC}\Delta t - B(t-\Delta t)\lambda_{BT}\Delta t - B(t-\Delta t)\lambda_0\Delta t$$
$$C(t) = B(t-\Delta t)\lambda_{BC}\Delta t - C(t-\Delta t)\lambda_{CB}\Delta t$$
$$T(t) = B(t-\Delta t)\lambda_{BT}\Delta t - T(t-\Delta t)\lambda_{TB}\Delta t$$
.....(5.2)

where B(t), C(t), and T(t) are the total blood lead, cortical bone lead, and trabecular bone lead at time t.

When Δt=1, *i.e.* the time step is chosen as 1 day, then the above equations can be written as:

$$B(t) = I_0 + C(t-1)\lambda_{CB} + T(t-1)\lambda_{TB} - B(t-1)\lambda_{BC} - B(t-1)\lambda_{BT} - B(t-1)\lambda_0$$
$$C(t) = B(t-1)\lambda_{BC} - C(t-1)\lambda_{CB} \qquad \text{.....(5.3)}$$
$$T(t) = B(t-1)\lambda_{BT} - T(t-1)\lambda_{TB}$$

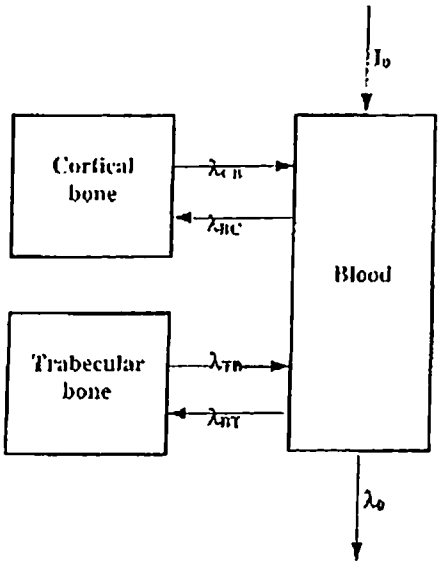

Figure 5-1 The simplified model proposed in this study, based on the available data

By choosing initial values for λ_{CB}, λ_{TB}, λ_{BC}, λ_{BT}, λ_0, and I_0, and given B_o, C_o, and T_o, the total blood lead, cortical bone lead, and trabecular bone lead for each day of the five year period will be calculated.

The goodness–of–fit function χ^2 is defined as:

$$\chi^2 = \sum\left[(B'(t) - B(t))/\sigma_{B(t)}\right]^2 + \sum\left[(C'(t) - C(t))/\sigma_{C(t)}\right]^2 + \sum\left[(T'(t) - T(t))/\sigma_{T(t)}\right]^2 \quad \ldots.(5.4)$$

where B'(t), C'(t), and T'(t) are the measured total blood, cortical bone, and trabecular bone lead for each individual at time t, while B(t), C(t), and T(t) are the corresponding predicted values. $\sigma_{C(t)}$ and $\sigma_{T(t)}$ are the uncertainties of the measured cortical and trabecular bone lead calculated from our data reduction algorithm. $\sigma_{B(t)}$ is the standard deviation of the blood lead of all individuals. The algorithm used to find the minimum χ^2 is the grid search method, which is described in detail by Bevington (Bevington 1969).

5.2.4 The bone and blood compartments in Leggett's model and the new simplified model

Figure 5-2 shows the bone and blood compartments in Leggett's model. The cortical and trabecular bone compartments are divided into three pools instead of only one compartment as used in the new model. Since the lead transfer between the blood and the bone surface, as well as the lead transfer between the bone surface and the exchangeable pool, are much faster than the transfer rate between the non-exchangeable pool and blood, the lead concentration in the blood, bone surface, and exchangeable pool

will reach equilibrium after a fairly short time. Therefore, for this long-term study, the lead can be seen as entering the non-exchangeable pool from blood with a certain transfer rate, and being released from the non-exchangeable pool to blood with another rate. This is the assumed mechanism for the new simplified model described in the previous section. In this way, the bone to blood transfer rates for these two models can be compared.

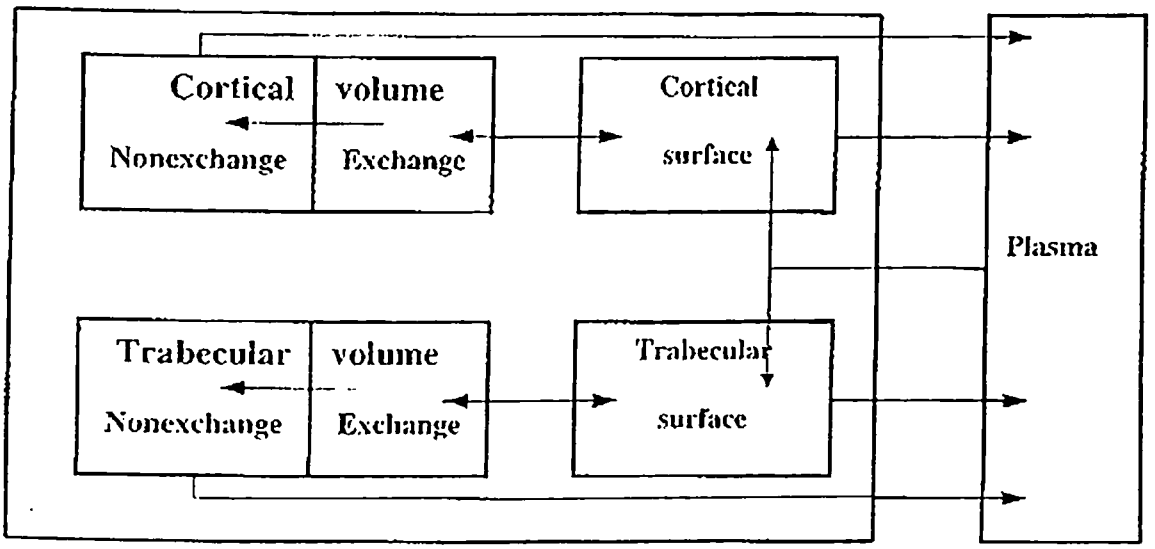

Figure 5-2 Bone and blood compartments in Leggett's model of lead metabolism

5.3 Results/Discussion

5.3.1 The predicted bone lead concentrations based on Leggett's model compared to the measured bone lead concentrations

Figure 5-3 shows the predicted and measured bone and blood lead concentrations for a retired employee (subject #270). The lead intake is regulated by the blood lead concentration history, so in the plot the predicted blood lead and the measured blood lead

are in good agreement. However, when comparing the predicted cortical bone lead and trabecular bone lead in 1994 and 1999 with the measured values, both predicted bone lead concentrations underestimate the measured values. The differences between the measured cortical bone lead concentrations and the predicted values are 3.3 and 3.7 times the uncertainties of the measured values for the year 1994 and 1999 respectively. The differences between the measured trabecular bone lead concentrations and the predicted values are even greater, with differences that are 12 and 18 times the uncertainties respectively.

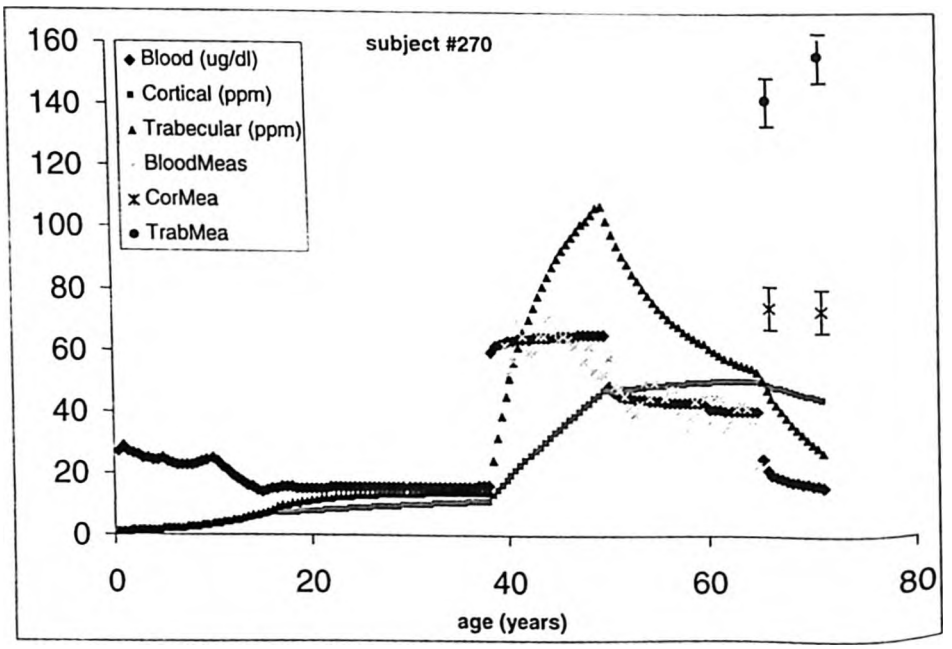

Figure 5-3 Predicted and measured bone and blood lead concentrations for subject #270

Figure 5-4 shows the same type of plots for all 9 retired workers for whom repeat bone lead data were available, and all of them indicate that the predicted cortical bone lead and trabecular bone lead concentrations greatly underestimate the measured values.

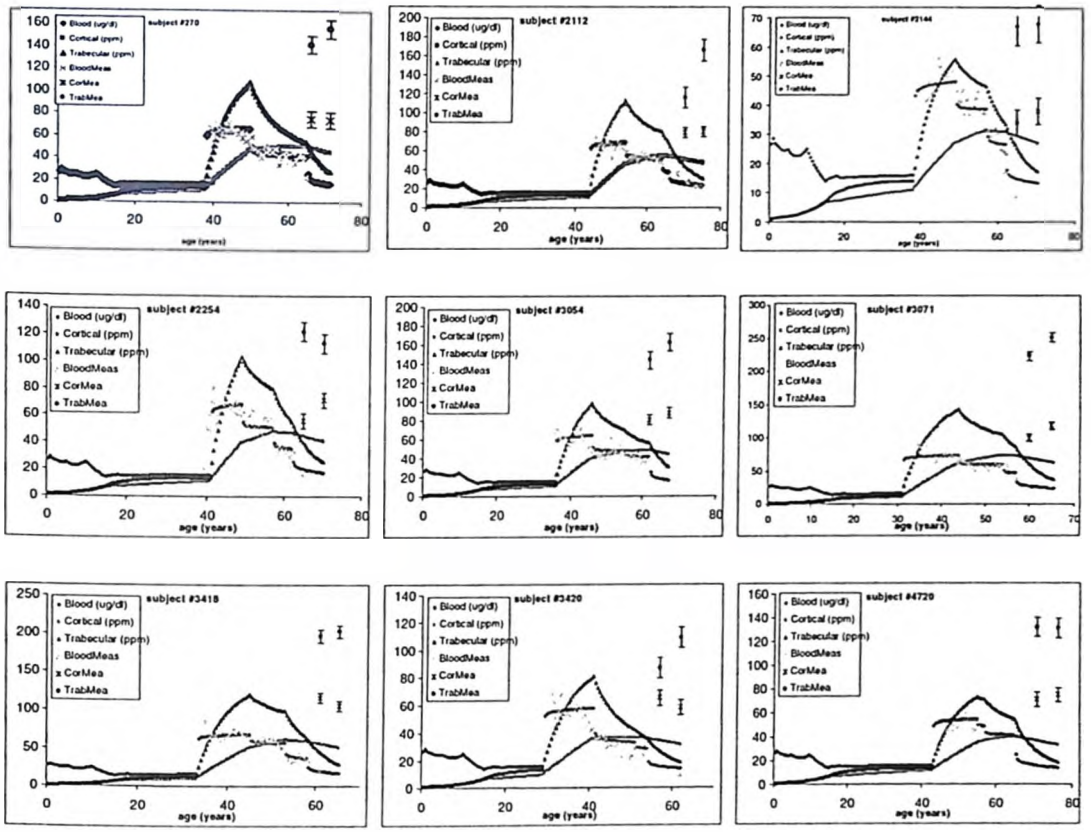

Figure 5-4 Predicted and measured bone and blood lead concentrations for 9 retired workers

5.3.2 The estimated transfer rates by the new model

The 327 workers with their bone lead measured twice were divided into five age groups. The new model was applied to these five age groups and Table 5-1 shows the calculated transfer rates for these groups.

Age	n	λ_{CB} (/day)	λ_{TB} (/day)	λ_{BC} (/day)	λ_{BT} (/day)
20s	42	(27±1)e-5	(22±2)e-5	(7.2±0.2)e-3	(6.2±0.1)e-3
30s	77	(7.6±0.2)e-5	(7.6±0.4)e-5	(3.7±0.1)e-3	(5.2±0.1)e-3
40s	140	(4.7±0.1)e-5	(8.9±0.2)e-5	(2.8±0.1)e-3	(5.7±0.1)e-3
50s	57	(1.0±0.1)e-5	(8.5±0.2)e-5	(1.6±0.1)e-3	(6.3±0.1)e-3
60s	11	(1.0±0.4)e-5	(0.4±0.4)e-5	(1.5±0.5)e-3	(2.8±0.3)e-3

Table 5-1: Calculated transfer rates for five age groups based on the simplified model

In order to confirm the validity of the new model, z tests of the differences between the predicted bone lead concentration and the measured bone lead concentration for the two time points are performed. Figure 5-5 shows the z-distribution of these differences. For a perfect fit the location should be 0 and the scale should be 1. The relatively greater width for the trabecular lead concentration is due to larger variability of these concentrations between individuals.

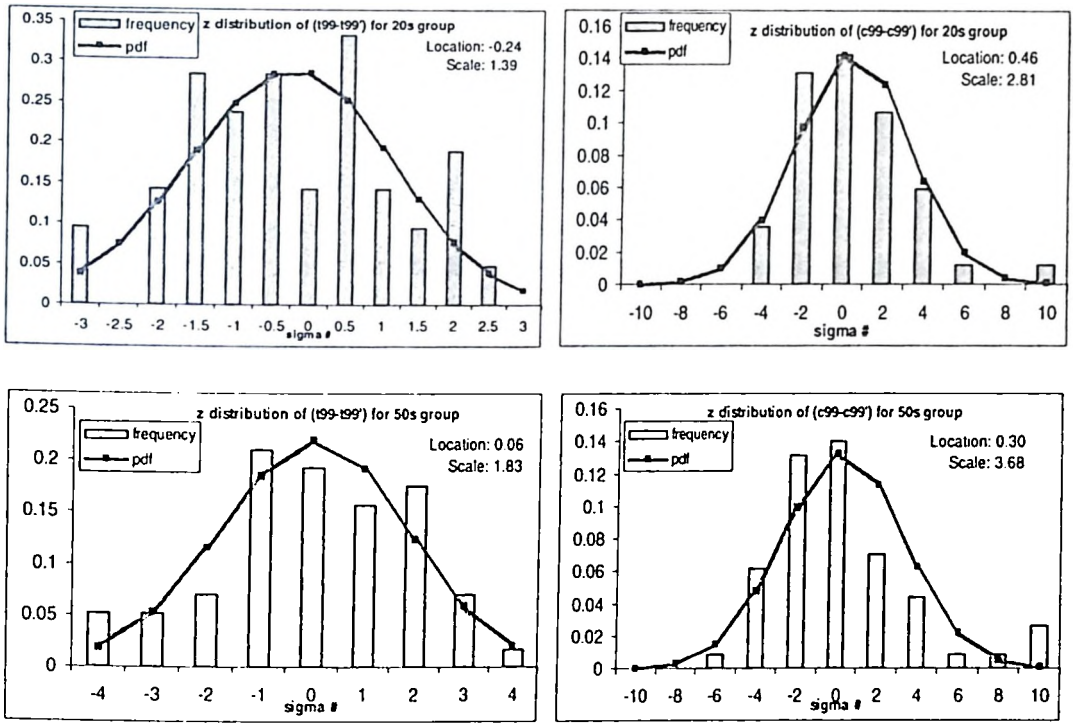

Figure 5-5 Z-distribution of the differences between the predicted and measured bone lead concentration; t99 and t99' are the predicted and measured tibia lead concentration for 1999, and c99 and c99' are the predicted and measured calcaneus lead concentrations for 1999, locations and scales are listed in the plots. Predicted values are based on the simplified model described in section 3.3.

The transfer rates from the non-exchangeable cortical bone to blood and from non-exchangeable trabecular bone to blood are 8.22e-5/day and 49.3e-5/day in Leggett's model for age 18 and older. It is assumed that the transfer rates from bone to blood stay the same for adults age 18 and older. This assumption is inconsistent with the transfer

rates derived from the new model. These values show that the transfer rate from cortical bone to blood decreases with age, with a relatively large value for subjects in their 20s, while the transfer rate from trabecular bone to blood decreases from the 20s to the 30s, and tends to be stable for subjects in their 40s and older. Overall, the transfer rates are smaller than the original values set in Leggett's model, except for the transfer from cortical bone to blood for subjects in their 20s. These findings are consistent with the underestimation of bone lead concentrations seen in Figures 5-3 and 5-4.

5.3.3 The predicted bone lead concentrations based on Leggett's model with new transfer rates, compared to the measured bone lead concentrations

Leggett's model is an age-specific model and all transfer rates are input into the model according to different age groups. The bone to blood transfer rates derived from the new model can be put directly into the input file to replace the original values. The population for the 60s age group is too small for statistical reliability, therefore the transfer rates for subjects in their 50s and older are considered to be the same. Figure 5-6 shows the predicted and measured bone and blood lead concentrations for subject #270, using the new transfer rates derived from the simplified model.

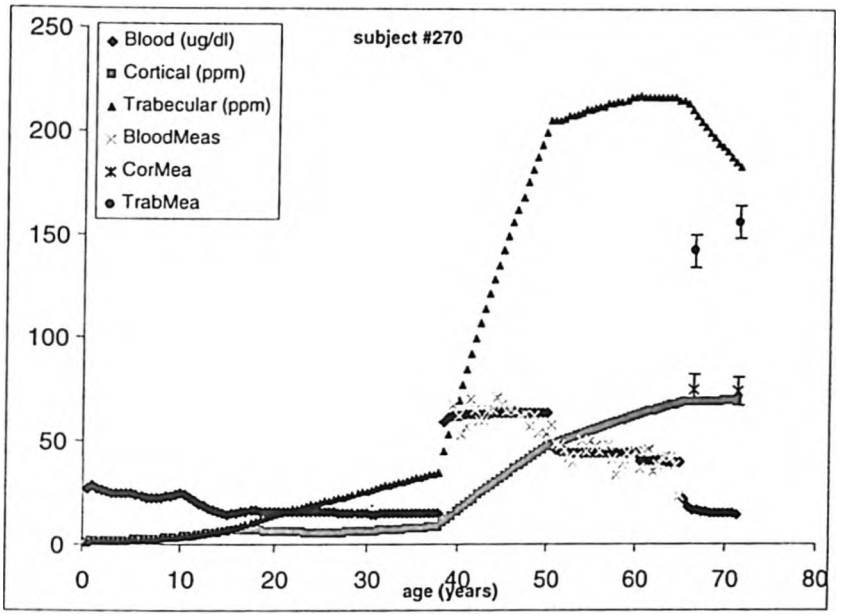

Figure 5-6 Predicted and measured bone and blood lead concentrations for subject #270. The predicted values are now calculated with Leggett's model using the new bone to blood transfer rates.

Figure 5-7 shows the same comparisons for all 9 retired workers. The predicted bone lead concentrations are much closer to the measured values compared to the results derived with the original bone to blood transfer rates. Table 5-2 shows the measured concentrations for the cortical and trabecular bones in the years 1994 and 1999, the modeled concentrations by using the original parameters and the derived new parameters. The results for cortical bone are better than for trabecular bone, suggesting that trabecular bone lead metabolism is more individually variable than cortical bone lead metabolism. These plots also show that the predicted trabecular bone lead concentrations now tend to overestimate the measured values slightly, which implies either an underestimation of the

trabecular bone to blood or an overestimation of the blood to trabecular bone transfer rate in the new model.

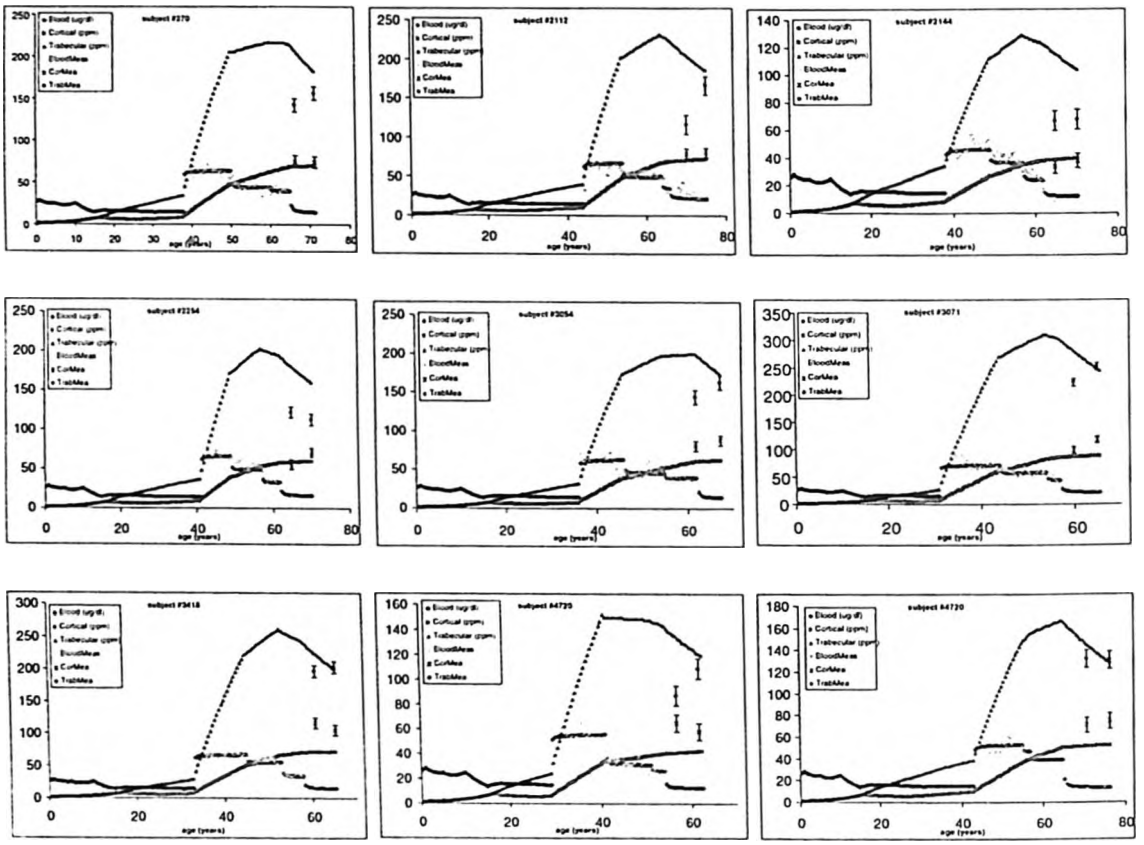

Figure 5-7 Predicted and measured bone and blood lead concentrations for 9 retired workers by using the new bone to blood transfer rates in Leggett's model

Overall, the new model and the XRF bone lead data give rise to a good approximation of the transfer rates between bone and blood, although there is clearly still room for improvement in predicting trabecular concentrations.

In this paper, only the predicted results for the retired workers are presented graphically for the original and modified Leggett model. This is because the retired workers have the

longest and most complicated pattern of lead exposure and therefore are the single group that tests the model most severely. However, it should be noted that data from all workers measured at two time points were used in establishing the rate constants summarized in Table 5-1, and these rate constants are used in generating the plots in figures 5-6 and 5-7.

Sub#	Cortical						Trabecular					
	1994			1999			1994			1999		
	meas	simulated		meas	simulated		meas	simulated		meas	simulated	
		orig	new		orig	new		orig	new		orig	new
270	75±6	49.2	68.6	74±8	44.7	69.5	142±8	45.4	207	156±7	27.7	183
2112	79±5	50.8	70.3	80±6	47.1	72.2	116±12	43.7	205	166±10	30.6	186
2144	34±4	29.4	38.5	38±5	27.0	39.7	67±7	25.2	116	68±6	17.2	104
2254	56±5	44.9	58.5	71±6	40.9	60.0	122±7	40.2	181	113±7	25.5	160
3054	81±5	48.8	61.0	88±6	44.1	62.1	144±9	56.1	200	163±9	31.0	174
3071	99±5	68.7	86.5	118±6	62.5	88.2	223±7	60.8	280	251±7	37.9	245
3418	116±5	55.8	71.2	105±8	51.0	72.0	197±9	45.2	225	232±8	29.0	201
3420	65±4	34.2	40.9	58±7	31.4	42.1	87±8	26.8	135	109±7	18.6	120
4720	71±5	36.6	51.5	75±7	33.3	52.5	132±8	28.6	145	131±7	18.9	129

Table 5-2 Calculated and modeled lead concentrations in cortical and trabecular bones

Note: sig is the uncertainties for the measurements; c_o99, c_o94, t_o99, t_o94 are the modeled lead concentration in cortical bone and trabecular bone in the years 1999 and 1994 by using the original parameters; c_n99, c_n94, t_n99, t_n94 are the modeled lead concentration in

cortical bone and trabecular bone in the years 1999 and 1994 by using the revised parameters.

The original transfer rates from non-exchangeable bone pool to blood in Leggett's model are based on histomorphometric measurements on human subjects. It is assumed that this rate is the same as the rate of bone resorption. Several authors have attempted to identify a single, long-term bone resorption rate of lead applicable to the adult human skeleton, and the estimates have ranged from about 0.007/year to about 0.15/year (Leggett 1993a), a range of a factor of 20. In this study, the new model shows that the bone to blood rate changes dramatically with age, especially for cortical bone. This suggests that the assumption of the equivalence of the transfer rate and the resorption rate is an incomplete picture, since the bone resorption rate would not be expected to change so dramatically with age in male subjects. Further study is required to investigate the cause of age dependence of bone to blood transfer rates; perhaps lead accumulation in the bone influences the transfer rate.

Bone lead concentration is an index of long-term lead exposure. XRF measurements provide an invaluable assessment of this index, and further refinements to long term aspects of human lead metabolism will be made possible through data derived from this method.

5.4 Conclusion/Future work

This study demonstrates that the default values of bone-to-blood lead transfer rates in Leggett's model are not suitable for occupationally exposed workers. By using an

XRF bone lead repeat data set, one can investigate bone lead metabolism with a simplified model. The model described in this paper indicates a lower lead transfer rate from bone to blood than previously modeled, especially for cortical bone. Future work in this area includes a third bone lead survey with the same population, which will provide a data set with a total time interval of 10 years. It is anticipated that such additional data will lead to further revisions of the current bone lead metabolism model.

Chapter 6

Left censoring: a statistical approach for XRF bone lead data analysis

6.1 Left censoring

A censored observation contains only partial information about the variable of interest. For example, in a clinical cancer therapy trial to investigate the patients' survival situation, incomplete information could occur in several ways: the patient may decide to move elsewhere and the researchers never see him again; the therapy may have such bad side effects that it is necessary to discontinue the treatment; termination of the study, etc.. Data collected for these situations are called censored data. There is both right censoring and left censoring depending on where the censoring occurs. Right censoring is observed when the censoring happens on the right, i.e. the variable of interest is not observed even at the end of the observation; left censoring is observed when the censoring happens on the left, i.e. the variable of interest is censored before we could observe it. For example, a Stanford psychiatrist wanted to know the age at which a certain group of African children learned to perform a particular task. When he arrived in the village, there were some children who already knew how to perform the task, so these children contributed left-censored observations. Some children learned the task while he was present, and their ages could be recorded. These children contributed uncensored observations. When he

left, there remained some children who had not yet learned the task, thereby contributing to right-censored observations. The detailed description about censoring and left-censoring can be found in Miller's book (1981). Censoring analysis is generally used in life sciences for the surveys related to people and animals, especially in the health related field. Recently, some scientists adapted this method to data analysis for trace element measurement (Kubala-Kukuś 2001, Pajek, Kubala-Kukuś 2002). In the trace element measurement, the concentration of the trace element may be below the detection limit (DL) of the detection system. In this case, the DL is recorded, instead of an exact concentration value. This is a left-censoring case, since the value is censored before we could observe it. When we measure bone lead by using XRF, sometimes the bone lead concentration is so low that it is below the detection limit of the bone lead measurement system. These are also examples of left-censored data. In our lab, we have an algorithm to calculate the concentration even if it is below DL or a negative value. We used to use these values for data analysis. One of the purposes of this study is to investigate the validity of our analysis procedure and to compare the conventional analysis process and the left-censoring approach.

6.2 Methods

The statistical methods that are used in this study are Inverse Variance Weighting (IVW) method, Kaplan-Meier (KM) method (Kaplan 1958), Nelson-Aalen (NA) Method (Nelson 1972, Aalen 1978), and Reconstruction Method (RM) (Kubala-Kukuś 2001). These are nonparametric estimation methods. A statistical package called Minitab is also

applied to analyze the data (Minitab Statistical Software 2000, Minitab Corp., State College, PA), and log-normal distribution was chosen for this analysis.

6.2.1 IVW method

IVW is the conventional method used in our lab to analyze the bone lead measurement data. It is used to determine the mean $\bar{x}$ and the associated error s on the mean and the formulae are listed below:

$$\bar{x} = \frac{\sum \frac{x_i}{\sigma_i^2}}{\sum \frac{1}{\sigma_i^2}} \quad \text{..... (6.1)}$$

$$s = \frac{1}{\sum \frac{1}{\sigma_i^2}} \quad \text{..... (6.2)}$$

where x_i is the concentration for an individual in the population, and σ_i is the uncertainty of the concentration. Although IVW takes into account the observational uncertainty on the measurements σ_i, it approximates the actual distribution by a delta function and provides no information about the distribution width. Moreover, it includes the individual concentrations below DL and negative concentrations, which means the actual mean should be higher than the calculated one.

6.2.2 KM method

KM method is also known as product-limit method. It can be applied for both left-censoring and right censoring. This method is described in detail in Kaplan's paper (Kaplan 1958). Let's look at a simple example for a set of left-censored data. A group of 67 people had their bone lead measured, and the bone lead concentrations for these people are listed in Table 6-1.

concentrations	(4,8]		(8,12]		(12,16]		(16,20]		(20,24]		(24,28]	
	True	DL	True	DL	True	DL	True	DL	True	DL	True	DL
No. of people	2	12	10	10	10	3	6	0	9	0	5	0

Table 6-1 Bone lead concentrations for 67 people

Note: Unit is μg Pb/g bone mineral (or ppm). True means the true concentration; DL means the detection limit.

So there were 2 people with measured concentrations between 4 ppm and 8 ppm, whereas there were 12 people whose results were below detection limits between 4 ppm and 8 ppm, and so on. The histogram for these data is showed in Figure 6-1. The conventional method to analyze censored data is called Reduced-Sample (RS) method, in which the censored data were ignored during the process. In the KM method, both uncensored and censored data were used for analysis. The cumulative distribution (CD) and the probability distribution (PD) of the bone lead concentrations are shown in Table 6-2 by using KM method.

Concentrations	CD	Ranges	PD
≤ 28 ppm	1-0/67 =1	(24,28]	1-62/67 = 5/67
≤ 24 ppm	1*(1-5/67)=62/67	(20,24]	62/67-53/67 = 9/67
≤ 20 ppm	(62/67)*(1-9/62) = 53/67	(16,20]	53/67-47/67 = 6/67
≤ 16 ppm	(53/67)*(1-6/53) = 47/67	(12,16]	47/67-37/67 = 10/67
≤ 12 ppm	(47/67)*(1-3/47) = 37/67	(8,12]	37/67-444/1139 = 0.162
≤ 8 ppm	(37/67)*(1-10/34) = 444/1139	(4,8]	444/1139-2664/7973 = 0.056
≤ 4 ppm	(444/1139)*(1-2/14) = 2664/7973	(0,4]	2664/7973-0 = 0.334
≤ 0 ppm	0	<0	0

Table 6-2 The cumulative distribution (CD) and the probability distribution (PD) of the bone lead concentrations by KM method

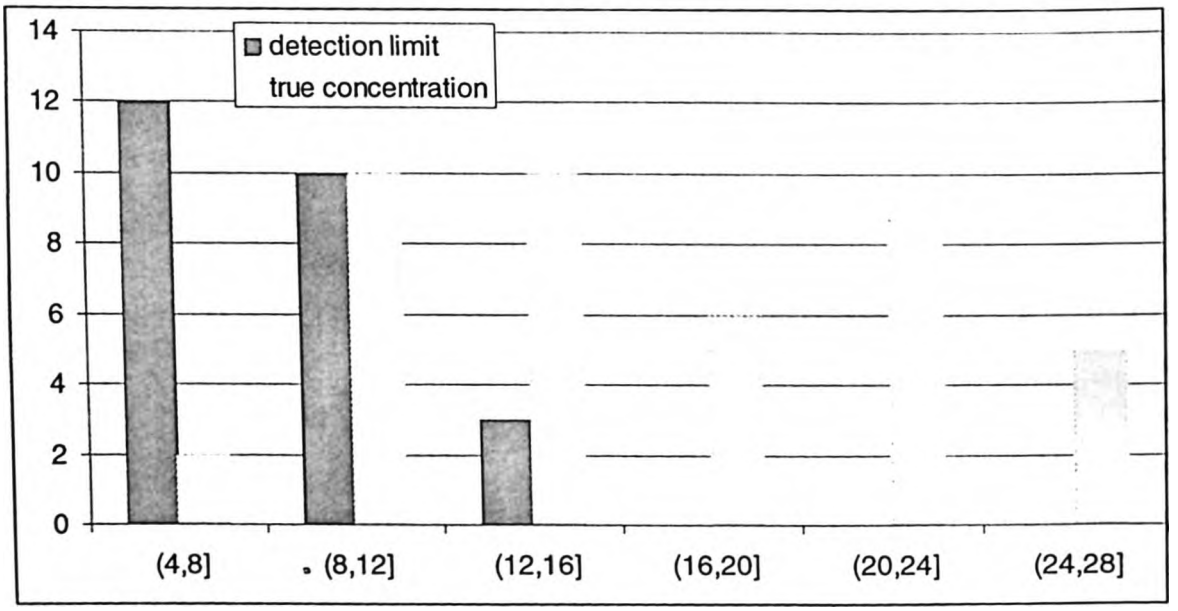

Figure 6-1 Histogram of bone lead concentrations for 67 people

The proportion of the people with bone lead concentration less than 28 ppm is 1. The proportion of the people with bone lead concentration less than 24 ppm is 1 minus the proportion of the people with bone lead concentration between 24 ppm and 28 ppm, which is 1 minus 5/67. The same calculations can be applied when there are no censored data present. For the concentrations between 12 ppm and 16 ppm, there are 10 exact concentrations and 3 detection limits, which means 10 people have concentrations between 12 ppm and 16 ppm, and 3 people have DL between 12 ppm and 16 ppm. In the left-censoring analysis, we assume these 3 people are on the left side of the range (12,16], i.e. these 3 people have bone lead concentration less than 12 ppm. So the proportion of the whole group of the people with bone lead concentration less than 12 ppm is the product of the proportion of the people who have concentration less than 16 ppm and the proportion of the rest of the people who have concentration less than 12 ppm, which is 47/67 times (1-10/47). This way, the censored data were counted. The probability distribution for one range can be subtracted from the proportions of two consecutive ranges, which is showed in Table 6-2. According to the above process, the cumulative distribution function F(x) for left-censored data by KM method can be written as

$$F_{KM}(x) = \prod_{x_i > x} [1 - d(x_i)/n(x_i)] \quad \text{..... (6.3)}$$

Here $d(x_i)$ denotes the number of measurements (events) with the result x_i, while $n(x_i)$ is the number of concentrations, which can be measured or censored for $x > x_i$.

Table 6-3 shows the mean and the standard error of mean (SEM) calculated from reduced samples method, inverse weighted method (IVW), and KM method.

Reduced sample		IVW		KM	
Mean	SEM	Mean	SEM	Mean	SEM
15.65	0.63	11.44	0.51	11.22	0.48

Table 6-3 Mean and SEM calculated from reduced sample, IVW, and KM method

6.2.3 NA method

The detail descriptions for NA method can be found in Aalen and Nelson's papers (Aalen. 1978, Nelson 1972). The idea also comes from the survival analysis. If at a point of time t_i, $d(t_i)$ lives out of a set of $n(t_i)$ lives die, then the hazard rate (or failure rate) at time t_i is $d(x_i)/n(x_i)$. Cumulatively sum these up from time zero to time t_i to get the cumulative hazard rate:

$$H(t) = \sum \frac{d(t_i)}{n(t_i)} \qquad (t>t_i) \ldots\ldots\ldots\ldots (6.4)$$

The survival function can be obtained by the exponential of the cumulative hazard rate:

$$S(t) = \exp[-\sum d(t_i)/n(t_i)] \ldots\ldots\ldots\ldots (6.5)$$

By adopting the above analysis, the cumulative distribution function F(x) by NA method is

$$F_{NA}(x) = \exp[-\sum d(x_i)/n(x_i)] \ldots\ldots\ldots\ldots (6.6)$$

Again, $d(x_i)$ is the number of measurements with the result x_i, while $n(x_i)$ is the number of concentrations that can be measured or censored for $x>x_i$. The number of measurements with the result x_i ($d(x_i)$) corresponding to the death number at time t_i ($d(t_i)$),

because for the measurements with result x_i, those measurements (or numbers) have gone, and not exist (died) anymore for the following regions.

6.2.4 RM method

The RM method was developed by Kubala-Kukuś et al. (Kubala-Kukuś et al. 2001). Denoting the measured concentration distribution of bone lead in a population of N samples by n(x) and the distribution of reported DLs by m(x), the original concentration distribution N(x) for the studied population can be deduced. The total numbers of measured concentrations and reported detection limits are

$$\begin{aligned} n &= \sum n(x_i) \\ m &= \sum m(x_i) \end{aligned} \quad \text{..... (6.7)}$$

The detection limits of the method for a given population of samples are characterized by some probability distribution P(x), and $\sum P(x_i) = 1$. The number of measured concentrations n(x) for a given concentration range x can be expressed as a product of original concentration distribution N(x)and the probability that the actual value of DL is smaller than x, namely

$$n(x) = N(x) \sum_{x<x_i} P(x_i) \text{ ..... (6.8)}$$

Similarly, the number of reported DLs m(x) for a given concentration range x can be expressed as a product of the probability P(x) and the number of samples in which the concentration is less than x, namely

$$m(x) = P(x) \sum_{x<x_i} N(x_i) \text{ ..... (6.9)}$$

By solving the equations (6.8) and (6.9), the original probability distribution can be expressed as

$$f(x)=\frac{N(x)}{N}=\frac{n(x)}{F(x)}\exp[-\sum_{x<x_i}\frac{n(x_i)}{F(x_i)}] \quad \text{..... (6.10)}$$

where $F(x)=\sum_{x<x_i}[n(x_i)+m(x_i)]$.

To make the formula consistent with those for the KM and NA methods, the formula can be rewritten as

$$f_{RM}(x)=\frac{d(x)}{n(x)}\exp\left(-\sum_{x<x_i}\frac{d(x_i)}{n(x_i)}\right) \quad \text{..... (6.11)}$$

Here $d(x_i)$ is the number of measurements with the concentration range x_i, while $n(x_i)$ is the number of concentrations that can be measured or censored for $x>x_i$.

6.2.5 Mean and uncertainty of the mean

Following the discussion above, the probability distribution function for left-censored bone lead concentration data can be obtained by KM, NA, or RM method. The mean and uncertainty of the mean for these data sets can then be calculated as

$$\begin{aligned} &< x >= \sum x_i f(x_i) \\ &\sigma^2 = \sum x_i^{\,2} f(x_i) - < x >^2 \quad \text{..... (6.12)} \\ &\sigma_{mean} = \frac{\sigma}{\sqrt{N-2}} \end{aligned}$$

where x_i is the average concentration of the ith range and $f(x_i)$ is the probability function for this range.

6.2.6 Log-normal distribution

The distribution of the trace element concentration in biomedical samples is asymmetric. This asymmetric distribution can be well described by a log-normal distribution. The probability distribution function for the log-normal distribution is

$$f(x) = \frac{1}{\sqrt{2\pi}\sigma x}\exp\left(-\frac{(\ln x - \mu)^2}{2\sigma^2}\right) \quad \text{..... (6.13)}$$

The mean, median, and variance of the concentrations for this group can be expressed as

$$\begin{aligned} &\text{mean} = \exp(\mu + \frac{1}{2}\sigma^2) \\ &\text{median} = \exp(\mu) \quad \text{..... (6.14)} \\ &\text{variance} = \exp(2\mu + \sigma^2)[\exp(\sigma^2 - 1) \end{aligned}$$

The window width for a log-normal distribution is

$$w_{opt} = 0.9An^{-\frac{1}{5}} \quad \text{..... (6.15)}$$

where A = min(standard deviation, interquartile range/1.34), and n is the sample number. The log-normal distribution fitting could be performed by using the data from the KM, NA, or RM method, but in this work, it was carried with Minitab statistical software for the simplicity of the analysis procedure. The lognormal distribution by using Minitab is fitted by a nonparametric Turnbull Method (Turnbull 1974, 1976).

6.3 Measurements and populations

KM, NA, RM method, and Minitab statistical software were used to investigate the mean, uncertainty of the mean, median, as well as the distribution properties of data

sets containing lead concentrations determined by ^{109}Cd γ-ray induced K XRF. Nine data sets were analyzed. Table 6-4 shows the characteristic of the populations.

Group	n	Measurement site	Exposure	Mean age (range)	Censored (%)
A. exposed men	101	tibia	Occupational	40.5 (24-97)	25
B. exposed women	108	tibia	Occupational	47.1 (31-82)	52
C. referent women	99	tibia	Environmental	46.9 (31-83)	87
D. exposed young men	134	tibia	Environmental	24.2 (19-29)	73
E. exposed young women	128	tibia	Environmental	24.7 (19-30)	75
F. referent young men	142	tibia	Environmental	24.5 (19-29)	96
G. referent young women	126	tibia	Environmental	23.9 (19-29)	91
H. exposed women	73	tibia	Occupational	46.4 (39-68)	40
I. exposed women	73	calcaneus	Occupational	46.4 (39-68)	29

Table 6-4 Characteristic of the populations

Group A and B consist of men and women, respectively, exposed to lead occupationally through working at a battery plant and primary lead smelter. Group C consists of women in the same age range as women in group B, who served as referents in the study conducted by the Agency of Toxic Substances and Disease Registry (ATSDR). Exposed young adult men (Group D) and women (Group E) were individuals who were exposed to high amounts of environmental lead in their childhood. They were from 9 months to 9 years of age in year 1974 and 1975, and at that time had lived in one

of five towns surrounding lead smelter in the Silver Valley, Idaho, USA. Groups F and G served as referents in the same age group, with no known exposure to lead. Bone lead concentrations in Group A were measured in 1998, and in 1994 in Groups B through G. A subset of women from Group B participated in a repeat study conducted in 2000, at which time concentrations of lead in both tibia (Group H) and calcaneus (Group I) bones were measured.

6.4 Results/discussion

The left-censoring analysis for the bone lead concentrations of these 9 groups were performed by using KM, NA, RM method, and Minitab statistical software. The data sets were grouped as measured concentrations and detection limits. As mentioned before, the data analysis of our lab can give an exact concentration and an uncertainty for the bone lead concentration for an individual. Since our uncertainty is around $\sqrt{2N_{bkg}}$, and DL is defined as around $3\sqrt{N_{bkg}}$, the concentrations less than 2*uncertainties will be grouped as a DL with a value of 2*uncertainty of the concentration. Table 6-5 shows the mean, error of the mean (EM) or standard error of the mean (SEM) determined by inverse variance weighted (IVW) averaging, KM, NA, RM, and Minitab statistic software.

	IVW Avg.		KM		NA		RM		Minitab	
	Mean	EM	Mean	SEM	Mean	SEM	Mean	SEM	Mean	SEM
A	22.30	0.42	23.70	1.95	22.93	1.97	23.33	2.10	24.40	2.31
B	14.36	0.50	14.94	1.69	14.60	1.69	14.22	1.70	15.96	1.56
C	3.22	0.50	5.32	0.37	5.20	0.37	5.09	0.37	5.62	0.96
D	0.026	0.313	3.37	0.19	3.37	0.16	3.36	0.19	3.35	0.74
E	1.63	0.43	4.76	0.31	4.74	0.31	4.72	0.31	4.90	0.75
F	4.54	0.31	6.07	0.55	6.03	0.55	5.98	0.55	6.53	0.65
G	5.61	0.43	7.04	0.58	6.97	0.58	6.83	0.58	7.94	0.68
H	14.58	0.48	13.75	1.40	13.27	1.41	12.67	1.43	15.27	1.43
I	24.45	0.78	26.49	2.45	25.43	2.49	24.07	2.55	28.86	2.79

Table 6-5 Mean, error of the mean (EM) or standard error of the mean (SEM) determined by inverse variance weighted (IVW) averaging, KM, NA, RM, and Minitab

If we only look at the absolute value, the means calculated from the conventional IVW method is smaller than those from the left-censoring methods, and the differences (compare to the uncertainties) are getting bigger as the censored proportion gets greater. This is because left-censoring methods counts the fact that the concentration has to be greater than 0, while the conventional method allows negative values. A more important purpose to calculate the means is to compare the bone lead concentration of two different groups to see what effect the bone lead concentrations. Table 6-6 shows the difference

between means of the given populations, expressed in number of uncertainties, as estimated by IVW and left-censoring methods.

Groups	IVW	KM	NA	RM	Minitab
B and C	15.75	5.56	5.43	5.25	5.64
D and F	10.20	4.64	4.64	4.50	3.23
E and G	6.54	3.47	3.39	3.21	3.00
D and E	3.02	3.82	3.93	3.74	1.47
F and G	2.02	1.21	1.18	1.06	1.50
B and H	0.317	0.542	0.604	0.698	0.326

Table 6-6 Difference between means of the given populations

Compare group B and C, both conventional IVW method and left-censoring methods show that B group has a significant higher mean bone lead concentration. This is a reasonable result because B group is an occupationally exposed group and C group is a control group. Compare group D and F, both conventional IVW method and left-censoring methods show that D group has a significant higher mean bone lead concentration. The D group is a group that was exposed to lead when they were children 20 years ago and F group is a group that has no lead exposure record. The result means lead exposure in childhood will affect the bone lead concentration in adulthood decades later. Both the conventional IVW method and left-censoring methods lead to the same conclusion. For group D and E, IVW and left censoring method show significant differences, but Minitab doesn't, which means Minitab may lead to incorrect conclusion

sometime. For group F and G, IVW method shows marginal significance, but the rest do not. So there is no definite conclusion for these two groups. For group B and H, none of these methods shows significant differences, when they probably shouldn't, because H is a repeated subset of B.

An advantage of the left-censoring method is that you can get the distribution function from the analysis. Figure 6-2 shows the histogram of bone lead concentrations for the referent young adult women (group G). Figure 6-3 shows the PDF as estimated by the four left-censoring methods for bone lead concentration measurements for the same group.

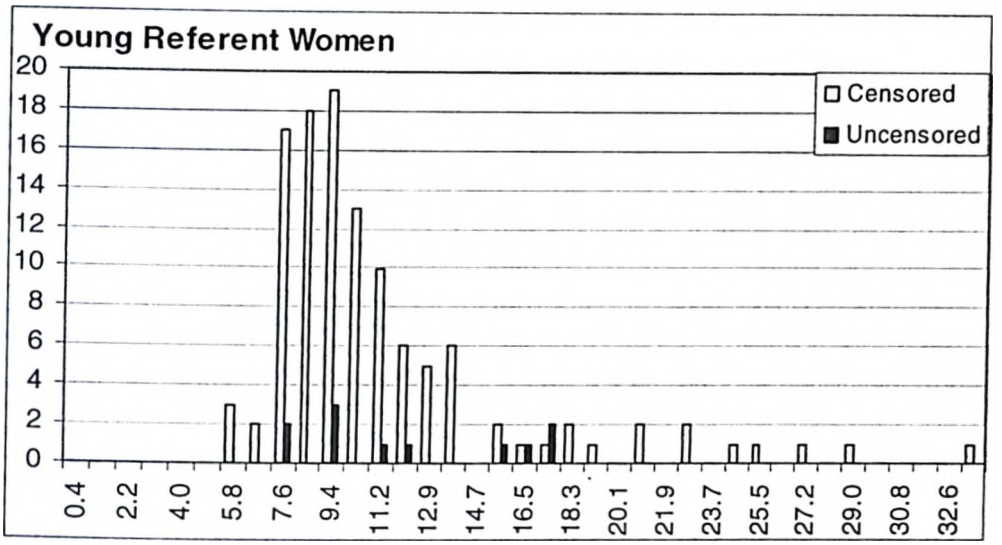

Figure 6-2 Histogram of bone lead concentrations for the referent young adult women

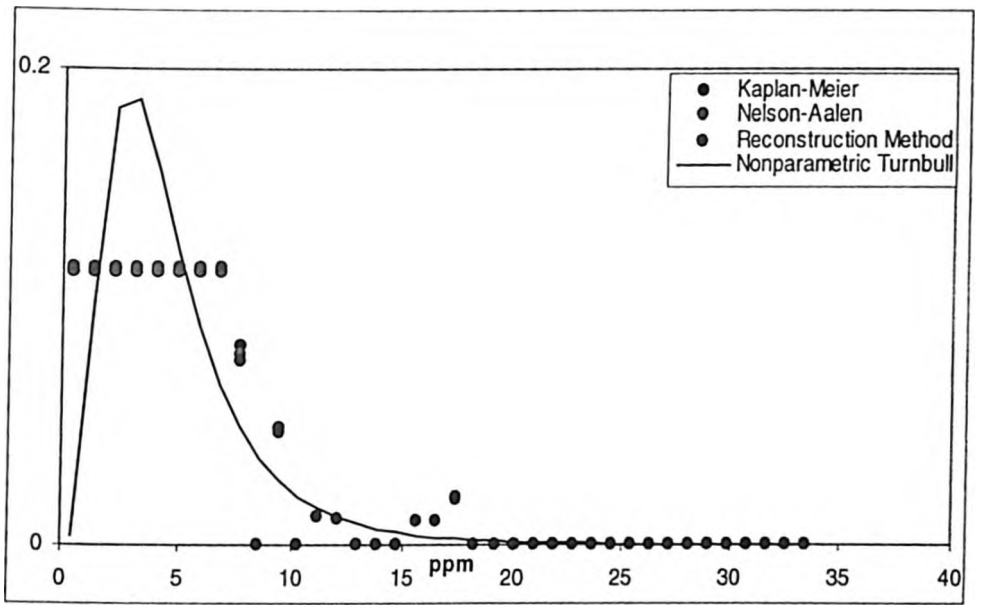

Figure 6-3 PDFs estimated by the four left-censoring methods for bone lead concentration measurements for the referent young adult women

6.5 Conclusion

In conclusion, left-censoring analysis has some advantages in analyzing the censored bone lead concentration data obtained by XRF measurement. For example, the absolute value of mean acquired from left-censoring analysis is closer to the true value compared to that acquired from the conventional IVW or RS analysis; left-censoring analysis provides a way to find the distribution of the data for a particular group. But if we are only concerned about the comparison between the means of two or more groups, then the conventional analysis is as valid as the left-censoring analysis. Furthermore, Minitab statistical software package is a very good and convenient tool to perform the left-censoring analysis.

References

Aalen OO, (1978) "Nonparametric inference for a family of counting process". *The annals of statistics* **6**: 701-726

Adachi JD, Arlen D, Webber CE, Chettle DR, Beaumont LF, Gordon CL, (1998) "Is there any association between the presence of bone disease and cumulative exposure to lead?" *Calcif Tissue Int* **63**: 429-432

Ahlgren L, Lidén K, Mattsson S, Tejning S, (1976) "X-ray fluorescence analysis of lead in human skeleton *in vivo*". *Scand J Work Environ Health* **2**:82-86

Ahlgren L, Haeger-Aronsen B, Mattsson S, and Schütz A, (1980) "*In vivo* determination of lead in the skeleton after occupational exposure to lead". *Br. J. Ind. Med.* **37**: 109-113

Alomran AH, Shleamoon MN. (1988) "The influence of chronic lead exposure on lymphocyte proliferative response and immunoglobulin levels in storage battery workers". *Journal of Biological Science Research* **19**:575-585

Annest JL, Pirkle JL, Makuc D, Neese JW, Bayse DD, Kovar MG, (1983) "Chronological trend in blood lead levels between 1976 and 1980". *N. Engl. J. Med* **308**:1373-1377

Ao Q, Lee SH, Gardner RP, (1997) "Optimization of *in vivo* x-ray fluorescence analysis methods for bone lead by simulation with the Monte Carlo code CEARXRF". *Appl Radiat Isot* **48**:1413-1423

Bert JL, Dusen V, Grace JR, (1989) "A generalized model for the prediction of lead body burdens". *Environ. Res.* **48**:117-127

Bevington PR, (1969) "Data reduction and error analysis for the physical sciences". McGraw-Hill, Inc.

Bleeker ML, McNeill FE, Lindgren KN, Masten VL, Ford DP, (1995) "Relationship between bone lead and other indices of lead exposure in smelter workers". *Toxicol Lett.* **77**:241-248

Brito JA, McNeill FE, Stronach I, Webber CE, Wells S, Richard N, Chettle DR, (2001) "Longitudinal changes in bone lead concentration: implications for modeling of human bone lead metabolism". *J Environ Monit* **3**: 343-351

Brito JA, McNeill FE, Webber CE, Wells S, Richard N, Carvalho ML, Chettle DR, (2002) "Evaluation of a novel structural model to describe the endogenous release of lead from bone". *J Environ Monit.* **4**: 194-201

Brody DJ, Pirkle JL, Kramer RA, Flegal KM, Matte TD, Gunter EW, Paschal DC, (1994) "Blood lead levels in the U.S. population from phase 1 of the Third National Health and Nutrition Examination Surveys". *JAMA* **272**:277-283

Chettle DR, Scott MC, Somervaille LJ, (1991) "Lead in bone: Sampling and quantitation using K x-rays excited by ^{109}Cd". *Environ Health Perspect* **91**:49-55

Cristy M, (1981) "Active bone marrow distribution as a function of age in humans". *Phys. Med. Biol* **3**: 389-400

EPA (1986) "Air quality criteria for lead". Research Triangle Park, NC: U.S. Environmental Protection Agency, Office of Research and Development, Office of Health and Environment Assessment, Environmental Criteria and Assessment Office. EPA 600/8-83-028F

Erkkilä J, Armstrong R, Riihimäki V, Chettle DR, Paakkari A, Scott M, Somervaille L, Starck J, Kock B, Aitio A, (1992) "*In vivo* measurements of lead in bone at four anatomical sites: long term occupational and consequent endogenous exposure". *Br J Ind Med* **49**: 631-644

Ewers U, Stiller-winkler R, Idel H. (1982) "Serum immunoglobulin, complement C3, and salivary IgA level in lead workers", *Environ Res* **29**:31-357

Fischbein A, Tsang P, Luo JC, Roboz JP, Jiang JD, Bekesi JG, (1993) "Phenotypic aberrations of CD3+ and CD4+ cells and functional impairments of lymphocytes at low-level occupational exposure to lead". *Clin Immunol Immunopathol* **66**:163-168

Fleming DEB, Boulay D, Richard NS, Robin JP, Gordon CL, Webber CE, Chettle DR, (1997) "Accumulated body burden and endogenous release of lead in employees of a lead smelter" *Environ Health Perspect* **105**: 224-233

Fleming DE, Chettle DR, Webber CE, O'Flaherty EJ, (1999) "The O'Flaherty model of lead kinetics: an evaluation using data from a lead smelter population". *Toxicol Appl Pharmacol* **161**:100-9

Frost HM, (1969) "Tetracycline-based histological analysis of bone remodeling". *Calc. Tiss. Res.* **3**:211-237

Gerhardsson L, Attewell R, Chettle DR, Englyst V, Lundström NG, Nordberg GF, Nyhlin H, Scott MC, Todd AC, (1993) "*In vivo* measurements of lead in bone in long-term exposed lead smelter workers". *Arch Environ Health* **48**: 147-156

Gonzalez-Riola J, Hernandez ER, Escribano A, Revilla M, Ca-Seco, Villa LF, Rico H, (1997) "Effect of lead on bone and cartilage in sexually mature rats: a morphometric and histomorphometry study". *Environ Res* **74**:91-93

Gordon CL, Chettle DR, Webber CE, (1993) "An improved instrument for the *in vivo* detection of lead in bone". *British Journal of Industrial Medicine* **50**:637-641

Goyer R, (1993) "Lead toxicity: Current concerns". *Environ Health Perspect* **100**:177-187

Gruber HE, Gonick HC, Khalil-manesh F, Sanchez TV, Motsinger S, Meyer M, Sharp CF, (1997) "Osteopenia induced by long-term, low- and high-level exposure of the adult rat to lead". *Miner Electrolyte Metab* **23**:65-73

Guo W, Gardner RP, Metwally WA, (2004) "Preliminary studies on K and L coincidence spectroscopy for optimizing the *in vivo* XRF measurement of lead in bone". *Nuclear Instruments and Methods in Physics Research* **213B**:574-578

Hu H, Aro A, Rotnitzky A, (1995) "Bone lead measured by x-ray fluorescence: epidemiologic methods". *Environ Health Perspect* **103**(suppl 1):105-110

Hu H, Hashimoto D, Besser M, (1996) "Levels of lead in blood and bone of women giving birth in a Boston hospital". *Arch Environ Health* **51**:52-58

ICRU, http://physics.nist.gov/PhysRefData/XrayMassCoef/tab4.html

José Brito. (2000) "Fluorescência de Raios X in vivo aplicada ao estudo da concentração de chumbo ósseo – contributo para modelos da toxicocinética do chumbo", thesis for PhD program, Faculdade de ciências da Universidande de Lisboa

Knoll G F, (1999) "Radiation Detection and Measurement", Third Edition, John Wiley and Sons, Inc.

Kubala-kukuś A, Banas D, Braziewicz J, Majewska U, Mrowczynski S, Pajek M, (2001) "Influence of detection limit on the measured concentration distribution of trace elements". *X-ray Spectrometry* **30**: 348-352

Kubala-kukuś A, Pajek M, (2002) "Simulations of censoring effects in XRF analysis". Poster for 5th IRRMA, Bologna, Italy

Laird EE, Chettle DR, Scott MC, (1982) "The factors effecting in vivo x-ray fluorescence of lead in bone". *Nuclear Instruments and Methods* **193**:377-382

Lederer CM, Shirley VS, eds.; Browne E, Doebler RE, Dairiki JM, Shihab-Eldin A, Jardine LJ, Tuli JK, Buyrn AB, (1978) "Tables of Isotopes", 7th edition, New York: Wiley

Lee SH, Gardner RP, Todd AC, (2001) "Preliminary studies on combining the K and L XRF methods for *in vivo* bone lead measurement". *Appl Radiat Isot* **54**:893-904

Leggett RW, (1993a) "An age-specific kinetic model of lead metabolism in humans". *Environ. Health. Perspect* **101**:598-616

Leggett RW, Eckerman KF, Williams LR, (1993b) "An elementary method for implementing complex biokinetic models". *Health Physics* **64**:260-271

Miller R G, Jr, (1981) "Survival analysis". John Wiley & Sons

Minitab statistic software, (2000) Release 13 for Windows, Minitab Inc.

Needleman HL, (1993) "The current Status of childhood low-level lead toxicity". *Neurotoxicology* **14**: 161-166

Nelson W, (1972) "Theory and applications for hazard plotting for censored failure data". *Technometrics* **14**: 945-965

Nie H, (2001) "The improvement of *in vivo* XRF lead measurement system". Thesis for M.Sc., Medical Physics, McMaster University

NIST: http://physics.nist.gov/PhysRefData/XrayMassCoef/tab4.html

O'Flaherty EJ, (1993) "Physiologically based models for bone-seeking elements. IV. Kinetics of lead disposition in humans". *Toxicol. Appl. Pharmacol* **118**:16-29

O'Flaherty EJ, (1995). "Physiologically based models for bone seeking elements. V. Lead absorption and disposition in childhood". *Toxicol. Appl. Pharmacol* **131**:297-308

O'Meara JM, (1999) "Measuring lead, mercury, and uranium by *in vivo* x-ray fluorescence", dissertation for PhD degree, McMaster University

Pajek M, Kubala-kukuś A, Banaś D, Braxiewicz J, Majewska U, (2002) "Random left-censoring: a statistical approach accounting for detection limits in x-ray fluorescence analysis". Poster for 5th International Topical Meeting on Industrial Radiation and Radioisotope Measurement Applications (IRRMA), Bologna, Italy

Perazella MA, (1996) "Lead and the kidney: nephropathy, hypertension, and gout". *Conn. Med* **60**: 521-526

Pirkle JL, Brody DJ, Gunter EW, Kramer RA, Paschal DC,Flegal KM, Matte TD, (1994) "The decline in blood lead levels in the United States: the National Health and Nutrition Examination Surveys". *JAMA* **272**:284-291

Pounds JG, Long GJ, Rosen JF, (1991) "Cellular and molecular toxicity of lead in bone". *Environ Health Perspect* **91**:17-32

Pounds JG, Leggett RW. (1998) "The ICRP age-specific biokinetic model for lead: validations, empirical comparisons, and explorations". *Environ Health Perspect* **106**:1505-1511

Puzas JE, Sickel MJ, Felter ME, (1992) "Osteoblasts and chondrocytes are important target cells for the toxic effects of lead". *Neurotoxicology* **13**:783-788

Schonfeld DJ, (1993) "New developments in pediatric lead poisoning". *Curr Opin Pediatr* **5**: 537-544

Rabinowitz MB, Wetherill GW, Koppel JD, (1976) "Kinetic analysis of lead metabolism in health humans". *J. Clin. Invest.* **58**:260-270

Research Triangle Institute, United States, Agency for Toxic Substances and Disease Rigistry, (1999) "Toxicological Profile for Lead", U.S. Dept. of Health and Human Services, Public Health Service, Agency for Toxic Substances and Disease Rigistry

Shimizu A, Onda T, Sakamoto Y, (2004) "Calculation of gamma-ray buildup factors up to depths of 100mfp by the method of invariant embedding (III), generation of an improved data set". *Journal of Nuclear Science and Technology* **41**: 413-424

Somervaille LJ, Laird EE, Chettle DR, Scott MC, (1983) "Lead body stores assessed *in vivo* by x-ray fluorescence". *International Conference on Heavy Metals in the Environment* **1**: CEP Consultants, Edinburgh, pp.521-524

Somervaille LJ, Chettle DR, Scott MC, (1985) "*In vivo* measurement of lead in bone using x-ray fluorescence". *Phys. Med. Biol* **30**:929-943

Somervaille LJ, Nilsson U, Chettle DR, Tell I, Scott MC, Schütz A, Mattsson S, and Skerfving S, (1989) "*In vivo* measurements of bone lead – a comparison of two x-ray fluorescence techniques used at three different bone sites". *Phys. Med. Biol* **34**: 1833-1845

Stern AH, (1994) "Derivation of lead in soil at residential sites corresponding to a de minimis contribution to blood lead concentration". *Risk Analysis* **14**:1049-1056

Stern AH, (1996) "Derivation of a target concentration of Pb in soil based on elevation of adult blood pressure". *Risk Analysis* **16**:201-210

The Royal Society of Canada. (1986) "Lead in the Canadian environment: science and regulation"

Todd AC, Chettle DR, Scott MC, and Somervaille LJ, (1991) "Monte Carlo modeling of *in vivo* x-ray fluorescence of lead in the kidney". *Phys. Med. Biol* **36**:439-448

Todd AC, McNeill FE, Palethorpe JE, Peach DE, Chettle DR, Tobin MJ, Strosko SJ, and Rosen JC, (1992) "*In vivo* x-ray fluorescence of lead in bone using K x-ray excitation with ^{109}Cd sources: radiation dosimetry studies". *Environmental Research* **57**: 117-132

Todd AC, (2002a) "L-shell x-ray fluorescence measurements of lead in bone: system development". *Phys Med Biol* **47**:507-522

Todd AC, (2002b) "L-shell x-ray fluorescence measurements of lead in bone: theoretical consideration". *Phys Med Biol* **47**:491-505

Todd AC, Carroll S, Geraghty C, Khan FA, Moshier EL, Tang S, Parsons PJ, (2002c) "L-shell x-ray fluorescence measurements of lead in bone: accuracy and precision". *Phys Med Biol* **47**:1399-1419

Turnbull BW, (1974) "Nonparametric estimation of a survivorship function with doubly censored data". *Journal of the American Statistical Association* **69**: 169-173.

Turnbull BW, (1976) "The empirical distribution function with arbitrarily grouped, censored and truncated data". *Journal of the Royal Statistical Society* **38**: 290-295.

Turner JE, (1995) "Atoms, Radiation, and Radiation Protection", 2nd edition, John Wiley and sons

U.S. Department of Commerce, (1969) "Photon cross sections, attenuation coefficients, and energy absorption coefficients from 10 keV to 100 GeV".

Victery W. (1988) "Evidence for effects of chronic lead exposure on blood pressure in experimental animals: An overview". *Environ Health Perspect* **78**: 71-76

Wielopolski L, Slatkin DN, Vartsky D, Ellis KJ, Cohn SH, (1981) "Feasibility study for the *in vivo* measurement of lead in bone using L-x-ray fluorescence". *IEEE Trans Nuclear Science* **NS-28**:114-116

Wielopolski L, Rosen JF, Slatkin DN, Vartsky D, Ellis KJ, Cohn SH, (1983) "Feasibility of noninvasive analysis of lead in the human tibia by soft x-ray fluorescence". *Med Phys* **10**:248-251

Wielopolski L, Ellis KJ, Vaswani AN, Cohn SH, Greeberg A, Puschett JB, Parkinson DK, Fetterolf DE, Landrigan PJ, (1986) "*In vivo* bone lead measurements: a rapid monitoring method for cumulative lead exposure". *Am J Ind Med* **9**:221-226

Wielopolski L, Slatkin DN, Kalef-ezra JA, Rosen JF, (1987) "Non-invasive detection of tibial bone lead in intact legs by L x-ray fluorescence". *The Toxicologist Abstract*, pp.77

Wieloposki L, Rosen JF, Slatkin DN, Zhang R, Kalef-ezra JA, Rothman JC, Maryanski M, Jenks ST, (1989) "*In vivo* measurement of cortical bone using polarized radiation". *Med Phys* **16**:521-528

Wilhelm M, Lombeck I, Hafner D, Ohnesorge FK, (1989) "Hair lead levels in young children from the F.R.G". *Journal of Trace Elements and Electrolytes in Health and Disease* **3**:165-170

Appendices: Introduction/Comments/Description

Part of the work described in the attached paper in Appendix I "An investigation of ^{109}Cd γ-ray induced K-x-ray fluorescence bone-lead measurement calibration procedure" was performed in the PhD program period, but was not included in the thesis. For those who are interested in that work, please refer to the paper and my Master's thesis.

The work described in Chapter 6 is a joint work collaborated with my colleague Marija Popovic. For some aspects of the work you may obtain a better idea by referring to our joint paper "Left-censoring: A Statistical Approach for XRF Bone Lead Data Analysis" listed in Appendix I.

Appendix IV described a collaborative work with Dr. R. B. Richardson (richardr@aecl.ca) in Radiation Biology and Health Physics Branch, Atomic Energy of Canada Limited, Chalk River Laboratories. This work calculates the dose absorption fraction for C-14 and Tritium in trabecular bone by Monte Carlo (MC) simulation and it is important to the application of a physiological bone compartmental model that Dr. Richardson has been developing.

Appendix I Papers

The attached are two papers that have been published during the period of my PhD program. Most of the work in these two papers was performed during my Master's program, and some of the complementary work was continued during my PhD program.

The titles of the attached papers, and the other papers that are published, submitted and/or in preparation are also listed below.

Nie HL, Chettle DR, McNeill FE, O'Meara JM, An Investigation of ^{109}Cd Induced K-XRF Lead Measurement Calibration, *Physics in Medicine and Biology* **49** (2004) N325

Nie HL, Chettle DR, Stronach IM, Arnold ML, Huang SB, McNeill FE, O'Meara J, A Study of MDL Improvement for the *in vivo* Measurement of Lead in Bone, *Nuclear Instruments and Methods in Physics Research* **B 213**(2004)579

Todd AC, Arnold ML, Aro ACA, Chettle DR, Fleming DEB, McNeill FE, Moshier EL, **Nie HL**, Stronach IM, corrections to "How to Calculate Lead Concentration and Concentration Uncertainty in XRF *in vivo* Bone Lead Analysis" by Kondrashov and Rothenberg, *Applied Radiation and Isotopes*, **58**(2003)41

Chettle DR, Arnold ML, Aro ACA, Fleming DEB, Kondrashov VS, McNiell FE, Moshier EL, **Nie HL**, Rothenberg SJ, Stronach IM, Todd AC, An Agreed Statement on Calculating Lead Concentration and Uncertainty in XRF *in vivo* Bone Lead Analysis, *Applied Radiation and Isotopes* **58**(2003)603

Nie HL, Chettle DR, Webber CE, Brito JAA, O'Meara JM, McNeill FE, X-ray Fluorescence Data in the Study of Human Bone Lead Metabolism, *Journal of environmental monitoring*, submitted

Popovic M, **Nie HL**, Chettle DR, McNeill FE, Kaye WE, Lee V, Stokes L, Left-censoring: A Statistical Approach for XRF Bone Lead Data Analysis, *Journal of environmental monitoring*, submitted

Nie HL, Chettle DR, Luo LQ, Dosimetry Study for a New *in vivo* Bone Lead Measurement System, *Health Physics*, in preparation

Luo LQ, Chettle DR, **Nie HL**, McNeill FE, Popvic M, Relationship of Compton Scatter and Pb K-series Peaks with Different Filters and Collimators in an in vivo Analytical System, in preparation

Luo LQ, Chettle DR, **Nie HL**, McNeill FE, Popovic M, Curve Fitting Using a Genetic Algorithm for the X-ray Fluorescence Measurement of Lead in Bone, submitted

Nie HL, Chettle DR, Luo LQ, O'Meara JM, *In vivo* Investigation by Using a New Bone Lead Measurement System, in preparation

Available online at www.sciencedirect.com
SCIENCE DIRECT®
ELSEVIER
Nuclear Instruments and Methods in Physics Research B 213 (2004) 579–583
NIM B
Beam Interactions with Materials & Atoms
www.elsevier.com/locate/nimb

A study of MDL improvement for the in vivo measurement of lead in bone

Huiling Nie [a,*], David Chettle [a], Ian Stronach [b], Michelle Arnold [c], Shibin Huang [d], Fiona McNeill [a], Joanne O'Meara [e]

[a] *Medical Physics and Applied Radiation Sciences Unit, McMaster University, Hamilton, ON, Canada L8S 4K1*
[b] *Department of Medical Physics, The Queen Elizabeth Hospital, UK*
[c] *Department of Physics, Weber State University, USA*
[d] *School of Medicine, Fudan University, China*
[e] *Department of Physics, Guelph University, Canada*

Abstract

^{109}Cd induced K XRF has been used for in vivo lead measurement for about two decades. Recently, the need for improvement of this system has been emphasized due to an increased understanding of low-level lead exposure. The conventional XRF bone-lead measurement system includes a 25 mm radius HPGe detector and one set of electronics. In this work, a cloverleaf detector system is investigated. This system consists of four 8 mm radius detectors and four sets of electronics. We measured bare plaster of Paris phantoms and phantoms in a soft tissue equivalent leg phantom to represent in vivo measurement. A Monte Carlo simulation for XRF measurement was also used to simulate this system. We compared both the experimental results and the simulation and found that the minimum detectable limit (MDL) is greatly improved by using the cloverleaf system and a stronger source. The effect of geometry is also discussed. An overall MDL ratio of about 0.3 (experimental value 0.278 ± 0.016 and simulation value 0.273) is obtained by using the cloverleaf system compared to the conventional system for in vivo measurement, which means a decrease of MDL from about 6–10 to about 2–3 μg/(g bone mineral).

PACS: 78.70.En
Keywords: MDL; Lead measurement; Cloverleaf system

1. Introduction

The first in vivo measurement of bone lead in human body by using XRF was reported in 1976 by Ahlgren et al. [1], where gamma rays from ^{57}Co were used to excite the K series X-rays of lead in finger bone with a 90° geometry. After that, a number of XRF systems have been designed and constructed for the in vivo measurement of lead concentrations in bone. According to Todd and Chettle's review in 1994, the majority of these studies adopted the ^{109}Cd K XRF method because of its several advantages: a robust measurement, a lower detection limit, and a lower effective radiation dose [2].

* Corresponding author.
E-mail address: nieh@mcmaster.ca (H. Nie).

0168-583X/$ - see front matter © 2003 Elsevier B.V. All rights reserved.
doi:10.1016/S0168-583X(03)01675-6

Although the ^{109}Cd K XRF method has been considered as an effective method, the capacity of this system is not good enough to satisfy the low-level lead concentration investigations. Generally, the average bone-lead concentration for the non-occupationally exposed adults is about 10–20 μg Pb/(g bone mineral) and the value maybe lower for children, while the minimum detectable limit (MDL) for a standard system (the optimal set-up for our conventional ^{109}Cd K XRF bone-lead measurement system) is about 6–10 μg Pb/(g bone mineral). So the bone-lead concentration for general population is comparable with the MDL, which means we would get a poor result for bone-lead measurements for the general population. Since the hazardous effects at low levels of lead for the general population especially for children have been increasingly of concern, the improvement of MDL and hence the improvement of this system is becoming an important aspect for bone-lead measurement.

In this work, both Monte Carlo simulations and practical experiments are used to investigate a cloverleaf system, which consists of four 8 mm detectors instead of the conventional one 25 mm detector. The advantage of small detector is that it has a better resolution and each of the four smaller detectors can process the same number of counts per unit time as the larger detector. This leads to a much better MDL by using a stronger source.

2. Experimental method and data analysis

2.1. Standard system

The standard system consists of a 25 mm radius HPGe detector (the resolution is about 750 eV for 88.035 keV peak), a preamplifier, a main amplifier, an analog-to-digital converter and a PC based multi-channel analyzer system.

2.2. Cloverleaf system

The cloverleaf system has the same electronic constituents as the standard system and the only difference is that its detector system consists of four 8 mm radius small detectors and therefore four sets of the same electronic systems are needed. In this work, experiments were based on a single 8 mm detector and assumed symmetry for the four detector elements in the cloverleaf system.

2.3. Geometry

For convenience of comparison, another set of arrangements has been used. It is similar to the standard system except that it has different geometries. For the standard system, the source-sample distance is fixed at 24 mm and gives rise to a detector-sample distance of 38 mm. The source-sample distance as well as the source detector distance were changed to compare the results for different geometries.

2.4. Samples

Two sets of samples have been used in this work. One is the bare phantom which is made of plaster of Paris. The other is the plaster of Paris phantom in soft tissue leg phantom which is used to simulate in vivo measurement. The latter is illustrated in Fig. 1.

2.5. Monte Carlo simulation

A Monte Carlo program was used to simulate the measurement of these two sets of phantoms. This program was developed by O'Meara and Stronach and it has been used in several previous studies [3–5].

2.6. Data analysis

2.6.1. MDL calculations for experiments

A non-linear least square fitting program was used to get the lead concentration and its uncertainty by alpha-fitting (the fitting for the $K_{\alpha 1}$ and $K_{\alpha 2}$ peaks) and beta-fitting (the fitting for the $K_{\beta 1}$

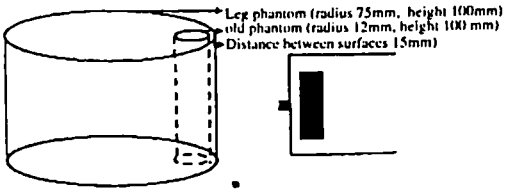

Fig. 1. Phantom in leg phantom measurement.

and $K_{\beta 3}$ peaks). The MDL of the lead concentration using alpha-fitting and beta-fitting was calculated by the following formula:

$$(\mathrm{MDL})_{\mathrm{alpha}} = 2 \times (\mathrm{uncertainty})_{\mathrm{alpha}}, \quad (1)$$

$$(\mathrm{MDL})_{\mathrm{beta}} = 2 \times (\mathrm{uncertainty})_{\mathrm{beta}}, \quad (2)$$

and the weighted MDL can be estimated as [6]

$$(\mathrm{MDL})_{\mathrm{weighted}} = [(\mathrm{MDL}_{\mathrm{alpha}})^{-2} + (\mathrm{MDL}_{\mathrm{beta}})^{-2}]^{-1/2}. \quad (3)$$

2.6.2. MDL calculations for Monte Carlo simulations

The formula for the MDL calculation for MC simulation is

$$\mathrm{MDL} = 2 \times C \times \frac{N_{x0}}{N_{\mathrm{coh}}} \times \sqrt{\frac{1}{N_{x0}} + \frac{1}{N_{\mathrm{coh}}}}, \quad (4)$$

where N_{x0} is the count at the X-ray energy for 0 ppm lead concentration, N_{coh} is the count in coherent peak and C (micro g Pb/g bone mineral) is calibration factor. C is derived from the N_x/N_{coh} versus phantom Pb concentration in μg Pb/(g bone mineral).

3. Results and discussion

Bare phantom and phantom in leg phantom were measured as well as simulated by Monte Carlo simulation in three sets of data – standard system, cloverleaf system and varied geometry. The different geometries are

DSD (detector-sample distance): 30, 25, 22 and 20 mm.
SSD (source-sample distance): 14, 9, 6 and 4 mm.

Tables 1 and 2 list the MDLs and MDL ratios for all the systems derived from experimental data (Table 1 is for bare phantom and Table 2 is for phantom in leg phantom). "Geo" ratio is the MDL ratio between the single detector in a particular geometry and standard system. "Overall" is the overall ratio between cloverleaf system in a particular geometry and standard system.

Tables 3 and 4 list the MDLs and MDL ratios for all the systems by Monte Carlo simulations (Table 3 is for bare phantom and Table 4 is for bone in soft tissue).

Table 1
Experimental results for bare phantom

Geometry	MDLs		Ratio (clove/geo)	MDLstan	Geo ratio MDLgeo/MDLsta	Overall ratio * geo
	$(\mathrm{MDL})_{\mathrm{clover}}$	$(\mathrm{MDL})_{\mathrm{geometry}}$				
30,14	0.896 ± 0.168	2.112 ± 0.308	0.423 ± 0.017	2.319 ± 0.428	0.915 ± 0.046	0.387 ± 0.011
25,9	0.821 ± 0.169	1.949 ± 0.320	0.420 ± 0.017		0.842 ± 0.018	0.353 ± 0.008
22,6	0.796 ± 0.145	1.903 ± 0.265	0.417 ± 0.017		0.825 ± 0.036	0.343 ± 0.004
20,4	0.778 ± 0.145	1.893 ± 0.252	0.409 ± 0.023		0.821 ± 0.042	0.336 ± 0.004

Note: Each experiment was done with three phantoms which have different lead concentrations. The listed values are the average values and the uncertainties are standard deviations for three sets of data.

Table 2
Experimental results for phantom in leg phantom

Geometry	MDLs		Ratio (clove/geo)	MDLstan	Geo ratio MDLgeo/MDLsta	Overall ratio * geo
	$(\mathrm{MDL})_{\mathrm{clover}}$	$(\mathrm{MDL})_{\mathrm{geometry}}$				
30,14	2.149 ± 0.321	4.701 ± 0.633	0.457 ± 0.009	5.898 ± 0.754	0.797 ± 0.038	0.364 ± 0.016
25,9	1.850 ± 0.375	4.089 ± 0.729	0.451 ± 0.010		0.691 ± 0.033	0.312 ± 0.022
22,6	1.657 ± 0.226	3.933 ± 0.219	0.421 ± 0.043		0.671 ± 0.047	0.281 ± 0.020
20,4	1.640 ± 0.224	3.870 ± 0.431	0.423 ± 0.015		0.658 ± 0.049	0.278 ± 0.016

Table 3
Monte Carlo simulation results for bare bone

Geometry	MDLs		Ratio (clove/geo)	MDLstan	Geo ratio MDLgeo/MDLsta	Overall ratio * geo
	$(MDL)_{clover}$	$(MDL)_{geometry}$				
30,14	1.879	4.042	0.465	4.698	0.860	0.400
25,9	1.704	3.779	0.451		0.804	0.363
22,6	1.627	3.702	0.439		0.788	0.346
20,4	1.599	3.714	0.431		0.791	0.340

Table 4
Monte Carlo simulation results for bone in soft tissue

Geometry	MDLs		Ratio (clove/geo)	MDLstan	Geo ratio MDLgeo/MDLsta	Overall ratio * geo
	$(MDL)_{clover}$	$(MDL)_{geometry}$				
30,14	3.276	7.019	0.467	9.087	0.773	0.361
25,9	2.781	6.162	0.451		0.679	0.306
22,6	2.559	5.950	0.430		0.655	0.282
20,4	2.482	6.184	0.401		0.681	0.273

3.1. Discussion

By comparing the different geometries with the standard system, we can see the biggest geometrical improvement occurred at geometry (20,4). The values are 0.821 for bare phantom and 0.658 for the old phantom in leg phantom. So, for the bare phantom measurement and the in vivo measurement, which is simulated by the old phantom in leg phantom, we can improve the MDL by a factor of 0.821 and 0.658 only by changing the geometry of the system without changing the source strength. The geometrical factor affects the in vivo measurement more than that it affects the bare phantom measurement. This is because the in vivo measurement at a further distance gives rise to a bigger background count from Compton scattering under the X-ray energy (relative to the signal count).

We can estimate the improvement by a simple deduction. We know that MDL $\propto 1/\sqrt{\text{coherent count}}$. For the cloverleaf system, we have four detectors and four electronics, which means four times coherent count compared to the conventional system (with only one detector) can be produced. So this can give rise to an MDL improvement by a factor of 0.5. Moreover, the smaller detector has a better resolution. Since MDL $\propto \sqrt{\text{background}} \propto \sqrt{\text{resolution}}$ and the resolutions for the 8 mm radius detector and the 25 mm radius detector are 550 and 750, respectively. Combining these two factors, an improvement factor of $0.5 \times \sqrt{550}/\sqrt{750} = 0.428$ can be obtained, which is very similar to that we got from the simulations and measurements without considering the geometry factor ("Ratio (clove/geo)").

4. Conclusion

The improvement of the MDL of the in vivo lead measurement system was investigated by both Monte Carlo simulation and measurement. For the current source, the MDL of the in vivo measurement would be improved by a factor of 0.658 ± 0.049 compare to the standard system only by changing its geometry. The corresponding Monte Carlo simulation value is 0.681, which is close to the measurement value. If we use a cloverleaf system instead of the conventional system, and at the same time change the geometry to an optimal state, the value would be 0.278 ± 0.016 for the measurement and 0.273 for the Monte Carlo simulation, which is dramatic.

References

[1] L. Ahlgren, K. Lidén, S. Mattson, S. Tejning, Scand. J. Work Environ. Health 2 (1976) 82.
[2] A.C. Todd, D.R. Chettle, Environ. Health Perspect. 102 (1994) 172, Review.

[3] J.M. O'Meara, D.R. Chettle, F.E. McNeill, W.V. Prestwich, C.E. Sevensson, Phys. Med. Biol. 43 (1998) 1413.
[4] J.M. O'Meara, J. Borjesson, D.R. Chettle, Appl. Radiat. Isot. 53 (2000) 639.
[5] I.M. Stronach, F.E. McNeill, D.R. Chettle, J.M. O'Meara, Physics in Canada (May/June) (2000) 62.
[6] P.R. Bevington, Data Reduction and Error Analysis for the Physical Sciences, McGraw-Hill, New York, 1969.

INSTITUTE OF PHYSICS PUBLISHING PHYSICS IN MEDICINE AND BIOLOGY

Phys. Med. Biol. 49 (2004) N325–N334 PII: S0031-9155(04)82179-1

NOTE

An investigation of the ^{109}Cd γ-ray induced K-x-ray fluorescence (XRF) bone-lead measurement calibration procedure

Huiling Nie[1], David R Chettle[1], Fiona E McNeill[1] and Joanne M O'Meara[2]

[1] Medical Physics and Applied Radiation Sciences Unit, McMaster University, Hamilton, ON, L8S 4K1, Canada

[2] Department of Physics, University of Guelph, Guelph, ON, N1G 2W1, Canada

Received 16 June 2004
Published 10 September 2004
Online at stacks.iop.org/PMB/49/N325
doi:10.1088/0031-9155/49/19/N02

Abstract

Two sets of phantoms have been used to calibrate a ^{109}Cd γ-ray induced K-XRF bone-lead measurement system. Both sets of phantoms are made of plaster of Paris, but the calibration lines are significantly different. This results in a significant difference for the derived concentrations of bone lead for the same person using these two sets of phantoms. This study shows that the different calibration lines are due to the different compositions of the phantoms, which can then be accounted for by adjusting the parameters related to the phantom composition in spectral analysis. Bone-lead concentrations for ten lead-exposed smelter workers were computed before and after analysis modification, and the results show that the bone-lead concentrations for the same person calculated from two sets of phantoms are not significantly different, only after the modifications are incorporated. Through these investigations, it was discovered that a common practice of setting the ratio of the calcium edge amplitude to the coherent scatter amplitude as a constant is only valid when all spectra are acquired at the same system resolution. When there is a change in the resolution between spectra, it has been determined that the ratio of the calcium edge amplitude to the coherent area should instead be used as the constant factor in the analysis program.

1. Introduction

The first *in vivo* x-ray fluorescence (XRF) measurements of lead in bone were performed by Ahlgren *et al* using a ^{57}Co source in a 90° geometry (Ahlgren *et al* 1976). The technique used in our group is ^{109}Cd γ-ray induced K-x-ray fluorescence in a backscatter geometry, which

was developed at the University of Birmingham (Laird *et al* 1982). Enhanced systems were developed elsewhere, including one at McMaster University (Gordon *et al* 1993), in which a ^{109}Cd source was mounted coaxial with, and in front of, the detector, resulting in a backscatter source-sample-detector geometry. Since both the coherently scattered photons and the lead K x-rays detected in this system are produced by unattenuated ^{109}Cd source γ-rays interacting in the bone, the ratio of the amplitudes of lead K x-rays and coherent peaks produces a robust estimate of lead concentration in bone mineral (Somervaille *et al* 1985).

System calibration is one of the essential steps in the calculation of the lead concentration of an unknown sample. In principle, if we know the lead concentration of a standard sample and the coherent conversion factor (CCF), we can obtain the concentration in an unknown sample by using the formula

$$(\text{concentration})_{\text{sample}} = \frac{(\text{K x-ray/coherent})_{\text{sample}}}{(\text{K x-ray/coherent})_{\text{standard}}} \times \text{CCF} \times (\text{concentration})_{\text{standard}} \qquad (1)$$

where $(\text{K x-ray/coherent})_{\text{sample}}$ and $(\text{K x-ray/coherent})_{\text{standard}}$ are the ratios of the amplitudes of the x-ray and the coherent scatter peaks in the sample and standard spectra, respectively. If the concentration of the standard is measured in μg Pb/g phantom material, then the resulting concentration of the sample will be given in μg Pb/g bone mineral. The coherent conversion factor accounts for slight differences in scattering between the phantom material and bone mineral. In practice, several phantoms are used to generate a calibration line.

In general, the phantoms used to calibrate the ^{109}Cd induced K-XRF system are made of plaster of Paris. The composition of plaster of Paris powder is $CaSO_4 \cdot \frac{1}{2}H_2O$, changing to $CaSO_4 \cdot 2H_2O$ during the preparation of the phantom. Previous studies have been performed to examine the purity of commercially available hemihydrate plaster and to illustrate how this will affect the subsequent calculation of bone lead (Todd 2000, Aro *et al* 1994). Specifically, a stoichiometric analysis of a commercially available plaster indicated that the concentration of $CaSO_4 \cdot 2H_2O$ was 92.3%. The impurities in the plaster gave rise to a coherent scattering cross-section that was 0.045% greater than that of the pure hemihydrate plaster. The change of CCF due to the impurities was negligible during the calculation of the bone lead (Todd 2000). Aro *et al* used inductively coupled plasma mass spectrometry (ICPMS) to evaluate the suitability of plaster of Paris phantoms as a calibration standard and found that the calculated phantom concentrations underestimated measured concentrations by 15% on average. These authors suggested that plaster of Paris phantoms used for calibration should be measured for lead concentration by ICPMS or another valid analytical technique (Aro *et al* 1994).

The phantoms used at McMaster University are made of plaster of Paris. There are two sets of phantoms: one set has a radius of 1.2 cm, while the second, more recent, set has a radius of 2.5 cm. The second set was made in an effort to improve the uniformity of the lead distribution. We found that the calibration lines for these two sets of phantoms, and hence the results of the bone-lead concentration calculated from them, were significantly different. The impurity of the material was then questioned, and several methods were employed to analyse the composition of the phantom material. The spectral fitting program was then modified according to the phantom composition.

Through these investigations of spectral fitting, it was observed that the calcium edge amplitude to coherent peak amplitude ratio depends on the system resolution. This ratio is typically set as a constant in the fitting algorithm, and these observations suggest that this practice is only valid if all spectra are acquired with the same system resolution. Therefore, a more robust ratio was sought in these studies, one which is not dependent on system variables such as the resolution.

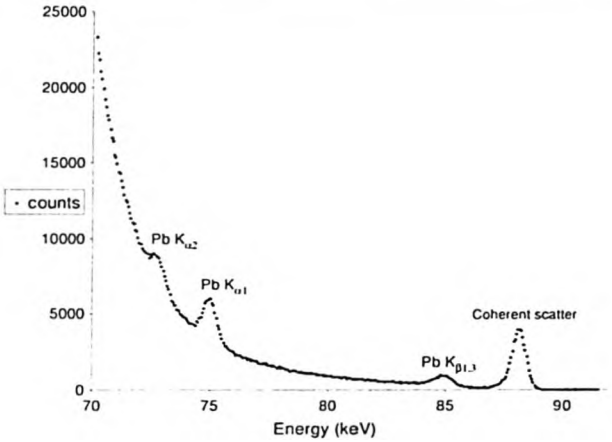

Figure 1. A representative lead XRF spectrum, collected from a 200 ppm phantom measured for 1800 s.

2. Methods and materials

2.1. The calibration lines for the old and new phantoms

The system used in this work is a standard ^{109}Cd K-XRF bone-lead measurement system. The system consists of a 25.5 mm radius HPGe detector, a preamplifier, a main amplifier, an analog-to-digital converter and a PC-based multi-channel analyser. A program originally developed by the Birmingham group, based on the Marquardt algorithm, is used to analyse the XRF spectrum, resulting in a measure of the peak amplitudes of the lead x-rays as well as the coherent scatter feature. The ratio of the x-ray to coherent peak amplitudes is then used, in conjunction with the calibration line, in order to calculate the lead concentration of the unknown sample. Figure 1 illustrates a typical lead x-ray fluorescence measurement spectrum, focusing on the energy region in which the key spectral features are found.

Prior to measuring unknown samples, the calibration line is determined by repeated measurements on a set of plaster of Paris phantoms, doped with known amounts of lead over a range of concentrations. The line is generated by plotting the x-ray to coherent peak amplitude ratios versus phantom concentration. Ten old phantoms and ten new phantoms were measured for 30 min to generate such calibration lines.

2.2. The composition of the new phantoms

The high energy tails of the Compton profile distribution from calcium and sulfur (for phantoms) or phosphorus (for bones) exhibit edge features that are close in energy to the lead $K_{\beta 1,3}$ x-ray peaks (Harding 1995), and an accurate accounting of these features is important in spectral analysis. Figure 2 illustrates these features, in a spectrum acquired from a phantom with zero added lead, collected for 70 h. In the previous fitting program, the amplitude of Ca and S edges was fixed as a constant fraction of the coherent scatter amplitude based on the composition of the matrix material.

To investigate the accuracy of these fixed ratios, three old phantoms with lead concentrations of 0 ppm, 2 ppm and 9 ppm were measured three times each, and three new

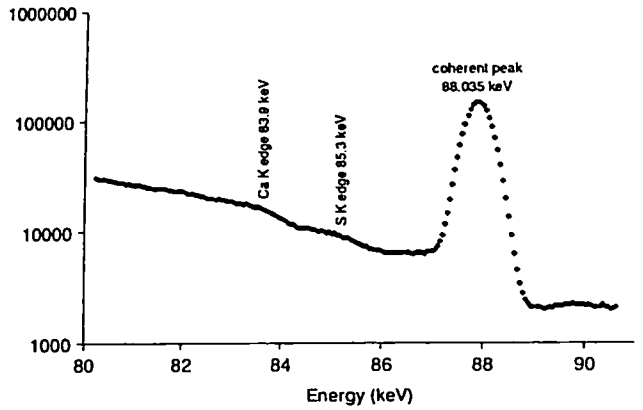

Figure 2. The Ca and S K edge features in a spectrum acquired from a 0 ppm plaster phantom over a 70 h measurement period.

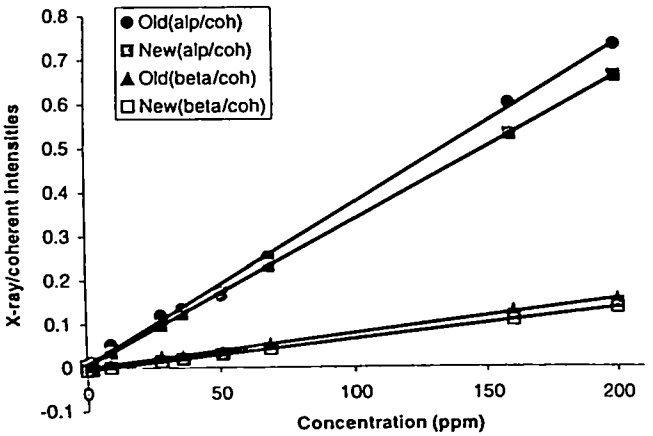

Figure 3. The K_α and K_β calibration lines for both sets of phantoms.

phantoms with lead concentrations of 0 ppm, 12 ppm and 21 ppm were measured four times each for 12 h. The ratio of the Ca edge to coherent peak amplitudes and the ratio of S edge to Ca edge amplitudes were allowed to vary in the analysis program. Based on these findings, more detailed analysis of the composition of the new phantoms was conducted by chemical analysis, neutron activation analysis (NAA), prompt-γ NAA and XRF.

3. Results/discussion

3.1. The calibration lines for the old and new phantoms

Figure 3 shows the calibration lines for the old and new phantoms. Note that there are two calibration lines for each set of phantoms: one line is generated by plotting the ratio of the K_α peak amplitude to coherent amplitude, whereas the other is generated by plotting the ratio of the K_β to coherent peak amplitudes.

Table 1. Composition-sensitive ratios for the 0 ppm phantoms.

New phantom set			Old phantom set		
Resolution (eV)	Ca/Coh	S/Ca	Resolution	Ca/Coh	S/Ca
577	0.037	0.227	564	0.026	0.53
624	0.041	0.218	620	0.033	0.51
703	0.045	0.248	630	0.036	0.39
			735	0.040	0.45
Average:	0.041	0.231	Average:	0.034	0.47
Standard deviation:	0.004	0.016	Standard deviation:	0.006	0.06

The functions of these lines are

$$\begin{aligned}
(\alpha/\mathrm{coh})_{\mathrm{Old}} &= (0.003\,66 \pm 0.000\,01) \times X(\mathrm{ppm}) + (0.006 \pm 0.006) \\
(\alpha/\mathrm{coh})_{\mathrm{New}} &= (0.003\,29 \pm 0.000\,01) \times X(\mathrm{ppm}) + (0.005 \pm 0.001) \\
(\beta/\mathrm{coh})_{\mathrm{Old}} &= (0.000\,78 \pm 0.000\,01) \times X(\mathrm{ppm}) - (0.0001 \pm 0.0001) \\
(\beta/\mathrm{coh})_{\mathrm{New}} &= (0.000\,71 \pm 0.000\,01) \times X(\mathrm{ppm}) - (0.0059 \pm 0.0007)
\end{aligned} \tag{2}$$

where α/coh and β/coh are the ratios of the amplitudes of the K_α and K_β peaks to the coherent peak amplitude respectively, and X is the concentration of the phantom. Note that there is a negative intercept for the new K_β calibration line, which is significantly non-zero, and also that the slopes of the new K_α and K_β calibration lines are about 10% lower than those obtained with the old set of phantoms. The lower slopes of the new calibration lines indicate that for the same lead concentration, the ratios of K_α and K_β to coherent amplitudes for the new phantoms are smaller than those for the old phantoms. This indicates that the cross-section for coherent scatter differs between the two phantom matrices: the cross-section is higher for the new phantoms relative to that of the old phantoms. The cross-section for coherent scatter will be strongly influenced by the concentration of high Z elements in the matrix, which implies that there are differences in concentrations of such elements in these two phantom materials. Detailed elemental analysis was therefore necessary to resolve the discrepancies in the slopes of the calibration lines of the two sets of phantoms. The significantly non-zero intercept for the new K_β calibration line suggests that there are inaccuracies in modelling the edge features close in energy to the peak. The following sections will pursue this hypothesis in more detail.

3.2. The composition of the new phantoms, from spectral analysis

Table 1 lists the Ca edge to coherent peak amplitude ratio and S edge to Ca edge amplitude ratio from the spectral analysis of 0 ppm phantoms. Note that system resolution (for 88 keV peak) was not constant, and is also listed in the table.

From table 1 it is clear that the measured ratios differ for the two phantom sets: the Ca edge to coherent amplitude ratios are 0.041 ± 0.004 and 0.034 ± 0.006 for the new and old phantoms, respectively, and the S to Ca edge amplitude ratios are 0.23 ± 0.02 and 0.47 ± 0.06 for the new and old phantoms, respectively. In the original analysis program, these two ratios were set as fixed values, with the Ca edge to coherent amplitude ratio set as 0.030 and the S to Ca edge amplitude ratio set as 0.44. These values are consistent with those returned in the analysis of the old phantoms, while the ratios for the new phantoms are quite different.

From table 1, the ratio of the S and Ca edge amplitudes for the new phantoms is about half of that of the old phantoms, implying that the concentration ratio of S to Ca in the new

Table 2. Concentration analysis results for the new phantoms.

Method	Ca	σ(Ca)	S	σ(S)	C	σ(C)	Mg	σ(Mg)	(S/Ca) atom	σ (S/Ca)
Fitting	n/a	n/a	n/a	n/a	n/a	n/a	n/a	n/a	0.374	0.027
Chemical	0.324	0.003	0.081	0.001	0.052	0.001	0.0024	0.0003	0.312	0.005
NAA1	0.304	0.002	0.096	0.007	n/a	n/a	0.0044	0.0001	0.395	0.029
NAA2	0.303	n/a	0.09	n/a	n/a	n/a	n/a	n/a	0.371	n/a
PGNAA	0.332	n/a	0.082	n/a	n/a	n/a	n/a	n/a	0.309	n/a
XRF1[a]	0.607	0.023	0.168	0.028	n/a	n/a	n/a	n/a	0.346	0.059
XRF2	0.321	n/a	0.098	n/a	0.048	n/a	n/a	n/a	0.382	n/a

[a] Only relative quantities of Ca and S were available in this analysis, therefore only the S/Ca ratio should be compared with the other techniques listed.

phantoms is about half of that in the old phantoms. Also, the higher Ca edge to coherent amplitude ratio observed with the new phantoms suggests that the concentration of Ca in the new plaster is greater than that in the old phantoms. From these preliminary findings, it was clear that the composition of the new phantoms needed a more detailed investigation.

3.3. The composition of the new phantoms, from more detailed analyses

Table 2 lists the results from a variety of analysis techniques, performed on the new phantom material at a number of different locations.

Unless otherwise stated, the concentrations of Ca, S, C and Mg in table 2 are given as fractions by weight. Fitting refers to analysis of that part of the spectrum in which Ca and S edges can be seen. Spectra from both old and new phantoms, each collected over a 70 h measurement period were analysed. The chemical analysis was conducted by the Guelph Chemical Lab Ltd (Guelph, ON, Canada) and the sample was analysed using a varian inductively coupled plasma–atomic emission spectroscopy (ICP-MS) as per standard techniques. NAA1 refers to neutron activation analysis, and was conducted by the nuclear analysis laboratory of the Chinese Institute of Atomic Energy (Beijing, China). NAA2 also refers to neutron activation analysis, and was conducted by the NAA laboratory of McMaster University, (Hamilton, ON, Canada). The PGNAA (prompt-γ NAA) was also completed at the NAA laboratory of McMaster University. XRF1 refers to x-ray fluorescence analysis performed by Professor Gama at the nuclear analysis laboratory of Lisbon University (Lisbon, Portugal). Note that this analysis only provided measures of the Ca and S present, and reports these only in relative terms. XRF2 refers to the x-ray fluorescence analysis performed by Ontario GEO Services Centre, Geosciences Laboratories (Sudbury ON, Canada). Initially it was anticipated that a single analysis would suffice, however, the results tabulated in table 2 illustrate that there is a range of S to Ca concentration ratios measured.

Based on these results, a weighting of each method's finding suggests the following molecular composition of the new phantom material:

$CaCO_3$: $(51 \pm 7)\%$

$CaSO_4 \cdot \frac{1}{2}H_2O$: $(41 \pm 6)\%$

$MgSiO_4$: $(1.70 \pm 0.04)\%$

H_2O: $(7 \pm 9)\%$

compared with the expected composition of 100% $CaSO_4 \cdot \frac{1}{2}H_2O$.

From the above values for composition by weight, the predicted $(S/Ca)_{atom}$ ratio for the new material is 0.356, compared with a value of 1 for the composition of the previous phantoms. Therefore, the S to Ca edge amplitude ratio in the analysis program should be

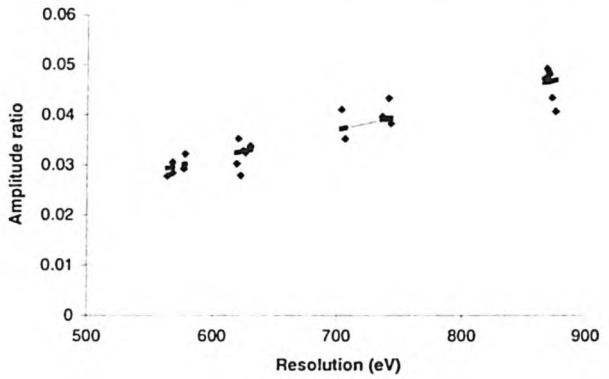

Figure 4. Ca edge to coherent peak amplitude ratio versus resolution.

changed by a corresponding amount: the amplitude ratio should decrease from 0.44 to 0.16. Furthermore, this predicted composition can be used to determine the degree to which other material-related parameters will be affected. Such calculations suggest that the Ca edge to coherent peak amplitude ratio should be changed from 0.030 to 0.036 in the analysis program. Furthermore, the value of the coherent conversion factor should be changed from 1.46 to 1.29 when using equation (1) to calculate the concentration of lead present in an unknown sample.

3.4. Influence of resolution on the Ca edge to coherent peak amplitude ratio

When the results discussed in 3.1 were first observed, it was noted that the ratio of Ca edge to coherent peak amplitude ratio was dependent on the system resolution (see table 1). More complete data are presented in figure 4.

The function of this curve is

$$\text{Ca/Coh} = (5.71 \times 10^{-5}) \times \text{resolution} - 0.0029.$$

Therefore, the Ca edge to coherent peak amplitude ratio has a linear relationship with resolution. If all measurements are conducted at the same system resolution, one fixed value of the Ca edge to coherent peak amplitude ratio can be used, such as the values of 0.030 and 0.036 given in the previous section for 100% $CaSO_4 \cdot \frac{1}{2}H_2O$ and the new plaster matrix, respectively. However, if system resolution is variable, this practice in spectral analysis may lead to errors. Instead it is proposed that a ratio based on that of the Ca edge amplitude to coherent peak area be implemented. Figure 5 demonstrates the relationship between the resolution and the ratio of Ca edge amplitude to the product of the coherent peak amplitude and full-width half-maximum (FWHM). (Note: peak area is proportional to the product of the amplitude and the FWHM for a Gaussian peak, and the FWHM is readily obtained from the spectral analysis of the coherent peak feature.)

A t-test shows that the slope of this curve is not significantly different from zero ($p = 0.327$), indicating that the ratio (Ca edge/(coherent peak amplitude $\times$ FWHM)) is independent of resolution, over the range tested here. It should be noted that other ratios relative to the coherent peak amplitude may similarly be influenced by variable system resolution, and care should be taken to ensure that the resolution remains fixed, or that a more robust ratio, such as that to the coherent peak area, is used in analysis in such scenarios.

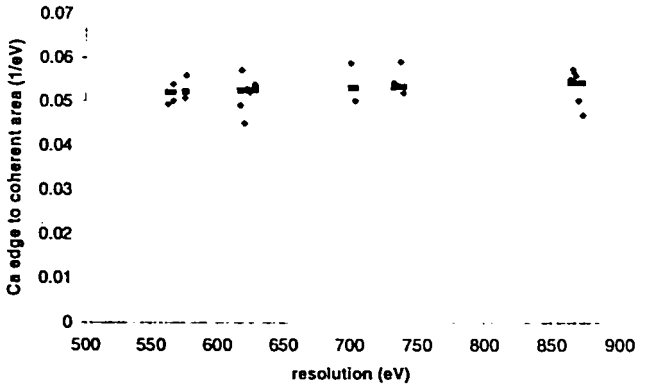

Figure 5. The Ca edge to coherent area ratio versus resolution.

Table 3. Results from the old and new phantom calibrations. New1 refers to analysis with the new phantoms before modifications to the procedure, whereas New2 determines the concentration based on the new phantoms and a modified analysis process, including updated values for the Ca edge to coherent peak amplitude ratio, the S to Ca edge amplitude ratio and the coherent conversion factor.

Sample no	Pb conc.1 (Old1)	Pb conc. 2 (New1)	Pb conc.3 (New2)
1	6.5 ± 5.1	13.6 ± 5.5	7.2 ± 4.9
2	28.6 ± 9.6	38.6 ± 10.4	28.6 ± 9.3
3	13.4 ± 5.4	21.6 ± 6.0	13.8 ± 5.2
4	5.0 ± 7.0	13.3 ± 7.6	5.6 ± 6.7
5	76.3 ± 6.7	90.0 ± 7.5	74.9 ± 6.5
6	73.5 ± 14.0	87.7 ± 15.4	72.1 ± 13.6
7	36.6 ± 5.7	47.6 ± 6.3	36.4 ± 5.5
8	57.0 ± 8.3	68.8 ± 9.0	56.1 ± 8.0
9	4.6 ± 6.1	10.8 ± 6.7	5.3 ± 5.8
10	53.4 ± 8.8	66.2 ± 9.8	52.6 ± 8.5

3.5. Impact of changes to the analysis process for in vivo data set

These studies have determined that the elemental composition of the new phantom material differs significantly from that of the previous phantoms. This has an effect on various parameters used both in the spectral analysis program and in converting x-ray intensities to lead concentrations via equation (1). Therefore, to emphasize the importance of these changes, table 3 shows the results for calcaneus lead concentrations of ten smelter workers, using the new phantom calibration before and after analysis modifications, as well as the results using the old phantom calibration. The matrix material and analysis procedure have been well established with the previous set of phantoms, therefore the worker concentrations obtained from this set will be used as the standard to test the new phantom calibration.

Z-tests show that there is a significant difference between the concentrations obtained with the previous phantom set and those calculated with the new phantoms before analysis modifications. However, there is no significant difference between the concentrations calculated from the old phantom set and those determined with the new phantoms after program modification (Z-test, $p = 0.897$).

Table 4. Comparing the results of setting either the Ca edge to coherent area ratio or the Ca edge to coherent amplitude ratio as a constant in the analysis program. See text for details.

Sample no	Pb conc. 1 (Old1)	Pb conc. 2 (Old2)	Pb conc. 3 (New2)	Pb conc. 4 (New3)
1	6.5 ± 5.1	6.6 ± 5.1	7.2 ± 4.9	8.0 ± 4.9
2	28.6 ± 9.6	28.4 ± 9.6	28.6 ± 9.3	29.0 ± 9.3
3	13.4 ± 5.4	13.8 ± 5.4	13.8 ± 5.2	14.8 ± 5.2
4	5.0 ± 7.0	5.3 ± 7.0	5.6 ± 6.7	6.5 ± 6.7
5	76.3 ± 6.7	77.0 ± 6.7	74.9 ± 6.5	76.0 ± 6.5
6	73.5 ± 14.0	73.9 ± 14.0	72.1 ± 13.6	73.2 ± 13.6
7	36.6 ± 5.7	36.8 ± 5.7	36.4 ± 5.5	37.1 ± 5.4
8	57.0 ± 8.3	56.8 ± 8.2	56.1 ± 8.0	56.4 ± 8.0
9	4.6 ± 6.1	8.6 ± 6.1	5.3 ± 5.8	9.7 ± 5.8
10	53.4 ± 8.8	54.1 ± 8.8	52.6 ± 8.5	52.8 ± 8.5

In the preceding section, it was also demonstrated that ratios involving the coherent peak amplitude may be sensitive to system resolution, and a more robust approach is the use of ratios relative to the coherent peak area. Table 4 therefore shows the effect of setting the Ca edge amplitude to coherent area ratio, rather than the Ca edge to coherent amplitude ratio, as a constant. Old1 uses the previous phantoms and sets the Ca edge to coherent amplitude ratio as a constant. Old2 uses the previous phantoms and sets the Ca edge to coherent area ratio as a constant. Similarly, New2 and New3 use the new phantoms, but set the Ca edge to coherent amplitude, and the Ca edge to coherent area as a constant, respectively. It should be noted that both New2 and New3 use analysis algorithms based on the measured composition of the matrix as reported in section 3.2.

Z-tests show no significant difference between the results when setting either the Ca edge to coherent peak amplitude or the Ca edge to the coherent peak area ratios as constants, for either the old or the new phantoms ($\alpha = 0.05$). In these studies, phantom calibration and subject measurement tend to be conducted with similar system configuration, and therefore there is little expected change in the detector resolution.

4. Conclusions

Accurate phantom calibration and analysis procedures are critical for the ^{109}Cd K-XRF bone-lead measurement system. This can be seen from table 3: inappropriate analysis parameters (New1) result in significant error for the subsequent calculation of the lead concentration in an unknown sample. The calibration procedure has been investigated in previous studies (Aro *et al* 1994, Todd 2000), but the emphasis in these previous works was the change in the CCF. In this work, it has been demonstrated that two additional composition-related parameters, namely the Ca edge to coherent amplitude ratio and the S edge to Ca edge amplitude ratio, will influence the accuracy of the analysis of unknown spectra, when there are changes in the matrix material used in phantom fabrication.

Calibration phantoms for the ^{109}Cd K-XRF bone-lead measurement tend to be made of plaster of Paris, which is usually considered to be $CaSO_4 \cdot \frac{1}{2}H_2O$, with some trace impurities. From these investigations, it is clear that this is not necessarily always the case, and care will be taken in future when procuring plaster of Paris for phantom preparation.

This work also demonstrates that the ratio of the calcium edge to the coherent peak area should be incorporated as a constant in spectral analysis, rather than the ratio of the calcium edge to the coherent peak amplitude, if there are significant changes in the system resolution

over the course of a series of calibration and subject measurements. However, it has also been demonstrated that in practice this change has only a minor effect on the resulting concentration calculations since detector resolution normally varies little during a set of measurements.

Acknowledgment

Support for this work from the Natural Sciences and Engineering Research Council of Canada, is gratefully acknowledged.

References

Ahlgren L, Lidén K, Mattsson S and Tejning S 1976 X-ray fluorescence analysis of lead in human skeleton *in vivo* *Scand. J. Work Environ. Health* 2 82–6

Aro A C A, Todd A C, Amarasiriwardena C and Hu H 1994 Improvements in the calibration of ^{109}Cd K x-ray fluorescence systems for measuring bone lead *in vivo* *Phys. Med. Biol.* 39 2263–71

Gordon C L, Chettle D R and Webber C E 1993 An improved instrument for the *in vivo* detection of bone lead *Br. J. Industrial Med.* 50 637–41

Harding G 1995 Comments on the article 'Photoelectron bremsstrahlung-analytical possibilities?' *Phys. Med. Biol.* 40 471–6

Lord E E, Chettle D R and Scott M C 1982 The factors effecting *in vivo* x-ray fluorescence of lead in bone *Nucl. Instrum. Methods* 193 577–82

Somervaille L J, Chettle D R and Scott M C 1985 *In vivo* measurement of lead in bone using x-ray fluorescence *Phys. Med. Biol.* 30 909–43

Todd A C 2000 Coherent scattering and matrix correction in bone-lead measurements *Phys. Med. Biol.* 45 1953–63

Appendix II Initial work in calculating the dose absorption fraction for ^{14}C and tritium in trabecular bone by Monte Carlo (MC) simulation

This is a collaborative work with Dr. R. B. Richardson (richardr@aecl.ca) in Radiation Biology and Health Physics Branch, Atomic Energy of Canada Limited, Chalk River Laboratories. Dr. Richardson is in the process of developing a physiological bone compartmental model. This model is being initially applied to the intake and dosimetry of ^{14}C and tritium. In order to calculate the committed equivalent dose to the critical target tissues in bone, it is necessary to evaluate the radionuclide absorbed fractions in those target tissues. The absorbed fraction can be estimated by using Monte Carlo simulations. This appendix will show some work performed to calculate the dose absorption fraction for ^{14}C and tritium in trabecular bone by MC simulation and some initial results.

The simulation is based on a trabecular bone cavity model designed by Dr. Richardson and he is still in the process of perfecting the model. Figure 1 shows the three dimensional plot for one cavity unit. This unit is shown as a cube of 1250μm*1250μm*1250μm. Clearly this unit is repeated many times in assemblies with widely varying geometries in actual bone. The grey part of the figure represent the bone plates and the transparent part is mainly bone marrow.

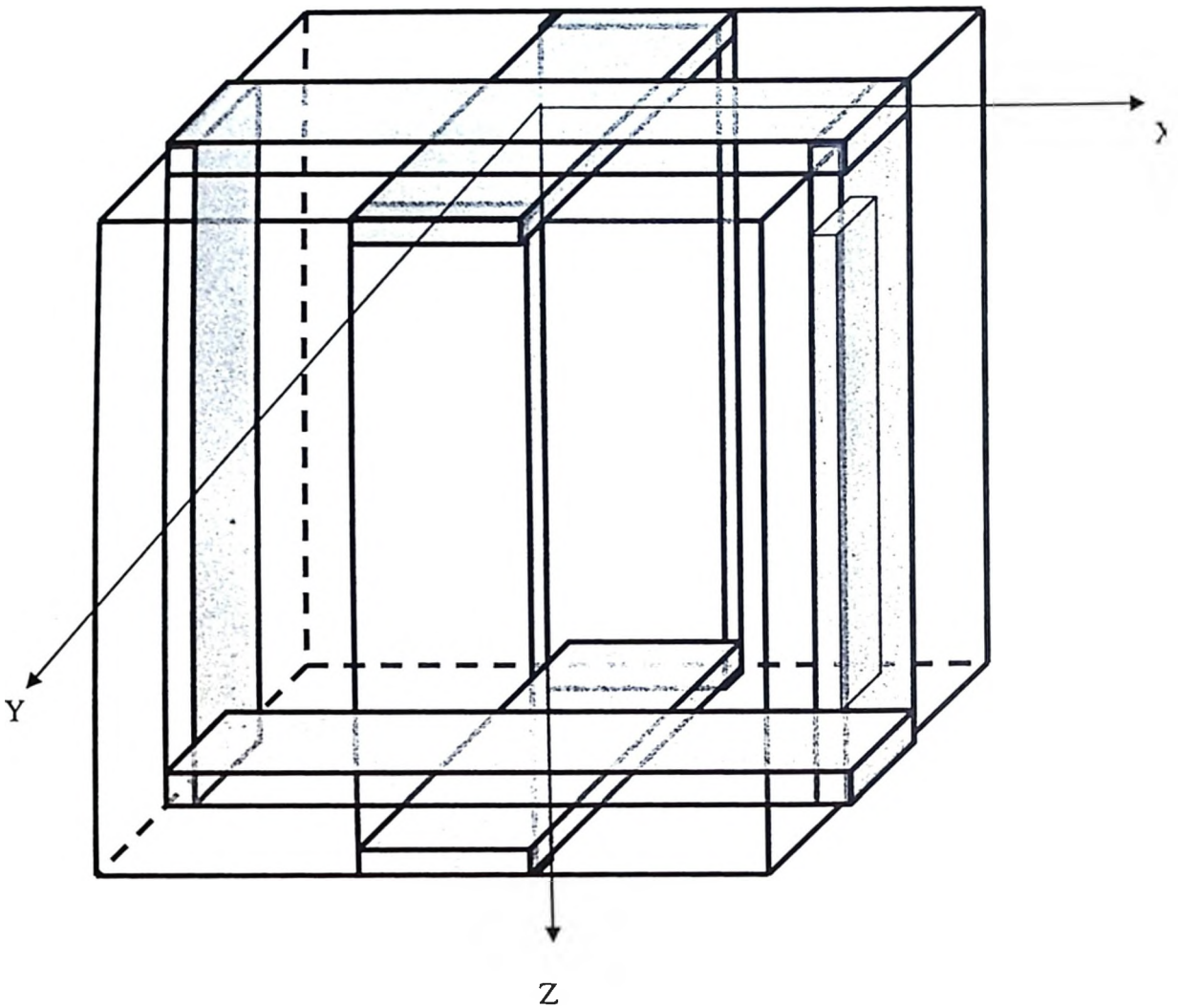

Figure 1 The three dimensional structure for the trabecular cavity unit

There are eight bone plates embedded in the unit; in one of them a bone remodeling unit (BMU) is inserted. A BMU is the unit that involves in the formation and resorption of the bone. The size of the bone plate is 1250μm*600μm*56μm (length*width*thickness). The size of the BMU is 1000μm*600μm*40μm (height*width*depth). The other regions within the cavity unit are bone marrow and some thin layers of bone lining cells and connective tissue. Figure 2 shows the two dimensional structure for the cavity unit in the X-Z plane. The slice is taken through the BMU.

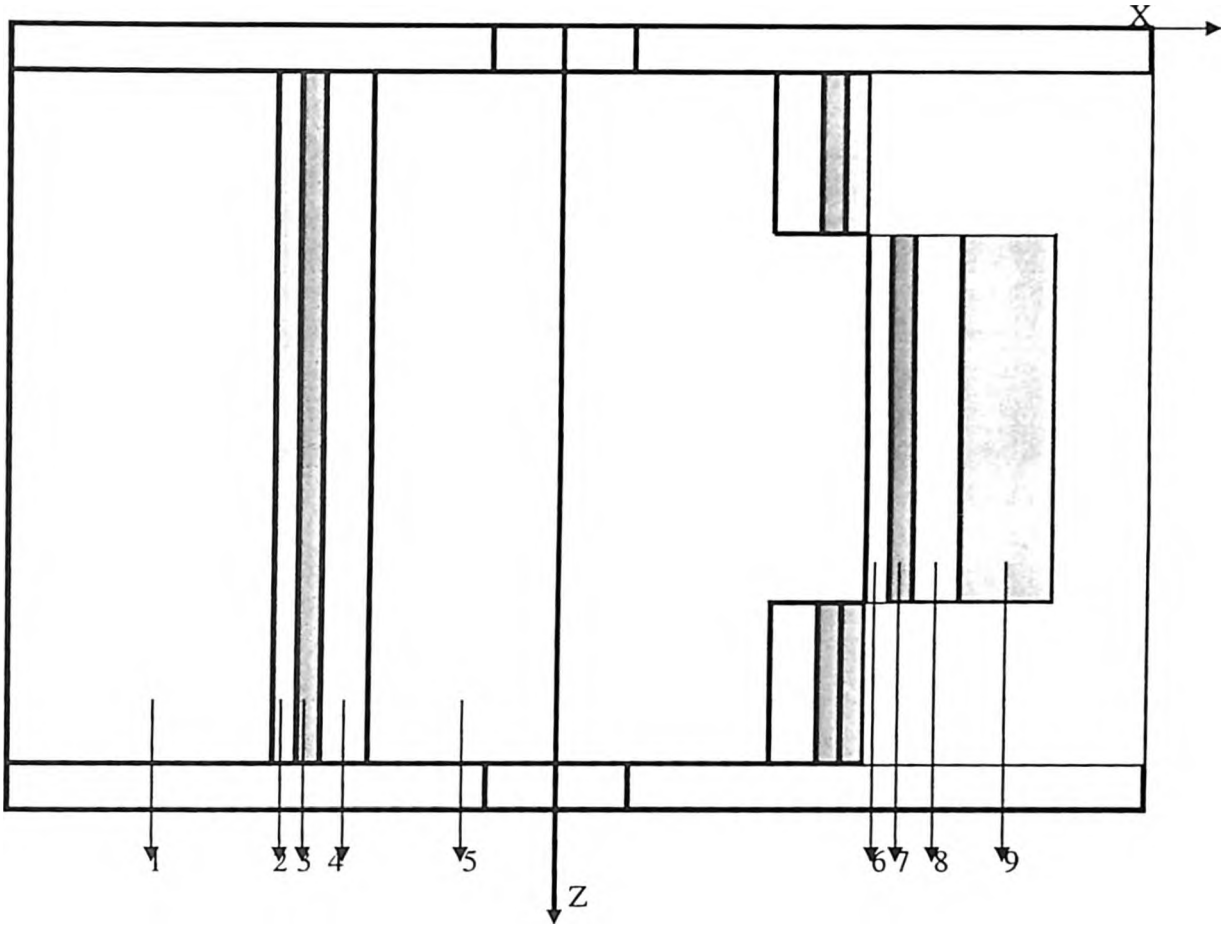

Figure 2 Two dimensional structure for the cavity unit at the X-Z plane
Note: the plot is not on scale.

1: bone, 56μm
2: connective tissue, 1μm
3: bone lining cells, 1μm
4: bone marrow, 8μm
2+3+4: endosteum, 10μm
5: bone marrow, 1118μm + 10μm
6: bone marrow, 9μm
7: osteoblast layer, 7μm
8: osteoid layer, 8μm
9: lamellae (new bone) layer, 16μm
6+7+8+9: BMU layer, 40μm

In the initial simulation, the cavity is calculated in 15 layers * 11 layers * 11 layers in X*Y*Z directions. Table 1 lists the tissues and their thicknesses for these layers.

Layers	X-direction	Y-direction	Z-direction
1	bone, 56μm	bone, 56μm	bone, 56μm
2	bone lining cells, 1μm	bone lining cells, 1μm	bone lining cells, 1μm
3	connective tissue, 1μm	connective tissue, 1μm	connective tissue, 1μm
4	bone marrow, 8μm	bone marrow, 8μm	bone marrow, 8μm
5	bone marrow, 259μm	bone marrow, 259μm	bone marrow, 59μm
6	bone plate, 600μm	bone plate, 600μm	BMU, 1000μm
7	bone marrow, 259μm	bone marrow, 259μm	bone marrow, 59μm
8	bone marrow, 8μm	bone marrow, 8μm	bone marrow, 8μm
9	connective tissue, 1μm	connective tissue, 1μm	connective tissue, 1μm
10	bone lining cells, 1μm	bone lining cells, 1μm	bone lining cells, 1μm
11	bone marrow, 9μm	bone, 56μm	bone, 56μm
12	osteoblast, 7μm		
13	osteoid, 8μm		
14	lamellae, 16μm		
15	bone, 56μm		

Table 1 Cavity structure

According to this structure, the number of regions for one cavity unit is 1821. ^{14}C and tritium were distributed homogeneously in each tissue, and the percentages of the ^{14}C and tritium in different tissue are calculated according to their compositions. The energy spectra for tritium and ^{14}C were shown in Table 2 (Cross et al. 1983). The cut off energies were set to be 10keV for both simulations (i.e. if the energy of the electron is less than 10keV, then the program assumes the energy is deposited locally).

tritium		^{14}C	
Energy (MeV)	N (Betas/MeV)	Energy (MeV)	N (Betas/MeV)
0.0000	82.762	0.0000	9.888
0.0004	86.202	0.0035	10.097
0.0008	92.999	0.0071	10.666
0.0013	97.536	0.0106	11.089
0.0017	100.355	0.0141	11.374
0.0021	101.883	0.0177	11.547
0.0025	102.402	0.0212	11.626
0.0029	102.111	0.0247	11.628
0.0034	101.154	0.0282	11.562
0.0038	99.643	0.0318	11.439
0.0042	97.664	0.0353	11.266
0.0046	95.292	0.0388	11.049
0.0050	92.586	0.0424	10.793
0.0055	89.598	0.0459	10.503
0.0059	86.374	0.0494	10.183
0.0063	82.953	0.0530	9.837
0.0067	79.370	0.0565	9.468
0.0071	75.658	0.0600	9.079
0.0076	71.845	0.0635	8.674
0.0080	67.958	0.0671	8.255
0.0084	64.022	0.0706	7.824
0.0088	60.059	0.0741	7.385
0.0092	56.092	0.0777	6.940
0.0097	52.139	0.0812	6.491
0.0101	48.221	0.0847	6.040
0.0105	44.355	0.0883	5.590
0.0109	40.557	0.0918	5.143
0.0113	36.845	0.0953	4.701
0.0118	33.234	0.0988	4.267
0.0122	29.739	0.1024	3.841
0.0126	26.374	0.1059	3.428
0.0130	23.153	0.1094	3.028
0.0134	20.090	0.1130	2.643
0.0139	17.198	0.1165	2.276
0.0143	14.489	0.1200	1.929
0.0147	11.975	0.1236	1.604
0.0151	9.668	0.1271	1.303
0.0155	7.580	0.1306	1.028
0.0160	5.723	0.1341	0.781
0.0164	4.107	0.1377	0.563
0.0168	2.743	0.1412	0.379
0.0172	1.642	0.1447	0.228
0.0176	0.813	0.1483	0.114
0.0181	0.269	0.1518	0.038
0.0185	0.017	0.1553	0.002

Table 2 Energy spectra for tritium and ^{14}C

The energy distributions were then fitted with polynomial functions by using Origin6.0 software. Both distributions of tritium and ^{14}C were input into the MC simulation through the fitted functions.

Table 3 lists the components and densities for different tissues. In the MC simulation, bone marrow is considered as a homogeneous mix of fat and haemopoietic marrow.

	Elemental composition (% by mass)											Density
Tissues	H	C	N	O	Na	Mg	P	S	Cl	K	Ca	(kg/m^3)
Fat[a]	12	77		11								920
Marrow	11.3	51.9	1.4	34.9	0.08		0.12	0.12	0.08	0.12		976
Connective tissue[b]	9.6	9.9	2.2	74.4	0.5		2.2	0.9	0.3			1100
Haemopoietic marrow	10.2	14.3	3.4	70.8	0.2		0.3	0.3	0.2	0.3		1060
Endosteum												
Osteoblasts												
Bone lining cells[c]												
Osteoid seam[c]	7.2	12.4	3.1	62.7	0.3	0.1	5.0	0.7	0.2		8.5	1410
New bone[c]	4.1	15.4	4.1	48.0	0.1	0.2	8.6	0.4			19.0	1800
Trabecular adult bone	3.5	16.2	4.4	45.4	0.1	0.2	9.1	0.3			20.8	1850

Table 3 Components and densities for different tissues

[a] ICRP 23 (1975)
[b] As cartilage, ICRP 23 (1975)
[c] Woodard and White (1986)
Note: Osteoid seam, 40% mineralization; new bone, 90% mineralization; marrow, 40% fat, 60% haemopoietic marrow.

Table 4 shows the volume and mass of different tissues for one cavity unit and C and H concentrations for different tissues.

Tissue	Density (mg/mm^3)	Volume (mm^3)	Mass (mg)	C-conc1*	C-mass	C-conc2**	H-conc1	H-mass	H-conc2
bone	1.80E+00	2.57E-01	4.62E-01	1.62E-01	7.48E-02	8.19E-02	3.50E-02	1.62E-02	7.97E-02
marrow	9.76E-01	1.64E+00	1.60E+00	5.19E-01	8.29E-01	9.07E-01	1.13E-01	1.81E-01	8.90E-01
bone lining cells	1.06E+00	4.14E-03	4.39E-03	1.43E-01	6.27E-04	6.86E-04	1.02E-01	4.47E-04	2.21E-03
connective tissue	1.10E+00	4.13E-03	4.54E-03	9.90E-02	4.50E-04	4.92E-04	9.60E-02	4.36E-04	2.15E-03
endosteum	1.06E+00	3.27E-02	3.46E-02	1.43E-01	4.95E-03	5.42E-03	1.02E-01	3.53E-03	1.74E-02
lamellae	1.80E+00	9.60E-03	1.73E-02	1.54E-01	2.66E-03	2.91E-03	4.10E-02	7.08E-04	3.49E-03
osteoid	1.41E+00	4.80E-03	6.77E-03	1.24E-01	8.39E-04	9.18E-04	7.20E-02	4.87E-04	2.40E-03
osteoblast	1.06E+00	4.20E-03	4.45E-03	1.43E-01	6.37E-04	6.96E-04	1.02E-01	4.54E-04	2.24E-03
Tatal		1.953			0.914			0.203	

Table 4 Volume and mass of different tissues and C concentrations

Note: Mass is the mass for the corresponding tissue; C-conc1 is the C concentration in the corresponding tissue; C-conc2 is C concentrations in the whole cavity unit.

The C and H concentrations in the whole cavity unit are used to normalize the C and H distributions in different tissues for the simulation.

Table 5 and 6 show the absorption fractions from source to target for one cavity unit for ^{14}C and tritium respectively. The values in the table are calculated as:

$$AF = \frac{\text{energy from the source that absorbed by the target}}{\text{tatal energy from the source}} \times (\text{C or H concentration in the source tissue})$$

or

$$AF = \frac{\text{energy from the carbon or tritium source absorbed by the target}}{\text{total energy from the carbon or tritium source in cavity}}$$

Source	Target 1	2	3	4	5	6	7	8	9	t
1	6.61E-02	5.38E-03	3.40E-04	3.06E-04	1.36E-03	1.02E-06	7.64E-07	5.88E-07	8.39E-03	8.1
2	1.37E-02	8.65E-01	6.47E-04	7.30E-04	4.77E-03	8.67E-04	7.72E-04	8.66E-04	2.01E-02	9.0
3	3.02E-04	2.21E-04	5.03E-05	2.98E-05	7.99E-05	0.00E+00	0.00E+00	0.00E+00	2.50E-06	6.8
4	1.98E-04	1.68E-04	2.02E-05	3.51E-05	6.89E-05	0.00E+00	0.00E+00	0.00E+00	1.94E-06	4.9
5	1.01E-03	1.33E-03	6.61E-05	8.04E-05	1.99E-03	2.93E-04	4.21E-05	2.07E-05	5.80E-04	5.4
6	5.83E-07	3.05E-04	0.00E+00	0.00E+00	3.66E-04	1.53E-03	2.73E-04	1.05E-04	3.28E-04	2.9
7	3.55E-07	2.11E-04	9.11E-09	7.72E-09	4.28E-05	2.12E-04	3.06E-04	1.03E-04	4.32E-05	9.1
8	3.63E-07	2.65E-04	3.26E-08	1.99E-08	2.55E-05	8.91E-05	1.13E-04	1.84E-04	1.89E-05	6.9

Table 5 Absorption fractions from source to target for one cavity unit for ^{14}C

Note: 1, bone; 2, marrow; 3, bone lining cells; 4, connective tissue; 5, endosteum; 6, lamellae; 7, osteoid seal; 8, osteoblast; 9, other regions outside the cavity unit.

Source	Target 1	2	3	4	5	6	7	8	9	total
1	7.96E-02	6.74E-06	4.40E-05	3.31E-06	1.09E-06	0.00E+00	0.00E+00	0.00E+00	6.32E-05	7.97E-
2	2.03E-05	8.90E-01	4.12E-06	4.20E-05	8.29E-05	1.40E-06	1.64E-06	1.84E-05	1.37E-04	8.90E-
3	1.13E-04	3.80E-06	1.98E-03	1.04E-04	7.60E-06	0.00E+00	0.00E+00	0.00E+00	0.00E+00	2.21E-
4	1.06E-05	2.94E-05	1.07E-04	1.92E-03	7.79E-05	0.00E+00	0.00E+00	0.00E+00	0.00E+00	2.15E-
5	1.69E-06	8.98E-05	6.58E-06	5.79E-05	1.72E-02	1.80E-05	0.00E+00	0.00E+00	1.66E-05	1.74E-
6	0.00E+00	6.08E-07	0.00E+00	0.00E+00	7.26E-06	3.48E-03	6.89E-06	0.00E+00	0.00E+00	3.49E-
7	0.00E+00	5.40E-07	0.00E+00	0.00E+00	0.00E+00	1.50E-05	2.37E-03	1.31E-05	0.00E+00	2.40E-
8	0.00E+00	1.82E-05	0.00E+00	0.00E+00	0.00E+00	0.00E+00	1.89E-05	2.20E-03	0.00E+00	2.24E-

Table 6 Absorption fractions from source to target for one cavity unit for tritium

Compare the results from table 5 and 6, the tritium dose is much more localized due to the smaller beta-particle range of tritium. For both tritium and ^{14}C, most of the dose is deposited in marrow due to the large proportion of marrow in the cavity unit.

Future work

The final version of the cavity model has not been completed, so the absorption fractions are only simulated for one cavity unit. Multiple cavities are needed to better simulate the real bone when the model is finalized. The uniqueness of Dr. Richardson's new bone compartmental model is that it allows for better accommodation of the dynamic physiological reality of the bone. However the MC simulation assumed that the

BMU is static in this work. So the dynamic nature of the BMU should be simulated in the future work. In future work, the chord distributions for marrow and bone should also be generated and compared to the data reported in the literature.

References

Cross WG, Ing H, Freedman N, (1983) "A short atlas of beta-ray Spectra", *Phys. Med. Biol.*, **28**: 1251-1260

International Commission on Radiological Protection (ICRP), (1975) "Reference man: Anatomical, physiological and metabolic characteristics", Oxford: Pergamon Press, ICRP Publication 23

Woodard HQ, White DR, (1986) "The composition of body tissues", *Brit J Radiol*, **59**: 1209-1219

Appendix III Fitting programs

Shell:

```
c MQINITA1.FOR ((Initial section of program))
c*****************************************************************
c VARIABLE DICTIONARY
c
c AA1() - first guess at parameters
c ADEV() - deviation
c AL1    - magnitude of alpha 1 peak
c AL1ERR - error of magnitude of alpha 1 peak
c BE1    - magnitude of beta 1 peak
c BE1ERR - error of magnitude of beta 1 peak
c CO1    - magnitude of coherent peak
c CO1ERR  - error of magnitude of coherent peak
c CPOS   - position of coherent peak (in channels)
c FNAM   - name of data file (eg. in c:\ff\ directory)
c       Up to 35 letters long, including path
c FT1    - variable used to remove magnitude of peak from FIT
c       to WORK
c FT1ERR - the error of the peak of FT1
c G      - gain (eV/channel)
c ICOM() - comments to add to output file (header)
c IDTE() - date to add to output file (header)
c IH2()  - random number seed
c III    - counter to keep track of number of files
c INUM   - the number of files that are in the data file
c IRES   - variable used to replace I in specifying ADEV(I)
c ISUB   - variable used to indicate if data is for phantoms or people
c       ISUB = 0 if people
c       ISUB = 1 if phantoms
c ITEST  - variable used to determine whether or not to plot data
c       ITEST = 1 if data IS to be plotted for each region
c       ITEST = 0 if NOT
c NF     - variable used to choose which subroutine is run
c NPTS   - number of channels
c NR     - number of parameters to be fitted over a restricted
c       range
c NST    - start channel
c NTERMS - number of parameters to be fitted (max 10)
c NTOP   - last channel number (NTOP = NPTS + NST -1)
c OFSET  - channel offset
c OUT1   - first output file - contains only peak amplitudes and
c       their errors
c OUT2   - second output file - contains the more complete output
c RA     - ratio of alpha 1 amplitude to coherent amplitude
```

```
c  RAERR   - error of RA  (std. dev)
c  RB      - ratio of beta 1 amplitude to coherent amplitude
c  RBERR   - error of RB  (std. dev)
c  SA      - slope of alpha calibration line
c  SAERR   - error of SA  (std. dev)
c  SB      - slope of beta calibration line
c  SBERR   - error of SB  (std. dev)
c  BA      - y-intercept of alpha calibration line
c  BAERR   - error of BA  (std. dev)
c  BB      - y-intercept of beta calibration line
c  BBERR   - error of BB  (std. dev)
c  COVA    - covariance between SA and BA for alpha calib. line
c  COVB    - covariance between SB and BB for beta calib. line
c  PPMA    - lead concentration obtained via alpha 1 peak amplitude
c  PPMAER - error of PPMA  (std. dev)
c  PPMB    - lead concentration obtained via beta 1 peak amplitude
c  PPMBER - error of PPMB  (std. dev)
c  PPM     - lead concentration obtained by a weighted mean of
c         PPMA and PPMB
c  PPMERR - error of PPM  (std. dev)
c  STPARA - name of file which contains the starting parameters
c  SBNAME - name of subroutine to add to output file (header)
c
c*****************************************************************
c
c  specification of variables
      CHARACTER*50 INFILE,OUTFILE,OUT1,OUT2,OUT3,OUT4,NAMEFILE
      CHARACTER*80 DATE, COMMENT1, COMMENT2, COMMENT3
      DIMENSION IRESS(10)
c
      CHARACTER*50 SBNAME, FNAM
      CHARACTER*30 IDTE
      CHARACTER*35 STPARA, SCALIB
      DIMENSION ICOM(108), AA1(10), ADEV(10), IH(2),
     + OFSETS(500), HH(500), WW(500)
      DATA AA1/10*0./
c
c  Initialize variables:
      IH(1) = 2
      IH(2) = 4
      CPOS  = 0.
      ALI   = 0.
      ALIERR = 0.
      BEI   = 0.
      BEIERR = 0.
      RA    = 0.
```

```
      RAERR  = 0.
      RB     = 0.
      RBERR  = 0.
      SA     = 0.
      SAERR  = 0.
      SB     = 0.
      SBERR  = 0.
      BA     = 0.
      BAERR  = 0.
      BB     = 0.
      BBERR  = 0.
      COVA   = 0.
      COVB   = 0.
      PPMA   = 0.
      PPMAER = 0.
      PPMB   = 0.
      PPMBER = 0.
      PPM    = 0.
      PPMERR = 0.
      COI    = 0.
      COIERR = 0.
      OUT1   = '                    '
      OUT2   = '                    '
      OUT3   = '                    '
      STPARA = '                      '
      SCALIB = '                      '
c
c  Tell that output will be written to disk and ask for filename
      WRITE(*,30)
   30 FORMAT(1X,'Please enter the name of the input file (including the
     +path and extension:'/,1X,'eg. C:\datafile\filelist.inp')
      WRITE(*,40)
   40 FORMAT(1X,'NOTE: The name of the file can have up to 45 characters
     + (including the path).'/,1X,'This file MUST already exist.')
      WRITE(*,*)
      READ(5,'(A)') NAMEFILE
      WRITE(*,*)
c
c  Read from file the names of the output files which are to be produced
      OPEN(UNIT=9, FILE=NAMEFILE, STATUS='OLD')
      READ(9, 50) OUTFILE
   50 FORMAT(A50)
 2010 CONTINUE
c
c  Add correct extensions to the OUTFILE name
c  and create OUT1,2,3,4 names, as same name, with .res, .ful, .dat
```

```
c  and .plt extensions
      OUT1=OUTFILE
      OUT2=OUTFILE
      OUT3=OUTFILE
      INCHECK = 0
      DO 100 I=1,50
       IF ((OUTFILE(I:I) .EQ. ' ') .AND. (INCHECK .EQ. 0)) THEN
        OUT1(I:I+3) = '.RES'
        OUT2(I:I+3) = '.FUL'
        OUT3(I:I+3) = '.DAT'
        INCHECK=1
       ENDIF
  100 CONTINUE
      WRITE(*,101)
  101 FORMAT(1X,'OUTPUT WILL BE WRITTEN TO FILES:')
      WRITE(*,110) OUT1, OUT2, OUT3
  110 FORMAT(1X,A50)
c
c  Open files for input and output
      L1=0
c  Open OUT1 as unit #3, OUT2 as unit #7, and OUT3 as unit #8
      OPEN(UNIT=3, FILE=OUT1, STATUS='NEW')
      OPEN(UNIT=7, FILE=OUT2, STATUS='NEW')
      OPEN(UNIT=8, FILE=OUT3, STATUS='NEW')
c  Write name of output files to top of OUT1, and OUT2:
      WRITE(3, 66) OUT1
      WRITE(7, 66) OUT2
      WRITE(8, 66) OUT3
   66 FORMAT(1X, 'Output filename: ',A35,/)
c
      READ(9, 120) DATE, COMMENT1, COMMENT2, COMMENT3
  120 FORMAT(A80,/,A80,/,A80,/,A80)
c     WRITE(*,122) DATE, COMMENT1, COMMENT2, COMMENT3
c  122 FORMAT(1X,A80,/,1X,A80,/,1X,A80,/,1X,A80)
c
      L1=L1+1
      WRITE(3,120) DATE, COMMENT1, COMMENT2, COMMENT3
      WRITE(7,120) DATE, COMMENT1, COMMENT2, COMMENT3
      WRITE(8,120) DATE, COMMENT1, COMMENT2, COMMENT3
c  Writing a line of -'s:
      WRITE(3,445)
      WRITE(7,445)
      WRITE(8,445)
  445 FORMAT(/75('-'))
      READ(9, 90) IFILES
   90 FORMAT(I6)
```

```
      WRITE(*,*) IFILES
      NFOLD=0
c  loop for number of files being analysed
c  end of loop must be outside all main individual analysis bits....
      DO 200 IOUTER = 1,IFILES
      READ(9,125) INFILE
      FNAM=INFILE
  125 FORMAT(A50)
      WRITE(*,*) INFILE
      READ(9,*) NF
      IF (NF .EQ. 11) THEN
       READ(9,*)  OFSET, NST, NPTS, G, ISUB, IH(1), IH(2)
       NTERMS = 7
       SBNAME = 'COHERENT with floating width and height          '
       IF (NFOLD .NE. NF) THEN
        WRITE(8,126)
  126  FORMAT('Init ChiSq',5X,'Init A1',6X,'Init A2',6X,'Init A3',6X,
     + 'Init A4',6X,'Init A5',6X,'Init A6',6X,'Init A7',4X,
     + 'Final ChiSq',4X,'Finl A1',6X,'Sig A1',7X,'Finl A2',6X,'Sig A2',
     + 7X,'Finl A3',6X,'Sig A3',7X,'Finl A4',6X,'Sig A4',7X,'Finl A5',
     + 6X,'Sig A5',7X,'Finl A6',6X,'Sig A6',7X,'Finl A7',6X,'Sig A7',
     + 24X,'Filename')
        NFOLD=NF
       ENDIF
      ELSE
       IF (NF .EQ. 1) THEN
        NTERMS = 5
        SBNAME = 'COHERENT with fixed width and height             '
        READ(9,*)  OFSET, NST, NPTS, G, ISUB, IH(1), IH(2), W, H
       ELSEIF (NF.EQ.2) THEN
        NTERMS = 4
        SBNAME = 'BETA with linked amplitudes, Ca linked to coherent'
        READ(9,*)  OFSET,NST,NPTS,G,ISUB,IH(1),IH(2),W,H,CPOS,CO1
       ELSEIF (NF.EQ.3) THEN
        NTERMS = 6
        SBNAME = 'ALPHA with linked amplitudes                     '
        READ(9,*)  OFSET, NST, NPTS, G, ISUB, IH(1), IH(2), W, H
        IF (NFOLD .NE. NF) THEN
        WRITE(8,127)
  127  FORMAT('Init ChiSq',5X,'Init A1',6X,'Init A2',6X,'Init A3',6X,
     + 'Init A4',6X,'Init A5',6X,'Init A6',4X,
     + 'Final ChiSq',4X,'Finl A1',6X,'Sig A1',7X,'Finl A2',6X,'Sig A2',
     + 7X,'Finl A3',6X,'Sig A3',7X,'Finl A4',6X,'Sig A4',7X,'Finl A5',
     + 6X,'Sig A5',7X,'Finl A6',6X,'Sig A6',24X,'Filename')
        NFOLD=NF
       ENDIF
```

```
      ENDIF
     ENDIF
     Write(*,*) SBNAME
c
     READ(9,*) (AA1(J), J=1,NTERMS)
c
c  Initialize all deviations, ADEV(), to zero:
     DO 1205, I = 1 , NTERMS
     ADEV(I) = 0.
     IRESS(I)=0
 1205 CONTINUE
c
     READ(9,*) NR
     READ(9,*) (IRESS(J), ADEV(IRESS(J)), J=1,NR)
c
     OUT4=INFILE
     INCHECK = 0
     DO 1001 I=1,50
      IF ((INFILE(I:I) .EQ. ' ') .AND. (INCHECK .EQ. 0)) THEN
       OUT4(I-4:I) = '.PLT'
       INCHECK=1
      ENDIF
 1001 CONTINUE
c
c  Open files for PLOT output
     OPEN(UNIT=2, FILE=OUT4, STATUS='NEW')
     WRITE(2,446) FNAM
  446 FORMAT('Plotting file ',A50)
     WRITE(2,447)
  447 FORMAT('Output from Marquardt fit.  Data is in columns:',
    +/,5x,'Channel number',2x,'Counts',2x,'Fitted counts')

c  Output to file OUT2, full output file
c  Writing the subroutine to OUT2:
     WRITE(7,448) SBNAME
  448 FORMAT(/,1X,'SUBROUTINE:  ',A50,)
c
c  Writing the number of channels and starting channel to OUT2:
     WRITE(7,449) NPTS, NST
  449 FORMAT(10X,I3,' channels starting in channel ',I3)
c
c  Write starting parameters to output location:
     WRITE(7,1218)
 1218 FORMAT(11X,'The starting parameters are:')
     DO 1203, I = 1, NTERMS
      WRITE(7,1217) I, AA1(I)
```

```
 1217  FORMAT(16X, 'A(',I2,') = ',G12.5)
 1203 CONTINUE
c
c  Output the number of parameters to be fitted over a restricted range
     WRITE(7,1201) NR
 1201 FORMAT(10X,I3,' RESTRICTED PARAMETERS:')
c
c  output restricted parameters and deviations
     DO 1202 J=1, NR
      IRES=IRESS(J)
     WRITE(7,310) IRES, AA1(IRES), ADEV(IRES)
  310 FORMAT(16X,'A(',I2,') = ',G12.5,' +/- ',G12.5)
 1202 CONTINUE
c
c  Write the 2 random numbers to desired output:
     WRITE(7,1211) IH(1), IH(2)
 1211 FORMAT(/,1X,'random number entry points ',I5,1X,I5)
c
c  Set ITEST = 0 so don't graph
     ITEST = 0
c  Set the last channel number (NTOP)
     NTOP=NPTS+NST-1
c  Re-initialize FT1 and FT1ERR:
     FT1    = 0.
     FT1ERR = 0.
c  SEED bit copied here from 2pbfit1 on
     CALL SEED(IH(1))
c  Run the fit program:
     CALL FIT(NTERMS, NPTS, NST, NTOP, NR, AA1, ADEV, IH, ITEST, FNAM,
    + OFSET, CPOS, FT1, FT1ERR, NF, G, W, H, ISUB, CO1)
c  Writing a line of -'s:
     WRITE(3,445)
     WRITE(7,445)
c  Close analysed spectrum file
     CLOSE(UNIT=2, STATUS='KEEP')
c  End of loop for multiple file analysis
  200 CONTINUE
c  Close all remaining units
     CLOSE(UNIT=9, STATUS='KEEP')
     CLOSE(UNIT=3, STATUS='KEEP')
     CLOSE(UNIT=7, STATUS='KEEP')
     CLOSE(UNIT=8, STATUS='KEEP')
c  End of program
     END
```

Subroutine 1:

```
c CERFVWA1.FOR ((Called as FUNCCW))
c Function for coherent and lead beta 2 peaks.
      FUNCTION FUNCCW(X, A, G, W, H)
c
c
c Variable Dictionary
c  A(1) - position of coherent
c  A(2) - amplitude of coherent
c  A(3) - width of coherent
c  A(4) - amplitude of LEAD beta 2
c       NOTE: in this program, the position of the beta 2 is fixed
c            with respect to the position of the coherent peak
c  A(5) - amplitude of exponential background
c  A(6) - exponent coefficient of exponential background
c  A(7) - step height (fraction of peak height)
c  SIGMAA(I) - error of A(I)
c  G - gain in eV/channel
c  X - channel number (position)
c  Z1 - gaussian parameter for the coherent peak
c  Z2 - gaussian parameter for the Beta 2 I
c  Z3 - gaussian parameter for the Beta 2 II
c  ZZ1 - exponential of gaussian for coherent: ZZ=exp(-Z*Z)
c      (depending on the magnitude of Z)
c  ZZ2 - exponential of gaussian for Beta 2 I
c  ZZ3 - exponential of gaussian for Beta 2 II
      DIMENSION A(10)
c
c Evaluation of gaussian parameters:
      Z1 = (X - A(1))/A(3)
      Z2 = (X - (A(1) - (668./G)))/A(3)
      Z3 = (X - (A(1) - (802./G)))/A(3)
c Evaluate the gaussian exponents, if they are large enough to avoid
c underflow, otherwise leave as zero:
      ZZ1=0.0
      ZZ2=0.0
      ZZ3=0.0
      IF(ABS(Z1).LT.5) ZZ1=EXP(-Z1*Z1)
      IF(ABS(Z2).LT.5) ZZ2=EXP(-Z2*Z2)
      IF(ABS(Z3).LT.5) ZZ3=EXP(-Z3*Z3)
c
c Function:
      FUNCCW = A(2)*(ZZ1 + A(7)*erfc(Z1))
     +       + A(4)*((ZZ2 + A(7)*erfc(Z2))
     +        + 0.509*(ZZ3 + A(7)*erfc(Z3)))
     +         + A(5)*EXP(A(6)*X)
      RETURN
```

```
      END
c
c  Subroutine to print peak amplitudes and their errors to OUT1
      SUBROUTINE FWRCW(A, SIGMAA, J)
      DIMENSION A(10), SIGMAA(10)
      WRITE(J,220) A(2), SIGMAA(2)
  220 FORMAT(1X, 'Coherent peak amplitude is: ',G12.5,' +/- ',G12.5)
      WRITE(J,225) A(1), SIGMAA(1)
  225 FORMAT(1X, 'Coherent peak position is:  ',G12.5,' +/- ',G12.5)
      WRITE(J,230) A(3), SIGMAA(3)
  230 FORMAT(1X, 'Coherent peak width is:    ',G12.5,' +/- ',G12.5)
c
c  Writing a line of -'s:
      WRITE(J,445)
  445 FORMAT(/75('-'))
c
      RETURN
      END
```

Subroutine 2:

```
c  MQALPH1.FOR  ((Called as FUNCA))
c
c  Function for lead alpha peaks.
c  Variable dictionary
c  A(1) - position of lead alpha 1
c  A(2) - amplitude of lead alpha 1
c  A(3) - amplitude of exponential background 1
c  A(4) - exponent coefficient of exponential background 1
c  A(5) - amplitude of exponential background 2
c  A(6) - exponent coefficient of exponential background 2
c  SIGMAA(I) - error of A(I)
c  W - width, in channels
c  H - height
c  G - gain in eV/channel
c  X - channel number
c  Z - gaussian parameter for lead alpha 1 peak (not squared)
c  V - gaussian parameter for lead alpha 2 peak
c  ZZ - exponential of gaussian for lead alpha 1
c  VV - exponential of gaussian for lead alpha 2
c
      REAL FUNCTION FUNCA(X, A, G, W, H)
      DIMENSION A(10)
c
c  Evaluation of gaussian parameters:
      Y = (X - (A(1) - (2165./G)))/W
      Z = (X - A(1))/W
```

```
c
c  Evaluate the gaussian exponents, if they are large enough to avoid
c  underflow, otherwise leave as zero:
      YY = 0.
      ZZ = 0.
      IF(ABS(Y).LT.5) YY=EXP(-Y*Y)
      IF(ABS(Z).LT.5) ZZ=EXP(-Z*Z)
c
c  Evaluate the function
      FUNCA = A(2) * (ZZ + H*ERFC(Z)) + (0.593*A(2)) * (YY + H*ERFC(Y))
     1 + A(3) * EXP(A(4)*X) + A(5) * EXP(A(6)*X)
      RETURN
      END
c
c
c  Subroutine to print alpha 1 peak amplitudes and error to OUT1
      SUBROUTINE FWRA(A, SIGMAA, J)
      DIMENSION A(10), SIGMAA(10)
      WRITE(J,220) A(2), SIGMAA(2)
  220 FORMAT(1X, 'Alpha 1 peak amplitude is:  ',G12.5,' +/- ',G12.5)
      RETURN
      END
```

Subroutine 3:

```
c  MQBETA1.FOR  ((called as FUNCB))
c  Function for lead beta peaks.
c  Variable Dictionary
c   A(1) - amplitude of beta 1
c   A(2) - amplitude of exponential background
c   A(3) - exponent coefficient of exponential background
c   A(4) - exponential on calcium & phosphorus edges
c   CO1  - height of coherent peak
c   CPOS - position of coherent peak (in channels)
c   ISUB - variable used to indicate if data is for phantoms or people
c        ISUB = 0 if people
c        ISUB = 1 if phantoms
c   SIGMAA(I) - error of A(I)
c   W - width, in channels (fixed)
c   H - height (fixed)
c   G - gain in eV/channel
c   X - channel number (position)
c   Y - gaussian parameter for beta 3 peak (not squared)
c   Z - gaussian parameter for beta 1 peak (not squared)
c   YY - exponential of gaussian for beta 3
c   ZZ - exponential of gaussian for beta 1
c   CA - gaussian parameter for calcium edge feature
```

```
c  POSCA - used to calculate CA and in Ca exponential background
c  P - gaussian parameter for phosphorus edge feature
c  POSP - used to calculate P and in P exponential background
c  S - gaussian parameter for sulphur edge feature
c  POSS - used to calculate S and in S exponential background
c
c
      REAL FUNCTION FUNCB(X, A, CPOS, G, W, H, ISUB, CO1)
      DIMENSION A(10)
c
c  Evaluate function depending on ISUB ( 0 = people, 1 = phantom)
      IF (ISUB.EQ.0) THEN
c
c  Evaluation of PEOPLE gaussian parameters:
          Z = (X - (CPOS - (3099./G)))/W
          Y = (X - (CPOS - (3585./G)))/W
          POSCA = X - (CPOS - (4038./G))
          CA = POSCA/W
          POSP = X - (CPOS - (2146./G))
          P = POSP/W
c
c  Evaluate the PEOPLE gaussian exponents, if they are large enough to
c  avoid underflow, otherwise leave as zero:
          ZZ = 0.
          YY = 0.
          IF(ABS(Z).LT.5)  ZZ = EXP(-Z*Z)
          IF(ABS(Y).LT.5)  YY = EXP(-Y*Y)
c
c  PEOPLE Function: (evaluating the gaussian peak, taking into account
c  the step function, and phosphorus and calcium edges):
        FUNCB = A(1) *(ZZ + H*ERFC(Z)) + (0.523*A(1)) *(YY+H*ERFC(Y))
     +  + A(2) * EXP(A(3)*X) + 0.0056*W *CO1 *(EXP(A(4)*POSCA) *
     1  ERFC(CA) + 0.21 * EXP(A(4)*POSP) * ERFC(P))
c
      ELSEIF (ISUB.EQ.1) THEN
c
c  Evaluation of PHANTOM gaussian parameters:
      Z = (X - (CPOS - (3099./G)))/W
      Y = (X - (CPOS - (3585./G)))/W
      POSCA = X - (CPOS - (4038./G))
      CA = POSCA/W
      POSS = X - (CPOS - (2472./G))
      S = POSS/W
c
c  Evaluate the PHANTOM gaussian exponents, if they are large enough to
c  avoid underflow, otherwise leave as zero:
```

```
      ZZ = 0.
      YY = 0.
      IF(ABS(Z).LT.5)  ZZ = EXP(-Z*Z)
      IF(ABS(Y).LT.5)  YY = EXP(-Y*Y)
c
c  PHANTOM Function: (evaluating the gaussian peak, taking into account
c  the step function, and phosphorus and calcium edges):
        FUNCB = A(1) *(ZZ + H*ERFC(Z)) + (0.523*A(1)) *(YY+H*ERFC(Y))
     +   + A(2) * EXP(A(3)*X) + 0.005*W*CO1 *(EXP(A(4)*POSCA) * ERFC(CA)
     +   + 0.16 * EXP(A(4)*POSS) * ERFC(S))
c
      ENDIF
c
      RETURN
      END
c
c  Subroutine to print peak amplitudes and their errors to the file
c  which was specified when asked for in DCWORK, namely: OUT1
      SUBROUTINE FWRB(A, SIGMAA, J)
      DIMENSION A(10), SIGMAA(10)
c
      WRITE(J,220) A(1), SIGMAA(1)
  220 FORMAT(1X, 'Beta 1 peak amplitude is:  ',G12.5,' +/- ',G12.5)
      RETURN
      END
```

Subroutine 4:

```
c  MQCOREA1.FOR  ((Called as FIT))
c     Calls to DERIVA to work out derivatives numerically
c
      SUBROUTINE FIT(NTERMS, NPTS, NST, NTOP, NR, A1, DEV, IH, ITEST,
     1 FNAM, OFSET, CPOS, FT1, FT1ERR, NF, G, W, H, ISUB, CO1)
c
c*****************************************************************
c  VARIABLE DICTIONARY
c
c  A1() - Initial guess at parameter
c  A() - New parameter value
c  CO1 - amplitude of coherent peak
c  CPOS - position of coherent peak (in channels)
c  DERIV() - derivative of parameter
c  DEV() - Deviation
c  FNAM - name of data file (in A: drive)
c  FT1    - variable used to remove magnitude of peak from FIT
c         to WORK
c  FT1ERR - the error of the peak of FT1
```

```
c  G - gain (eV/channel)
c  IH() - Random number seed
c  ISUB  - variable used to indicate if data is for phantoms or people
c        ISUB = 0 if people
c        ISUB = 1 if phantoms
c  ITEST - determines whether or not to plot data
c        ITEST = 1 if data IS to be plotted for each region
c        ITEST = 0 if NOT
c  NF - variable used to choose which subroutine is to be run
c  NFREE - number of degrees of freedom (NFREE = NPTS - NTERMS)
c  NPTS - number of channels
c  NR - number of parameters to be fitted over restricted
c     range
c  NST - start channel
c  NTERMS - number of parameters
c  NTOP - last channel number
c  OFSET - channel offset
c  OUT1 - first output file - contains only peak amplitudes and
c       their errors
c  OUT2 - second output file - contains the more complete output
c  SIGMAA(i) - error of A(i)
c  SPEC() - used to read data from data file
c  TEMPY - temporary Y used in loop
c  X() - channel numbers
c  Y() - data values
c  YFIT() - data values of fit function
c
c*****************************************************************
c
c  specification of variables
     CHARACTER*35 FNAM
     INTEGER*4 SPEC,CH,CHFT
     REAL*8 TEMPY
     DIMENSION SPEC(32,64)
     DOUBLE PRECISION ARRAY
     DIMENSION X(1024), Y(2048), YFIT(1024), WEIGHT(1024), A(10),
    + A1(10), B(10), BETA(10), ALPHA(10,10), ARRAY(10,10), DERIV(10),
    + DEV(10), SIGMAA(10), IH(2), YFITO(1024)
c
c  Set all Y and YFIT values to zero (avoid problems if input file is short)
     DO 2000 I=1,1024
      Y(I)=0.
      Y(I+1024)=0.
      YFIT(I)=0.
      YFITO(I)=0.
2000 CONTINUE
```

```
c  Initialize new parameters to initial parameter guesses:
      DO 898 I=1,NTERMS
      A(I)=A1(I)
  898 CONTINUE
c
c  If are running the first analysis model (ie. coherent) then write
c  the spectrum file name to OUT1 and OUT2, and its offset to OUT2
c  Write to screen that are analyzing the datafile:
c  Write to OUT1 and OUT2 which program is being run:
      IF (NF.EQ.11) THEN
       WRITE(6,2190)
       WRITE(3,2190)
       WRITE(7,2190)
       WRITE(3,36) FNAM
       WRITE(7,36) FNAM
       WRITE(7,2180) OFSET
      ELSEIF (NF.EQ.1) THEN
       WRITE(6,2200)
       WRITE(3,2200)
       WRITE(7,2200)
       WRITE(3,36) FNAM
       WRITE(7,36) FNAM
       WRITE(7,2180) OFSET
      ELSEIF (NF.EQ.2) THEN
       WRITE(6,2210)
       WRITE(3,2210)
       WRITE(7,2210)
      ELSEIF (NF.EQ.3) THEN
       WRITE(6,2220)
       WRITE(3,2220)
       WRITE(7,2220)
      ENDIF
      WRITE(6,39) FNAM
   36 FORMAT(/, /, 1X, 'FILE ANALYZED: ',A50)
   39 FORMAT(1X,'analyzing ', A35)
 2180 FORMAT(1X,'OFFSET:', 2X, f6.0,/)
 2190 FORMAT(1X,'COHERENT PROGRAM, floating width:')
 2200 FORMAT(1X,'COHERENT PROGRAM, fixed width:')
 2210 FORMAT(1X,'BETA PROGRAM:')
 2220 FORMAT(1X,'ALPHA PROGRAM:')
c  Open the data file, specifying the record length RECL.  Read data:
      OPEN(1,FILE=FNAM,ACCESS='DIRECT',RECL=128)
      DO 99 J=1,64
      READ(1,REC=J+1) (SPEC(I,J),I=1,32)
   99 CONTINUE
```

```
      CH=1
c
c  Put the data in Y():
      DO 600 J=1,64
      DO 700 K=1,32
      Y(CH)=SPEC(K,J)
      CH=CH+1
  700 CONTINUE
  600 CONTINUE
c
      CHFT=1
c
c  Shift the Y(I)'s so they start at the channel offset:
      DO 650 I=OFSET,2048
      TEMPY=Y(I)
      Y(CHFT)=TEMPY
c  Added 19/4/99; set Y(I) to zero after picking up value.  Otherwise
c  data will repeat from OFSET upwards
c     Y(I)=0.
      CHFT=CHFT+1
  650 CONTINUE
c
      CLOSE(UNIT=1,STATUS='KEEP')
c
c  Set X(I) = channel # (This is done for the channels from start
c  channel, NST, to last channel, NTOP):
      DO 211 I=NST,NTOP
      X(I)=I
  211 CONTINUE
c
c  Initialize flambda:
      FLAMDA=0.001
c
c  Calculate number of degrees of freedom:
   11 NFREE=NPTS-NTERMS
      IF(NFREE.LE.0) THEN
         CHISQR=0.
         GOTO 170
      ENDIF
c
c  Evaluate YFIT() using the functions FUNCA, FUNCB, FUNCC:
   20 DO 680 I=NST,NTOP
         IF (NF.EQ.11) THEN
            YFIT(I) = FUNCCW(X(I), A, G, W, H)
         ELSEIF (NF.EQ.1) THEN
            YFIT(I) = FUNCC(X(I), A, G, W, H)
```

```
      ELSEIF (NF.EQ.2) THEN
         YFIT(I) = FUNCB(X(I), A, CPOS, G, W, H, ISUB, CO1)
      ELSEIF (NF.EQ.3) THEN
         YFIT(I) = FUNCA(X(I), A, G, W, H)
      ENDIF
  680 CONTINUE
c  Evaluate chi-squared:
     CHISQ1=FCHIS(Y,NST,NTOP,NFREE,YFIT)
     CHIINI=CHISQ1
c  Evaluate Weights:
     DO 30 I=NST,NTOP
      IF(Y(I).LT.0) THEN
        WEIGHT(I) = 1./(-Y(I))
      ELSEIF(Y(I).GT.0) THEN
        WEIGHT(I) = 1./Y(I)
      ELSE
        WEIGHT(I) = 1.
      ENDIF
   30 CONTINUE
c
c  Evaluate Alpha and Beta matrices:
   31 DO 34 J=1,NTERMS
     BETA(J)=0.
     DO 34 K=1,J
   34 ALPHA(J,K)=0.
   41 DO 50 I=NST,NTOP
     CALL DERIVA(X(I), A, DERIV, G, W, H, CPOS, ISUB, CO1, NTERMS, NF)
     DO 46 J=1,NTERMS
      IF (NF.EQ.11) THEN
        BETA(J)=BETA(J)+WEIGHT(I)*(Y(I)-FUNCCW(X(I),A,G,W,H))
     1   * DERIV(J)
      ELSEIF (NF.EQ.1) THEN
        BETA(J)=BETA(J)+WEIGHT(I)*(Y(I)-FUNCC(X(I),A,G,W,H))
     1   * DERIV(J)
      ELSEIF (NF.EQ.2) THEN
       BETA(J)=BETA(J)+WEIGHT(I)*(Y(I)-
     1       FUNCB(X(I),A,CPOS,G,W,H,ISUB,CO1)) * DERIV(J)
      ELSEIF (NF.EQ.3) THEN
        BETA(J)=BETA(J)+WEIGHT(I)*(Y(I)-FUNCA(X(I),A,G,W,H))
     1         * DERIV(J)
      ENDIF
     DO 46 K=1,J
   46  ALPHA(J,K)=ALPHA(J,K)+WEIGHT(I)*DERIV(J)*DERIV(K)
   50 CONTINUE
   51 DO 53 J=1,NTERMS
     DO 53 K=1,J
```

```
  53 ALPHA(K,J)=ALPHA(J,K)
c
c  Evaluate Chi Square at starting point
  61  DO 62 I=NST,NTOP
        IF (NF.EQ.11) THEN
          YFIT(I) = FUNCCW(X(I), A, G, W, H)
        ELSEIF (NF.EQ.1) THEN
          YFIT(I) = FUNCC(X(I), A, G, W, H)
        ELSEIF (NF.EQ.2) THEN
          YFIT(I) = FUNCB(X(I), A, CPOS, G, W, H, ISUB, CO1)
        ELSEIF (NF.EQ.3) THEN
          YFIT(I) = FUNCA(X(I), A, G, W, H)
        ENDIF
  62 CONTINUE
  63 CHISQ1=FCHIS(Y,NST,NTOP,NFREE,YFIT)
c
c  Write chi squared and new parameter values to screen and unit 7 (.ful)
      WRITE(6,120) CHISQ1,(A(I),I=1,NTERMS)
      WRITE(7,120) CHISQ1,(A(I),I=1,NTERMS)
  120 FORMAT(1X,'CHI SQ =',1X,G12.5,/,5(1X,G12.5),/,5(1X,G12.5))
c
c  Added bit to hold Yfit values from this chisq while testing
c  if it is best.  To be retrieved later if so....
      DO 620 I=NST,NTOP
        YFITO(I) = YFIT(I)
  620 CONTINUE
c
c  Invert modified curvature matrix to find new parameters
    71 DO 74 J=1,NTERMS
         DO 73 K=1,NTERMS
    73   ARRAY(J,K)=DBLE(ALPHA(J,K)/DSQRT(ALPHA(J,J))/DSQRT(ALPHA(K,K)))
    74 ARRAY(J,J)=DBLE(1.+FLAMDA)
    80 CALL MATINV(ARRAY,NTERMS,DET)
    81 DO 84 J=1,NTERMS
         B(J)=A(J)
         DO 84 K=1,NTERMS
    84 B(J)=B(J)+BETA(K)*SNGL(ARRAY(J,K))/DSQRT(ALPHA(J,J))
     +   /DSQRT(ALPHA(K,K))
       IF(NR.EQ.0) GO TO 91
       DO 308 J=1,NTERMS
        IF(DEV(J).EQ.0) GO TO 308
        IF(ABS(B(J)-A1(J)).LT.DEV(J)) GO TO 308
c
c  Get random number to reset variable(s) which have hit limits
        CALL RANDOM(YFL)
c  Line below modified 28/4/99 (IMS) to have *1.8 instead of *2
```

```
      B(J) = (YFL-.5)*1.8*DEV(J)+A1(J)
  308 CONTINUE
c  If Chi Square increases, increase FLAMDA and try again
   91 DO 92 I=NST,NTOP
      IF (NF.EQ.11) THEN
        YFIT(I) = FUNCCW(X(I), B, G, W, H)
      ELSEIF (NF.EQ.1) THEN
        YFIT(I) = FUNCC(X(I), B, G, W, H)
      ELSEIF (NF.EQ.2) THEN
        YFIT(I) = FUNCB(X(I), B, CPOS, G, W, H, ISUB, CO1)
      ELSEIF (NF.EQ.3) THEN
        YFIT(I) = FUNCA(X(I), B, G, W, H)
      ENDIF
   92 CONTINUE
   93 CHISQR=FCHIS(Y,NST,NTOP,NFREE,YFIT)
      CHIDIF=CHISQ1-CHISQR
      IF(CHIDIF)94,101,101
   94 IF(ABS(CHIDIF)-1.E-03) 33,33,95
   95 FLAMDA=10.*FLAMDA
      GOTO 71
c  Evaluate parameters and test for convergence
  101 FLAMDA=FLAMDA/10.
      DO 103 J=1,NTERMS
      A(J) = B(J)
  103 CONTINUE
      IF(CHIDIF-.001*CHISQR)115,31,31
   33 CHISQR=CHISQ1
c  Added bit to retrieve YFIT values from chisq1 from earlier
      DO 621 I=NST,NTOP
       YFIT(I) = YFITO(I)
  621 CONTINUE
  115 CALL MATINV(ARRAY,NTERMS,DET)
      FLAMDA = 0.001
      DO 709 J=1,NTERMS
       ARRAY(J,J) = DBLE(1.+FLAMDA)
  709 CONTINUE
      CALL MATINV(ARRAY,NTERMS,DET)
c
c  Write the final value of chi-squared to OUT1 and OUT2:
      WRITE(3,55) CHISQR
      WRITE(7,55) CHISQR
   55 FORMAT(1X, 'FINAL chi squared  = ',G12.5)
c  Calculate the errors and write the final parameter values and
c  errors to OUT2:
      DO 107 J=1,NTERMS
      SIGMAA(J)=DSQRT(SNGL(ARRAY(J,J))/ALPHA(J,J))
```

```
      WRITE(7,130) J, A(J), SIGMAA(J)
  130 FORMAT(5X,'    A(',I1,') = ',G12.5,' +- ',G12.5)
  107 CONTINUE
c
c  Added section to write out ChiSq, Peak amp, error, position,
c  error, width, error, ETC and file name to file for excel
      IF (NF .EQ. 11) THEN
       WRITE(8,135) CHIINI,A1(1),A1(2), A1(3), A1(4), A1(5),
     + A1(6),A1(7), CHISQR,A(1),SIGMAA(1),A(2),SIGMAA(2),A(3),
     + SIGMAA(3),A(4),SIGMAA(4),A(5),SIGMAA(5),A(6),SIGMAA(6),
     + A(7), sigmaa(7), FNAM
  135  FORMAT(23(G12.5,1X),A50)
      ENDIF
      IF (NF .EQ. 3) THEN
       WRITE(8,136) CHIINI,A1(1),A1(2),A1(3),A1(4),A1(5),A1(6),
     + CHISQR,A(1),SIGMAA(1),A(2),SIGMAA(2),A(3),SIGMAA(3),
     + A(4),SIGMAA(4),A(5),SIGMAA(5),A(6),SIGMAA(6),FNAM
  136  FORMAT(20(G12.5,1X),A50)
      ENDIF
c     Nieh
      IF (NF .EQ. 2) THEN
       WRITE(8,137) CHIINI, A1(1),A1(2),A1(3),A1(4),CHISQR,
     + A(1),SIGMAA(1),A(2),SIGMAA(2),A(3),SIGMAA(3),A(4),
     + SIGMAA(4),FNAM
  137  FORMAT(14(G12.5,1X),A50)

      END IF
c
      WRITE(6,*)
c
c  Experimental writing out of ch, counts, fitted counts - not sure
c  that final values of y and yfit are those corresponding to best fit...
      IOF=50
      IF (NST .LE. IOF) IOF=NST
      DO 1080 IPR = NST-IOF+1, NTOP+IOF
       IF (IPR .LT. NST) then
        WRITE(2,109) IPR+OFSET-1, Y(IPR)
       ELSEIF (IPR .LE. NTOP) THEN
        WRITE(2,108) IPR+OFSET-1, Y(IPR), YFIT(IPR)
       ELSE
        WRITE(2,109) IPR+OFSET-1,Y(IPR)
       ENDIF
 1080 CONTINUE
  108 FORMAT(G12.5, 2X, G12.5, 2X, G12.5)
  109 FORMAT(G12.5, 2X, G12.5)
```

```
c  Setting FT1 equal to the peak amplitude, and FT1ERR equal to the
c  error of the peak amplitude to take these values out of FIT to WORK.
c  For the coherent program, also set CPOS equal to the coherent peak
c  position.
c  Also writing the required amplitudes and errors and width to the
c  file OUT1 which is unit #3
      IF (NF.EQ.11) THEN
         FT1 = A(2)
         FT1ERR = SIGMAA(2)
         CPOS = A(1)
         CALL FWRCW(A, SIGMAA, 3)
      ELSEIF (NF.EQ.1) THEN
         FT1 = A(2)
         FT1ERR = SIGMAA(2)
         CPOS = A(1)
         CALL FWRC(A, SIGMAA, 3)
      ELSEIF (NF.EQ.2) THEN
         FT1 = A(1)
         FT1ERR = SIGMAA(1)
         CALL FWRB(A, SIGMAA, 3)
      ELSEIF (NF.EQ.3) THEN
         FT1 = A(2)
         FT1ERR = SIGMAA(2)
         CALL FWRA(A, SIGMAA, 3)
      ENDIF
c
      GOTO 38
c
c  Error message if have 0 or less d.o.f.
  170 WRITE(6,180)
  180 FORMAT(1X,'<=0 Degrees of Freedom',/)
c
c  Error message if cannot find spectrum file
   16 WRITE(6,37) FNAM
   37 FORMAT(1X,'Cannot find ',8A2)
c
   38 RETURN
c
c  not clear what purpose of this statement is, as it is beyond the
c  return from the subroutine....
 1099 CONTINUE
      END
```

Subroutine 5:

```
      SUBROUTINE MATINV(ARRAY,NORDER,DET)
      DOUBLE PRECISION ARRAY,AMAX,SAVE
```

```
      DIMENSION ARRAY(10,10),IK(10),JK(10)
   10 DET=1.
   11 DO 100 K=1,NORDER
C
C       FIND LARGEST ELEMENT ARRAY(I,J) IN REST OF MATRIX
C
      AMAX=0.
   21 DO 30 I=K,NORDER
      DO 30 J=K,NORDER
   23 IF(DABS(AMAX)-DABS(ARRAY(I,J)))24,24,30
   24 AMAX=ARRAY(I,J)
      IK(K)=I
      JK(K)=J
   30 CONTINUE
C
C     INTERCHANGE ROWS AND COLUMS TO PUT AMAX IN ARRAY(K,K)
C
   31 IF(AMAX)41,32,41
   32 DET=0.
      GOTO 140
   41 I=IK(K)
      IF(I-K)21,51,43
   43 DO 50 J=1,NORDER
      SAVE=ARRAY(K,J)
      ARRAY(K,J)=ARRAY(I,J)
   50 ARRAY(I,J)=-SAVE
   51 J=JK(K)
      IF(J-K)21,61,53
   53 DO 60 I=1,NORDER
      SAVE=ARRAY(I,K)
      ARRAY(I,K)=ARRAY(I,J)
   60 ARRAY(I,J)=-SAVE
C
C       ACCUMULATE ELEMENTS OF INVERSE MATRIX
C
   61 DO 70 I=1,NORDER
      IF(I-K)63,70,63
   63 ARRAY(I,K)=-ARRAY(I,K)/AMAX
   70 CONTINUE
   71 DO 80 I=1,NORDER
      DO 80 J=1,NORDER
      IF(I-K)74,80,74
   74 IF(J-K)75,80,75
   75 ARRAY(I,J)=ARRAY(I,J)+ARRAY(I,K)*ARRAY(K,J)
   80 CONTINUE
   81 DO 90 J=1,NORDER
```

```
   IF(J-K)83,90,83
  83 ARRAY(K,J)=ARRAY(K,J)/AMAX
  90 CONTINUE
     ARRAY(K,K)=1./AMAX
 100 DET=DET*AMAX
C
C       RESTORE ORDERING OF MATRIX
C
 101 DO 130 L=1,NORDER
     K=NORDER-L+1
     J=IK(K)
     IF(J-K)111,111,105
 105 DO 110 I=1,NORDER
     SAVE=ARRAY(I,K)
     ARRAY(I,K)=-ARRAY(I,J)
 110 ARRAY(I,J)=SAVE
 111 I=JK(K)
     IF(I-K)130,130,113
 113 DO 120 J=1,NORDER
     SAVE=ARRAY(K,J)
     ARRAY(K,J)=-ARRAY(I,J)
 120 ARRAY(I,J)=SAVE
 130 CONTINUE
 140 RETURN
     END
```

Subroutine 6:

```
c MQDERIV1.FOR  ((Called as DERIVA))
c Subroutine to calculate derivatives:
c Calculates derivatives numerically, thus removing need to have
c separate set of derivative formulae for each function.
c Changes each parameter by a set fraction.  Derivative is
c then be found by calculating the function at A+deltaA (giving F(A+)),
c and the function at A-deltaA (giving F(A-)); and then taking dF/dA to
c be (F(A+)-F(A-))/(2*deltaA)
c
      SUBROUTINE DERIVA(X,A,DERIV,G,W,H,CPOS,ISUB,CO1,NTERMS,NF)
c
      DOUBLE PRECISION AOLD,ACHAN,ADIFF
      DIMENSION A(10),DERIV(10)
      DOUBLE PRECISION YVAL,YPOS,YNEG
c
c Produce derivative for each parameter
      DO 1720 J1=1, NTERMS
c
c Store initial value for each parameter, as Double Precision
```

```
      AOLD = DBLE(A(J1))
c  Set value for fraction by which to change parameter.
      ACHAN=1.0d+02
c
c  Select function to find derivatives for, and calculate
c  the F(A+) and F(A-) values for this function.
c  Note that the SNGL and DBLE statements here are critical
 1730  IF (NF.EQ.11) THEN
          A(J1) = SNGL(AOLD * (1.0D+00 + 1.0D+00/ACHAN))
          YPOS = DBLE(FUNCCW(X, A, G, W, H))
          A(J1) = SNGL(AOLD * (1.0D+00 - 1.0D+00/ACHAN))
          YNEG = DBLE(FUNCCW(X, A, G, W, H))
          A(J1) =SNGL(AOLD)
       ELSEIF (NF.EQ.1) THEN
          A(J1) = SNGL(AOLD * (1.0D+00 + 1.0D+00/ACHAN))
          YPOS = FUNCC(X, A, G, W, H)
          A(J1) = SNGL(AOLD * (1.0D+00 - 1.0D+00/ACHAN))
          YNEG = FUNCC(X, A, G, W, H)
          A(J1) = AOLD
       ELSEIF (NF.EQ.2) THEN
          A(J1) = SNGL(AOLD * (1.0D+00 + 1.0D+00/ACHAN))
          YPOS = FUNCB(X, A, CPOS, G, W, H, ISUB, CO1)
          A(J1) = SNGL(AOLD * (1.0D+00 - 1.0D+00/ACHAN))
          YNEG = FUNCB(X, A, CPOS, G, W, H, ISUB, CO1)
          A(J1) = AOLD
       ELSEIF (NF.EQ.3) THEN
          A(J1) = SNGL(AOLD * (1.0D+00 + 1.0D+00/ACHAN))
          YPOS = FUNCA(X, A, G, W, H)
          A(J1) = SNGL(AOLD * (1.0D+00 - 1.0D+00/ACHAN))
          YNEG = FUNCA(X, A, G, W, H)
          A(J1) = AOLD
       ENDIF
c
c  Calculate derivative
c  (Note: no SNGL statement used here... may be worth adding if
c   fitting proves difficult)
      DERIV(J1) = (YPOS-YNEG)/(2.0D+00*AOLD/ACHAN)
c
c  If problems arise, may need line below....
c       if (DERIV(J1) .EQ. 0) DERIV(J1)=1.0E-16
c
 1720 CONTINUE
c
      RETURN
      END
```

Subroutine 7:

```
c  MQERFC1.FOR  ((Called as ERFC))
c  Function to calculate the complementary error function
      FUNCTION ERFC(X)
c
c  Calculation of the complementary error function
c  based on the algorithm given by Spanier and Oldham
c  (Spanier J and Oldham KB, 1987.  An Atlas of Functions.)
c  (Hemisphere Publishing Corporation, p385-393)
c
c  All variables are taken as double precision, and constants
c  are truncated with d+00 to provide maximum accuracy.
c  Note that DBLE and SNGL statements are very important
      DOUBLE PRECISION T, TA, CPAR, F, PI
      DATA PI/3.14159265D+00/
c
      T = DBLE(X)
      TA = DABS(T)
c
c  Algorithm is provided in two alternative versions for absolute
c  values of T less than 1.5 and greater (equal) to 1.5
      IF (TA .GE. 1.5D+00) GOTO 200
c
c  section 1 from Spanier and Oldham (T < 1.5)
      CPAR = 1.0D+00
      JE = 3 + DINT(9.0D+00 * TA)
      F = 1.0D+00
 10   CONTINUE
      F = 1 + F*T*T * ( 5.0D-01 - JE ) / ( JE * ( 5.0D-01 + JE ))
      JE = JE - 1
      IF (JE .NE. 0) THEN
       GOTO 10
      ELSE
       F = CPAR + F*T * ( 2.0D+00 - 4.0D+00 * CPAR ) / DSQRT(PI)
       GOTO 300
      ENDIF
c
c  section 2 from Spanier and Oldham (T >= 1.5)
 200  CPAR = TA / T
      JE = 3 + DINT(32.0D+00 / TA)
      F = 0.0D+00
 20   CONTINUE
      F = 1.0D+00 / ( F*JE + DSQRT(2.0D+00 * T * T) )
      JE = JE - 1
      IF (JE .NE. 0) GOTO 20
      F = F * ( CPAR*CPAR + CPAR - 1.0D+00) * (DSQRT(2.0D+00/PI) )
```

```
     +              * DEXP(-T*T) + ( 1.0D+00 - CPAR )
c
c  common section - store values of erfc
c  value of erfc ranges from 2 to 0, but erfc used in fitting needs to
c  be from 1 to 0, therefore divide by 2 before passing back to main
 300  ERFC = SNGL(F/2.0D+00)
      TOUT = T
c
     RETURN
     END
```

Subroutine 8:

```
c  MQFCHIS1.FOR  ((Called as FCHIS))
c  Function to calculate Chi Squared
c  Not clear why all lines are numbered....
     FUNCTION FCHIS(Y,NST,NTOP,NFREE, YFIT)
     DIMENSION Y(4097),YFIT(2300)
c
  11  CHISQ = 0.
c
c  Accumulate Chi Square
c
  20  DO 30 I=NST,NTOP
  30  CHISQ=CHISQ+ABS((Y(I)-YFIT(I))*(Y(I)-YFIT(I))/YFIT(I))
c
c  Divide by number of Degrees of Freedom
  31  FREE=NFREE
  32  FCHIS=CHISQ/FREE
c
  40  RETURN
     END
```

Shell:

```
C 2PBWORK.FOR
C
    INCLUDE 'FGRAPH.FI'
C
C*****************************************************************
C VARIABLE DICTIONARY
C
C AA1() - first guess at parameters
C ADEV() - deviation
C AL1   - magnitude of alpha 1 peak
C AL1ERR - error of magnitude of alpha 1 peak
C BE1   - magnitude of beta 1 peak
C BE1ERR - error of magnitude of beta 1 peak
C CO1   - magnitude of coherent peak
C CO1ERR - error of magnitude of coherent peak
C CPOS  - position of coherent peak (in channels)
C FNAM  - name of data file (eg. in c:\ff\ directory)
C       Up to 35 letters long, including path
C FT1   - variable used to remove magnitude of peak from FIT
C       to WORK
C FT1ERR - the error of the peak of FT1
C G     - gain (eV/channel)
C ICOM() - comments to add to output file (header)
C IDTE() - date to add to output file (header)
C IH2() - random number seed
C III   - counter to keep track of number of files
C INUM  - the number of files that are in the data file
C IRES  - variable used to replace I in specifying ADEV(I)
C ISUB  - variable used to indicate if data is for phantoms or people
C       ISUB = 0 if people
C       ISUB = 1 if phantoms
C ITEST - variable used to determine whether or not to plot data
C       ITEST = 1 if data IS to be plotted for each region
C       ITEST = 0 if NOT
C NF    - variable used to choose which subroutine is run
C NPTS  - number of channels
C NR    - number of parameters to be fitted over a restricted
C       range
C NST   - start channel
C NTERMS - number of parameters to be fitted (max 10)
C NTOP  - last channel number (NTOP = NPTS + NST -1)
C OFSET - channel offset
C OUT1  - first output file - contains only peak amplitudes and
C       their errors
C OUT2  - second output file - contains the more complete output
```

```
C RA     - ratio of alpha 1 amplitude to coherent amplitude
C RAERR  - error of RA  (std. dev)
C RB     - ratio of beta 1 amplitude to coherent amplitude
C RBERR  - error of RB  (std. dev)
C SA     - slope of alpha calibration line
C SAERR  - error of SA  (std. dev)
C SB     - slope of beta calibration line
C SBERR  - error of SB  (std. dev)
C BA     - y-intercept of alpha calibration line
C BAERR  - error of BA  (std. dev)
C BB     - y-intercept of beta calibration line
C BBERR  - error of BB  (std. dev)
C COVA   - covariance between SA and BA for alpha calib. line
C COVB   - covariance between SB and BB for beta calib. line
C PPMA   - lead concentration obtained via alpha 1 peak amplitude
C PPMAER - error of PPMA  (std. dev)
C PPMB   - lead concentration obtained via beta 1 peak amplitude
C PPMBER - error of PPMB  (std. dev)
C PPM    - lead concentration obtained by a weighted mean of
C          PPMA and PPMB
C PPMERR - error of PPM  (std. dev)
C STPARA - name of file which contains the starting parameters
C SBNAME - name of subroutine to add to output file (header)
C
C*****************************************************************
C
C SPECIFICATION OF VARIABLES
C
      CHARACTER*50 SBNAME
      CHARACTER*30 IDTE
      CHARACTER*35 FNAM, OUT1, OUT2, OUT3, STPARA, SCALIB, INFILE
      CHARACTER*35 FNAMS(500), files
      DIMENSION ICOM(108), AA1(10), ADEV(10), IH(2),
     1 OFSETS(500), HH(500), WW(500)
      DATA AA1/10*0./
!
! Initialize variables:
      IH(1) = 2
      IH(2) = 4
      CPOS  = 0.
      AL1   = 0.
      AL1ERR = 0.
      BE1   = 0.
      BE1ERR = 0.
      RA    = 0.
      RAERR  = 0.
```

```
      RB    = 0.
      RBERR = 0.
      SA    = 0.
      SAERR = 0.
      SB    = 0.
      SBERR = 0.
      BA    = 0.
      BAERR = 0.
      BB    = 0.
      BBERR = 0.
      COVA  = 0.
      COVB  = 0.
      PPMA  = 0.
      PPMAER = 0.
      PPMB  = 0.
      PPMBER = 0.
      PPM   = 0.
      PPMERR = 0.
      CO1   = 0.
      CO1ERR = 0.
      OUT1  = '                    '
      OUT2  = '                    '
      OUT3  = '                    '
      STPARA = '                   '
      SCALIB = '                   '
!
! Tell that output will be written to disk and ask for filename
!
      WRITE(*,14)
   14 FORMAT(/,1X,'All results from this analysis program will be writte
     1n to disk.'/)
  999 CONTINUE
      WRITE(*,15)
   15 FORMAT(1X,'Please enter the name of the input/output files (includ
     +ing the path)'/,1x,'with NO extension.'/,1X,
     +'There should be three input files, each with the same name, but d
     +ifferent extensions:')
      write(*,16)
   16 format(1x,'????????.PAR  start parameters file'/,1x,
     +'????????.FIL  spectra file names, offset, width and step'/,1x,
     +'????????.001  gain plus alpha and beta calibration data')
      Write(*,*)
      READ(5,'(A)') files
      WRITE(*,*)

      WRITE(*,19)
   19 FORMAT(1X,'Output files will be written as follows:'/,1x,
     +'????????.FUL  complete output (ie final parameters of the fit)',
     +/,1x,'????????.DAT  concentrations and errors only'/,1x,
     +'????????.RES  peak amplitudes, errors and lead concentrations')
      WRITE(*,*)

c  .res = OUT1
c  .ful = OUT2
c  .dat = OUT3
c  .par = STPARA
c  .fil = INFILE
c  .001 = SCALIB
      OUT1=files
      OUT2=files
      OUT3=files
      STPARA = files
      INFILE = files
      SCALIB = files
      INCHECK = 0
      DO 100 I=1,50
       IF ((files(I:I) .EQ. ' ') .AND. (INCHECK .EQ. 0)) THEN
        OUT1(I:I+3) = '.RES'
        OUT2(I:I+3) = '.FUL'
        OUT3(I:I+3) = '.DAT'
        STPARA(I:I+3) = '.PAR'
        INFILE(I:I+3) = '.FIL'
        SCALIB(I:I+3) = '.001'
        INCHECK=1
       ENDIF
  100 CONTINUE
      WRITE(*,101)
  101 FORMAT(1X,'OUTPUT WILL BE WRITTEN TO FILES:')
      WRITE(*,110) OUT1, OUT2, OUT3
  110 FORMAT(1X,A50)


!
! Input the name of the file containing the starting parameters
! Open OUT1 as unit #3, OUT2 as unit #7, and OUT3 as unit #8
!
      OPEN(UNIT=3, FILE=OUT1, STATUS='NEW')
      OPEN(UNIT=7, FILE=OUT2, STATUS='NEW')
      OPEN(UNIT=8, FILE=OUT3, STATUS='NEW')
!
! Write name of output files to top of OUT1, and OUT2:
      WRITE(3, 66) OUT1
```

```
      WRITE(7, 66) OUT2
   66 FORMAT(1X, 'Output filename: ',A35,/)
      WRITE(*,*)
!
! Input whether the spectra are from people or phantoms.
!
      WRITE(*,5)
    5 FORMAT(/,1X,'Please indicate whether the spectra are from people o
     1r phantoms.',/,11x,'0 = people',10x,'1 = phantoms')
      READ(5,'(BN,I1)') ISUB
c  comma added in line above by ims, 3/3/99 (was a space)
!
      IF ((ISUB.NE.0) .AND. (ISUB.NE.1)) GOTO 999
!
! Open the data file which contains the filenames, etc.
!
      OPEN(UNIT=4, FILE=INFILE, STATUS='OLD')
!
! Read in the number of data files to be analyzed.
      READ(4,'(BN,I4)') INUM
c  comma added in line above by ims, 3/3/99 (was a space)
      WRITE(*,*)
!
! Read in the file names to the array FNAMS(), the offsets to the
! array OFSETS(), the widths to the array WW() and the heights to
! the array HH(),  Write filenames to screen.
!
      WRITE(*,13) INUM
   13 FORMAT(I4,' files will be analyzed.  These files are:')
      DO 7, I = 1, INUM
      READ(4,10) FNAMS(I), OFSETS(I), WW(I), HH(I)
   10 FORMAT(A35, 4X, F5.0, 4X, F6.4, 4X, F8.6)
      WRITE(*,11) I, FNAMS(I)
   11 FORMAT(1X, '#',I3,': ',A35)
    7 CONTINUE
      CLOSE(UNIT=4, STATUS='KEEP')
!
! Input the date (for header)
!
      WRITE(6,439)
  439 FORMAT(' DATE?')
      READ(5,'(A30)') IDTE
!
! Input any comments (for header)
!
      WRITE(6,443)
```

```
 443 FORMAT(1X,'Any comments?  Three lines available')
     READ(5,444)(ICOM(I),I=1,36)
 444 FORMAT(36A2)
     READ(5,444)(ICOM(I),I=37,72)
     READ(5,444)(ICOM(I),I=73,108)
!
! Writing information (the header) to the output files OUT1 and OUT2:
!
! Write a blank line and a line of *'s:
     WRITE(3, 445)
     WRITE(7, 445)
 445 FORMAT(/75('*'))
!
! Writing the date:
     WRITE(3,447) IDTE
     WRITE(7,447) IDTE
 447 FORMAT(' DATE:  ',A30)
!
! Writing the comments:
     WRITE(3,887) (ICOM(I),I=1,108)
     WRITE(7,887) (ICOM(I),I=1,108)
 887 FORMAT(1X,36A2)
!
! Writing a line of *'s:
  18 WRITE(3,445)
     WRITE(7,445)
!
! Set counter to use for files equal to 0
     III = 0
!
! Set ITEST = 0 so don't graph
     ITEST = 0
!
! Set NTEST = 1 so keep doing new files with same fit until the last
! file is found at which time NTEST will be changed.
     NTEST = 1
!-------------------------------------------------------
! WRITE INFORMATION ABOUT THE FITS TO THE FILE OUT2:
! FIND CALIBRATION AND GAIN DATA
        OPEN (UNIT=5, FILE=SCALIB, STATUS='OLD')
        READ(5,*) G
        READ(5,*) SA
        READ(5,*) SAERR
        READ(5,*) BA
        READ(5,*) BAERR
        READ(5,*) COVA
```

```
      READ(5,*) SB
      READ(5,*) SBERR
      READ(5,*) BB
      READ(5,*) BBERR
      READ(5,*) COVB
      CLOSE(UNIT=5, STATUS='KEEP')
!
! Open file containing start parameters as unit #4
   OPEN(UNIT=4, FILE=STPARA, STATUS='OLD')
!
! Read the first line telling the length of the measurement that the
! start parameters are for (is a dummy line)
   READ(4,'(A50)') SBNAME
   DO 1200, NF = 1, 3
   IF (NF.EQ.1) THEN
      NTERMS = 5
      SBNAME = 'COHERENT with fixed width and height '
   ELSEIF (NF.EQ.2) THEN
      NTERMS = 4
      SBNAME = 'BETA with linked amplitudes, Ca linked to coherent'
   ELSEIF (NF.EQ.3) THEN
      NTERMS = 6
      SBNAME = 'ALPHA with linked amplitudes '
   ENDIF
! Writing the subroutine to OUT2:
   WRITE(7,448) SBNAME
 448 FORMAT(/,1X,'SUBROUTINE: ',A50,)
!
! Input a dummy character (as are description lines in the file
! with the start parameters)
   READ(4,'(A50)') SBNAME
! Input the initial guesses from the file
 1208 DO 1209, I=1, NTERMS
   READ(4,*) AA1(I)
 1209 CONTINUE
! Input the number of channels and the start channel from the file
   READ(4,*) NPTS,NST
! Writing the number of channels and starting channel to OUT2:
   WRITE(7,449) NPTS, NST
 449 FORMAT(10X,I3,' channels starting in channel ',I3)
! Write starting parameters to output location:
   WRITE(7,1218)
 1218 FORMAT(11X,'The starting parameters are:')
   DO 1203, I = 1, NTERMS
      WRITE(7,1217) I, AA1(I)
 1217 FORMAT(16X, 'A(',I2,') = ',G12.5)
```

```
1203 CONTINUE
!
! Initialize all deviations, ADEV(), to zero:
    DO 1205, I = 1 , NTERMS
    ADEV(I) = 0.
1205 CONTINUE
!
! Input the number of parameters to be fitted over a restricted range
    READ(4,*) NR
    WRITE(7,1201) NR
1201 FORMAT(10X,I3,' RESTRICTED PARAMETERS:')
!
! Input the deviations for the specific A(I)'s and write to OUT2:
    DO 1202, I = 1 , NR
!   input:
    READ(4,*) IRES , ADEV(IRES)
!   output:
    WRITE(7,310) IRES, AA1(IRES), ADEV(IRES)
 310 FORMAT(16X,'A(',I2,') = ',G12.5,' +/- ',G12.5)
1202 CONTINUE
!
1200 CONTINUE
!
! Write the 2 random numbers to desired output:
    WRITE(7,1211) IH(1), IH(2)
1211 FORMAT(/,1X,'random number entry points ',I5,1X,I5)
!
! Write a line of *'s to OUT2:
    WRITE(7,445)
!
! Close the start parameters file:
    CLOSE(UNIT=4, STATUS='KEEP')
!-------------------------------------------------------
!
! Here is where the fit to the next file starts
!
! Increment file counter III
!
 998 III = III + 1
!
! Set FNAM to the (next) file in FNAMS(), OFSET to the corresponding
! OFSETS(), W to WW(), and H to HH()
    FNAM = FNAMS(III)
    OFSET = OFSETS(III)
    W = WW(III)
    H = HH(III)
```

```
!
! Open file containing start parameters as unit #4
    OPEN(UNIT=4, FILE=STPARA, STATUS='OLD')
!
! Read the first line telling the length of the measurement that the
! start parameters are for (is a dummy line)
    READ(4,'(A50)') SBNAME
!
! Run the programs.  When NF = 1, do the fixed width coherent
! program.  When NF = 2, do the beta program, and when NF = 3, do
! the alpha program.
!
c  Call Seed moved from 2pbfit, to ensure changing random numbers are
c  generated....
    CALL SEED(IH(1))
    DO 309, NF = 1, 3
!
    IF (NF.EQ.1) THEN
       NTERMS = 5
    ELSEIF (NF.EQ.2) THEN
       NTERMS = 4
    ELSEIF (NF.EQ.3) THEN
       NTERMS = 6
    ENDIF
!
! Input a dummy character (as are description lines in the file
! with the start parameters)
    READ(4,'(A50)') SBNAME
!
! Input the initial guesses from the file
   8 DO 9 I=1,NTERMS
    READ(4,*) AA1(I)
   9 CONTINUE
!
! Input the number of channels and the start channel from the file
    READ(4,*) NPTS,NST
!
! Set the last channel number (NTOP)
    NTOP=NPTS+NST-1
!
! Initialize all deviations, ADEV(), to zero:
    DO 305 I = 1 , NTERMS
    ADEV(I) = 0.
 305 CONTINUE
!
! Input the number of parameters to be fitted over a restricted range
```

```
    READ(4,*) NR
! Input the deviations for the specific A(I)'s:
    DO 302 I = 1 , NR
    READ(4,*) IRES , ADEV(IRES)
 302 CONTINUE
!
! Re-initialize FTI and FTIERR:
    FTI   = 0.
    FTIERR = 0.
! Run the fit program:
    CALL FIT(NTERMS, NPTS, NST, NTOP, NR, AAI, ADEV, IH, ITEST, FNAM,
   1 OFSET, CPOS, FTI, FTIERR, NF, G, W, H, ISUB, COI)
! Set the peak magnitudes to keep their values
    IF (NF.EQ.1) THEN
       COI = FTI
       COIERR = FTIERR
    ELSEIF (NF.EQ.2) THEN
       BEI = FTI
       BEIERR = FTIERR
    ELSEIF (NF.EQ.3) THEN
       ALI = FTI
       ALIERR = FTIERR
    ENDIF
 309 CONTINUE
    CLOSE(UNIT=4, STATUS='KEEP')
! Calculate the ratios and their errors.
    RA = ALI/COI
    RAERR = RA * (((ALIERR/ALI)**2. + (COIERR/COI)**2.)**0.5)
    RB = BEI/COI
    RBERR = RB * (((BEIERR/BEI)**2. + (COIERR/COI)**2.)**0.5)
! Set parameters (calb. line slope, intercept, etc.) depending
! on which system (tibia or calcaneus) was used
! Note:  ISYS = 4 for calcaneus,  ISYS = 5 for tibia
! Calculate Concentrations:
! Via Alpha:
    PPMA = (RA - BA) / SA
    PPMAER = RAERR*RAERR + BAERR*BAERR
    PPMAER = PPMAER + PPMA*PPMA*SAERR*SAERR + 2*PPMA*COVA
    PPMAER = (PPMAER**0.5) / SA
!
! Via Beta:
    PPMB = (RB - BB) / SB
    PPMBER = RBERR*RBERR + BBERR*BBERR
    PPMBER = PPMBER + PPMB*PPMB*SBERR*SBERR + 2*PPMB*COVB
    PPMBER = (PPMBER**0.5) / SB
!
```

```
! If people (ISUB=0) then multiply these #s by 1.29 to compensate for
! different cross-sections between bone and plaster of paris
!    IF (ISUB.EQ.0) THEN
!       PPMA = PPMA * 1.29
!       PPMAER = PPMAER * 1.29
!       PPMB = PPMB * 1.29
!       PPMBER = PPMBER * 1.29
!    ENDIF
! If people (ISUB=0) then multiply these #s by 1.29 to compensate for
! different cross-sections between bone and plaster of paris
    IF (ISUB.EQ.0) THEN
       PPMA = 1.29*RA/SA
       PPMAER = PPMA*PPMA*(RAERR*RAERR/RA/RA+SAERR*SAERR/SA/SA)
            PPMAER = (PPMAER)**0.5
       PPMB = 1.29*RB/SB
       PPMBER = PPMB*PPMB*(RBERR*RBERR/RB/RB+SBERR*SBERR/SB/SB)
            PPMBER = (PPMBER)**0.5
    ENDIF
! Weighted mean of these:
    PPMERR = 1/((PPMBER)**2.) + 1/((PPMAER)**2.)
    PPMERR = (1/PPMERR)**0.5
    PPM = (PPMB/((PPMBER)**2.) + PPMA/((PPMAER)**2.)) * (PPMERR**2.)
! Write the concentrations to the output files.
! To OUT1:
    WRITE(3,460) PPMA, PPMAER
    WRITE(3,461) PPMB, PPMBER
    WRITE(3,462) PPM, PPMERR
 460 FORMAT(/,1X, 'The concentration via alpha 1 is: ', F9.4,
   1 ' +/- ', F9.4, ' ppm.')
 461 FORMAT(1X, 'The concentration via beta 1 is:  ', F9.4,
   1 ' +/- ', F9.4, ' ppm.')
 462 FORMAT(1X, 'The weighted mean concentration is:', F9.4,
   1 ' +/- ', F9.4, ' ppm.'/)
!
! To OUT3:
    WRITE(8,1002) RA, RAERR, RB, RBERR
1002 FORMAT(4(2X, F12.6))
!
! Write the peak amplitudes and the concentrations to the screen:
!
    WRITE(*,463) FNAM
 463 FORMAT(1X, 'The results of analyzing the file ',A35,' are: '/)
    WRITE(6,303) CO1, CO1ERR
    WRITE(6,304) BE1, BE1ERR
    WRITE(6,306) AL1, AL1ERR
 303 FORMAT(1X, 'Coherent peak amplitude is:',G12.5,' +/- ', G12.5)
```

```
 304 FORMAT(1X, 'Beta 1 peak amplitude is: ',G12.5,' +/- ', G12.5)
 306 FORMAT(1X, 'Alpha 1 peak amplitude is: ',G12.5,' +/- ', G12.5)
     WRITE(6,460) PPMA, PPMAER
     WRITE(6,461) PPMB, PPMBER
     WRITE(6,462) PPM, PPMERR
1001 WRITE(*,*)
!  If have just finished the last data file (ie. III = INUM) then
!  stop by setting NTEST = 0
     IF(III.EQ.INUM) THEN
        NTEST = 0
        IFILES = 1
     ENDIF
!
!  If NTEST is 0, go to 1000, if NTEST is 1, go to 998,
!  if NTEST is 2 go to 999:
     IF(NTEST-1)1000,998,999
!
!  Close the files OUT1 and OUT2:
 1000 CLOSE(UNIT=3, STATUS='KEEP')
     CLOSE(UNIT=7, STATUS='KEEP')
     CLOSE(UNIT=8, STATUS='KEEP')
!  End of program
     END
```

Subroutine1:

```
C  2PBCOH.FOR
C
C  Subroutine for analysing coherent and lead beta 2 peaks.
C
C*****************************************************************
C  VARIABLE DICTIONARY
C
C  A(1) - position of coherent
C  A(2) - amplitude of coherent
C  A(3) - amplitude of LEAD beta 2
C       NOTE: in this program, the position of the beta 2 is fixed
C             with respect to the position of the coherent peak
C  A(4) - amplitude of exponential background
C  A(5) - exponent coefficient of exponential background
C
C  SIGMAA(I) - error of A(I)
C  G - gain in eV/channel
C  X - channel number (position)
C  Y - gaussian parameter for the Beta 2 I
C  Z - gaussian parameter for the coherent peak
C  V - gaussian parameter for the Beta 2 II
```

```
C  YY - exponential of gaussian for Beta 2 I
C  ZZ - exponential of gaussian for coherent: ZZ=exp(-Z*Z)
C       (depending on the magnitude of Z)
C  VV - exponential of gaussian for Beta 2 II
C
C*****************************************************************
C
      REAL FUNCTION FUNCC(X, A, G, W, H)
      DIMENSION A(10)
!
! Evaluation of gaussian parameters:
      Z = (X - A(1))/W
      Y = (X - (A(1) - (668./G)))/W
      V = (X - (A(1) - (802./G)))/W
!
! Evaluate the gaussian exponents, if they are large enough to avoid
! underflow, otherwise leave as zero:
      VV=0.0
      YY=0.0
      ZZ=0.0
      IF(ABS(V).LT.5) VV=EXP(-V*V)
      IF(ABS(Y).LT.5) YY=EXP(-Y*Y)
      IF(ABS(Z).LT.5) ZZ=EXP(-Z*Z)
!
! Function:   (evaluating the gaussian peak, taking into account
! the step function):
      FUNCC = A(2)*(ZZ + H*ERFC(Z)) + A(4)*EXP(A(5)*X)
     1+ A(3)*((YY + H*ERFC(Y)) + .509*(VV + H*ERFC(V)))
!
      RETURN
      END
!
! Subroutine to calculate derivatives:
      SUBROUTINE FDERVC(X, A, DERIV, G, W, H)
      DIMENSION A(10),DERIV(10)
!
! Evaluation of gaussian parameters:
      Z = (X - A(1))/W
      Y = (X - (A(1) - (668./G)))/W
      V = (X - (A(1) - (802./G)))/W
!
! Evaluate the gaussian exponents, if they are large enough to avoid
! underflow, otherwise leave as zero:
      VV=0.0
      YY=0.0
      ZZ=0.0
```

```
      IF(ABS(V).LT.5) VV=EXP(-V*V)
      IF(ABS(Y).LT.5) YY=EXP(-Y*Y)
      IF(ABS(Z).LT.5) ZZ=EXP(-Z*Z)
!
! Evaluation of partial derivatives of function:
! DERIV(i) = d(FUNCTION)/dA(i)
      DERIV(1) = A(2)*ZZ*(2.*Z/W+H) + A(3)*YY*(2.*Y/W+H)
     1  + 0.509*A(3)*VV*(2.*V/W+H)
      DERIV(2) = ZZ + H * ERFC(Z)
      DERIV(3) = YY + H * ERFC(Y) + .509 * (VV + H * ERFC(V))
      DERIV(4) = EXP(A(5)*X)
      DERIV(5) = A(4)*X*EXP(A(5)*X)
!
      RETURN
      END
!
! Subroutine to print peak amplitudes and their errors to OUT1
!
      SUBROUTINE FWRC(A, SIGMAA, J)
      DIMENSION A(10), SIGMAA(10)
      WRITE(J,220) A(2), SIGMAA(2)
  220 FORMAT(1X, 'Coherent peak amplitude is: ',G12.5,' +/- ',G12.5)
      RETURN
      END
```

Subroutine 2:

```
C  2PBALPH.FOR
C
C  Subroutine to analyze lead alpha peaks.
C
C*****************************************************************
C  VARIABLE DICTIONARY
C
C  A(1) - position of lead alpha 1
C  A(2) - amplitude of lead alpha 1
C  A(3) - amplitude of exponential background 1
C  A(4) - exponent coefficient of exponential background 1
C  A(5) - amplitude of exponential background 2
C  A(6) - exponent coefficient of exponential background 2
C
C  SIGMAA(I) - error of A(I)
C  W - width, in channels
C  H - height
C  G - gain in eV/channel
C  X - channel number
C  Z - gaussian parameter for lead alpha 1 peak (not squared)
```

```
C  V - gaussian parameter for lead alpha 2 peak
C  ZZ - exponential of gaussian for lead alpha 1
C  VV - exponential of gaussian for lead alpha 2
C
C*****************************************************************
C
      REAL FUNCTION FUNCA(X, A, G, W, H)
      DIMENSION A(10)
!
! Evaluation of gaussian parameters:
      Y = (X - (A(1) - (2165./G)))/W
      Z = (X - A(1))/W
!
! Evaluate the gaussian exponents, if they are large enough to avoid
! underflow, otherwise leave as zero:
!
      YY = 0.
      ZZ = 0.
      IF(ABS(Y).LT.5) YY=EXP(-Y*Y)
      IF(ABS(Z).LT.5) ZZ=EXP(-Z*Z)
!
! Evaluate the function
!
      FUNCA = A(2) * (ZZ + H*ERFC(Z)) + (0.593*A(2)) * (YY + H*ERFC(Y))
     1 + A(3) * EXP(A(4)*X) + A(5) * EXP(A(6)*X)
      RETURN
      END
!
! Subroutine to calculate derivatives:
!
      SUBROUTINE FDERVA(X, A, DERIV, G, W, H)
      DIMENSION A(10),DERIV(10)
!
! Evaluation of gaussian parameters:
      Z = (X - A(1))/W
      Y = (X - (A(1) - (2165./G)))/W
!
! Evaluate the gaussian exponents, if they are large enough to avoid
! underflow, otherwise leave as zero:
!
      ZZ = 0.
      YY = 0.
      IF(ABS(Z).LT.5) ZZ=EXP(-Z*Z)
      IF(ABS(Y).LT.5) YY=EXP(-Y*Y)
!
! Evaluation of partial derivatives of the function:
```

```
! DERIV(i) = d(FUNCTION)/dA(i)
    DERIV(1) = A(2) * ZZ * (2.*Z/W+H) + (0.593*A(2)) * YY * (2.*Y/W+H)
    DERIV(2) = (ZZ + H*ERFC(Z)) + (0.593) * (YY + H*ERFC(Y))
    DERIV(3) = EXP(A(4)*X)
    DERIV(4) = A(3) * X * EXP(A(4)*X)
    DERIV(5) = EXP(A(6)*X)
    DERIV(6) = A(5) * X * EXP(A(6)*X)
    RETURN
    END
!
! Subroutine to print alpha 1 peak amplitudes and error to OUT1
!
    SUBROUTINE FWRA(A, SIGMAA, J)
    DIMENSION A(10), SIGMAA(10)
    WRITE(J,220) A(2), SIGMAA(2)
 220 FORMAT(1X, 'Alpha 1 peak amplitude is: ',G12.5,' +/- ',G12.5)
    RETURN
    END-
```

Subroutine 3:

```
C  2PBBETA.FOR - to use in combined program
C
C  Subroutine to analyse lead betas
C
C*****************************************************************
C  VARIABLE DICTIONARY
C
C  A(1) - amplitude of beta 1
C  A(2) - amplitude of exponential background
C  A(3) - exponent coefficient of exponential background
C  A(4) - exponential on calcium & phosphorus edges
C
C  CO1  - height of coherent peak
C  CPOS - position of coherent peak (in channels)
C  ISUB - variable used to indicate if data is for phantoms or people
C       ISUB = 0 if people
C       ISUB = 1 if phantoms
C  SIGMAA(I) - error of A(I)
C  W - width, in channels (fixed)
C  H - height (fixed)
C  G - gain in eV/channel
C  X - channel number (position)
C  Y - gaussian parameter for beta 3 peak (not squared)
C  Z - gaussian parameter for beta 1 peak (not squared)
C  YY - exponential of gaussian for beta 3
C  ZZ - exponential of gaussian for beta 1
```

```
C  CA - gaussian parameter for calcium edge feature
C  POSCA - used to calculate CA and in Ca exponential background
C  P - gaussian parameter for phosphorus edge feature
C  POSP - used to calculate P and in P exponential background
C  S - gaussian parameter for sulphur edge feature
C  POSS - used to calculate S and in S exponential background
C
C*****************************************************************
C
      REAL FUNCTION FUNCB(X, A, CPOS, G, W, H, ISUB, CO1)
      DIMENSION A(10)
!
! Evaluate function depending on ISUB ( 0 = people, 1 = phantom)
!
      IF (ISUB.EQ.0) THEN
!
! Evaluation of PEOPLE gaussian parameters:
         Z = (X - (CPOS - (3099./G)))/W
         Y = (X - (CPOS - (3585./G)))/W
         POSCA = X - (CPOS - (4038./G))
         CA = POSCA/W
         POSP = X - (CPOS - (2146./G))
         P = POSP/W
!
! Evaluate the PEOPLE gaussian exponents, if they are large enough to
! avoid underflow, otherwise leave as zero:
         ZZ = 0.
         YY = 0.
         IF(ABS(Z).LT.5)  ZZ = EXP(-Z*Z)
         IF(ABS(Y).LT.5)  YY = EXP(-Y*Y)
!
! PEOPLE Function: (evaluating the gaussian peak, taking into account
! the step function, and phosphorus and calcium edges):
        FUNCB = A(1) *(ZZ + H*ERFC(Z)) + (0.523*A(1)) *(YY+H*ERFC(Y))
     1  + A(2) * EXP(A(3)*X) + 0.0056*W *CO1 *(EXP(A(4)*POSCA) *
     1  ERFC(CA) + 0.21 * EXP(A(4)*POSP) * ERFC(P))
!
      ELSEIF (ISUB.EQ.1) THEN
!
! Evaluation of PHANTOM gaussian parameters:
      Z = (X - (CPOS - (3099./G)))/W
      Y = (X - (CPOS - (3585./G)))/W
      POSCA = X - (CPOS - (4038./G))
      CA = POSCA/W
      POSS = X - (CPOS - (2472./G))
      S = POSS/W
```

```
!
! Evaluate the PHANTOM gaussian exponents, if they are large enough to
! avoid underflow, otherwise leave as zero:
    ZZ = 0.
    YY = 0.
    IF(ABS(Z).LT.5)  ZZ = EXP(-Z*Z)
    IF(ABS(Y).LT.5)  YY = EXP(-Y*Y)
!
! PHANTOM Function: (evaluating the gaussian peak, taking into account
! the step function, and phosphorus and calcium edges):
      FUNCB = A(1) *(ZZ + H*ERFC(Z)) + (0.523*A(1)) *(YY+H*ERFC(Y))
     1  + A(2) * EXP(A(3)*X) + 0.005*W*CO1 *(EXP(A(4)*POSCA) *
     1 ERFC(CA) + 0.16 * EXP(A(4)*POSS) * ERFC(S))
!
    ENDIF
!
    RETURN
    END
!
! Subroutine to calculate derivatives:
!
    SUBROUTINE FDERVB(X, A, DERIV, CPOS, G, W, H, ISUB, CO1)
    DIMENSION A(10),DERIV(10)
!
! Evaluate the function depending on ISUB (0 = people, 1 = phantom)
!
    IF (ISUB.EQ.0) THEN
!
! Evaluation of PEOPLE gaussian parameters:
        Z = (X - (CPOS - (3099./G)))/W
        Y = (X - (CPOS - (3585./G)))/W
        POSCA = X - (CPOS - (4038./G))
        CA = POSCA/W
        POSP = X - (CPOS - (2146./G))
        P = POSP/W
!
! Evaluate the PEOPLE gaussian exponents, if they are large enough to
! avoid underflow, otherwise leave as zero:
        ZZ = 0.
        YY = 0.
        IF(ABS(Z).LT.5)  ZZ = EXP(-Z*Z)
        IF(ABS(Y).LT.5)  YY = EXP(-Y*Y)
!
! Evaluation of partial derivatives of the PEOPLE function:
! DERIV(i) = d(FUNCTION)/dA(i)
        DERIV(1) = (ZZ + H*ERFC(Z)) + (0.523) * (YY+H*ERFC(Y))
```

```
      DERIV(2) = EXP(A(3)*X)
      DERIV(3) = A(2) * X * EXP(A(3)*X)
      DERIV(4) = 0.0056*W * CO1 * (POSCA * EXP(A(4)*POSCA) *
     1   ERFC(CA) + 0.21 * POSP * EXP(A(4)*POSP) * ERFC(P))
!
   ELSEIF (ISUB.EQ.1) THEN
!
! Evaluation of PHANTOM gaussian parameters:
      Z = (X - (CPOS - (3099./G)))/W
      Y = (X - (CPOS - (3585./G)))/W
      POSCA = X - (CPOS - (4038./G))
      CA = POSCA/W
      POSS = X - (CPOS - (2472./G))
      S = POSS/W
!
! Evaluate the PHANTOM gaussian exponents, if they are large enough to
! avoid underflow, otherwise leave as zero:
      ZZ = 0.
      YY = 0.
      IF(ABS(Z).LT.5)  ZZ = EXP(-Z*Z)
      IF(ABS(Y).LT.5)  YY = EXP(-Y*Y)
!
! Evaluation of partial derivatives of the function:
! DERIV(i) = d(FUNCTION)/dA(i)
      DERIV(1) = ZZ + H*ERFC(Z) + 0.523 * (YY + H*ERFC(Y))
      DERIV(2) = EXP(A(3)*X)
      DERIV(3) = A(2) * X * EXP(A(3)*X)
      DERIV(4) = 0.005*W * CO1 * (POSCA * EXP(A(4)*POSCA) *
     1   ERFC(CA) + 0.16 * POSS * EXP(A(4)*POSS) * ERFC(S))
!
   ENDIF
!
   RETURN
   END
!
! Subroutine to print peak amplitudes and their errors to the file
! which was specified when asked for in DCWORK, namely: OUT1
!
   SUBROUTINE FWRB(A, SIGMAA, J)
   DIMENSION A(10), SIGMAA(10)
!
   WRITE(J,220) A(1), SIGMAA(1)
 220 FORMAT(1X, 'Beta 1 peak amplitude is:  ',G12.5,' +/- ',G12.5)
   RETURN
   END
```

Subroutine 4:

```
            FUNCTION ERFC(X)
      DIMENSION P1(3),Q1(3),P2(5),Q2(5),P3(2),Q3(2)
      DATA CONST/0.564189584/
      DATA XMAX/8.9/
      DATA XUNIT/4.4/
      DATA P1(1),P1(2),P1(3)/21.3853322,1.72227577,.316652891/
      DATA Q1(1),Q1(2),Q1(3)/18.9522572,7.84374571,1.0/
      DATA P2(1),P2(2),P2(3)/7.37388831,6.86501848,3.03179934/
      DATA P2(4),P2(5)/.563169619,4.31877874E-5/
      DATA Q2(1),Q2(2)/7.37396089,15.1849082/
      DATA Q2(3),Q2(4),Q2(5)/12.7955295,5.35421679,1.0/
      DATA P3(1),P3(2)/-4.25799644E-2,-1.96068974E-1/
            DATA Q3(1),Q3(2)/.150942071,.921452412/
      T=X
      A=ABS(T)
      IF(T.GE.-XUNIT)GO TO 1
      ERFC=1.0
      RETURN
    1 IF(T.LE.XMAX)GO TO 2
      ERFC=0.0
      RETURN
    2 S=T**2
      IF(A.GT.0.47)GO TO 4
      Y=T*(P1(1)+S*(P1(2)+S*P1(3)))/(Q1(1)+S*(Q1(2)+S*Q1(3)))
      ERFC=(1.0-Y)/2.0
      RETURN
    4 IF(A.GT.4.0)GO TO 5
      Y=EXP(-S)*(P2(1)+A*(P2(2)+A*(P2(3)+A*(P2(4)+A*P2(5)))))
     1 /       (Q2(1)+A*(Q2(2)+A*(Q2(3)+A*(Q2(4)+A*Q2(5)))))
      GO TO 6
    5 R=1.0/A
      U=R**2
      Y=R*EXP(-S)*(CONST+U*(P3(1)+U*P3(2))/(Q3(1)+U*Q3(2)))
    6 IF(T.LT.0.0)Y=2.0-Y
      ERFC=Y/2.0
      RETURN
      END
```

Subroutine 5:

```
     REAL FUNCTION FCHIS(Y,NST,NTOP,NFREE, YFIT)
     DIMENSION Y(4097),YFIT(2300)
   11  CHISQ = 0.
C
C       ACCUMULATE CHI SQUARE
C
```

```
  20 DO 30 I=NST,NTOP
  30  CHISQ=CHISQ+ABS((Y(I)-YFIT(I))*(Y(I)-YFIT(I))/YFIT(I))
C
C       DIVIDE BY NUMBER OF DEGREES OF FREEDOM
C
  31 FREE=NFREE
  32 FCHIS=CHISQ/FREE
  40 RETURN
     END
```

Subroutine 6:

```
C 2PBWORK.FOR
C
    INCLUDE 'FGRAPH.FI'
C
C*****************************************************************
C VARIABLE DICTIONARY
C
C AA1() - first guess at parameters
C ADEV() - deviation
C AL1    - magnitude of alpha 1 peak
C AL1ERR - error of magnitude of alpha 1 peak
C BE1    - magnitude of beta 1 peak
C BE1ERR - error of magnitude of beta 1 peak
C CO1    - magnitude of coherent peak
C CO1ERR  - error of magnitude of coherent peak
C CPOS   - position of coherent peak (in channels)
C FNAM   - name of data file (eg. in c:\ff\ directory)
C        Up to 35 letters long, including path
C FT1    - variable used to remove magnitude of peak from FIT
C        to WORK
C FT1ERR - the error of the peak of FT1
C G      - gain (eV/channel)
C ICOM() - comments to add to output file (header)
C IDTE() - date to add to output file (header)
C IH2()  - random number seed
C III    - counter to keep track of number of files
C INUM   - the number of files that are in the data file
C IRES   - variable used to replace I in specifying ADEV(I)
C ISUB   - variable used to indicate if data is for phantoms or people
C        ISUB = 0 if people
C        ISUB = 1 if phantoms
C ITEST  - variable used to determine whether or not to plot data
C        ITEST = 1 if data IS to be plotted for each region
C        ITEST = 0 if NOT
C NF     - variable used to choose which subroutine is run
```

```
C NPTS  - number of channels
C NR    - number of parameters to be fitted over a restricted
C         range
C NST   - start channel
C NTERMS - number of parameters to be fitted (max 10)
C NTOP  - last channel number (NTOP = NPTS + NST -1)
C OFSET - channel offset
C OUT1  - first output file - contains only peak amplitudes and
C         their errors
C OUT2  - second output file - contains the more complete output
C RA    - ratio of alpha 1 amplitude to coherent amplitude
C RAERR - error of RA (std. dev)
C RB    - ratio of beta 1 amplitude to coherent amplitude
C RBERR - error of RB (std. dev)
C SA    - slope of alpha calibration line
C SAERR - error of SA (std. dev)
C SB    - slope of beta calibration line
C SBERR - error of SB (std. dev)
C BA    - y-intercept of alpha calibration line
C BAERR - error of BA (std. dev)
C BB    - y-intercept of beta calibration line
C BBERR - error of BB (std. dev)
C COVA  - covariance between SA and BA for alpha calib. line
C COVB  - covariance between SB and BB for beta calib. line
C PPMA  - lead concentration obtained via alpha 1 peak amplitude
C PPMAER - error of PPMA (std. dev)
C PPMB  - lead concentration obtained via beta 1 peak amplitude
C PPMBER - error of PPMB (std. dev)
C PPM   - lead concentration obtained by a weighted mean of
C         PPMA and PPMB
C PPMERR - error of PPM (std. dev)
C STPARA - name of file which contains the starting parameters
C SBNAME - name of subroutine to add to output file (header)
C
C*****************************************************************
C
C SPECIFICATION OF VARIABLES
C
      CHARACTER*50 SBNAME
      CHARACTER*30 IDTE
      CHARACTER*35 FNAM, OUT1, OUT2, OUT3, STPARA, SCALIB, INFILE
      CHARACTER*35 FNAMS(500), files
      DIMENSION ICOM(108), AA1(10), ADEV(10), IH(2),
     1 OFSETS(500), HH(500), WW(500)
      DATA AA1/10*0./
!
```

```
! Initialize variables:
    IH(1) = 2
    IH(2) = 4
    CPOS  = 0.
    ALI   = 0.
    ALIERR = 0.
    BEI   = 0.
    BEIERR = 0.
    RA    = 0.
    RAERR  = 0.
    RB    = 0.
    RBERR  = 0.
    SA    = 0.
    SAERR  = 0.
    SB    = 0.
    SBERR = 0.
    BA    = 0.
    BAERR  = 0.
    BB    = 0.
    BBERR  = 0.
    COVA  = 0.
    COVB  = 0.
    PPMA  = 0.
    PPMAER = 0.
    PPMB  = 0.
    PPMBER = 0.
    PPM   = 0.
    PPMERR = 0.
    COI   = 0.
    COIERR = 0.
    OUT1  = '                    '
    OUT2  = '                    '
    OUT3  = '                    '
    STPARA = '                     '
    SCALIB = '                     '
!
! Tell that output will be written to disk and ask for filename
!
     WRITE(*,14)
  14 FORMAT(/,1X,'All results from this analysis program will be writte
    In to disk.'/)
 999 CONTINUE
     WRITE(*,15)
  15 FORMAT(1X,'Please enter the name of the input/output files (includ
    +ing the path)'/,1x,'with NO extension.'/,1X,
    +'There should be three input files, each with the same name, but d
    +ifferent extensions:')
     write(*,16)
  16 format(1x,'????????.PAR  start parameters file'/,1x,
    +'????????.FIL  spectra file names, offset, width and step'/,1x,
    +'????????.001  gain plus alpha and beta calibration data')
     Write(*,*)
     READ(5,'(A)') files
     WRITE(*,*)

     WRITE(*,19)
  19 FORMAT(1X,'Output files will be written as follows:'/,1x,
    +'????????.FUL  complete output (ie final parameters of the fit)',
    +/,1x,'????????.DAT  concentrations and errors only'/,1x,
    +'????????.RES  peak amplitudes, errors and lead concentrations')
     WRITE(*,*)

c  .res = OUT1
c  .ful = OUT2
c  .dat = OUT3
c  .par = STPARA
c  .fil = INFILE
c  .001 = SCALIB
     OUT1=files
     OUT2=files
     OUT3=files
     STPARA = files
     INFILE = files
     SCALIB = files
     INCHECK = 0
     DO 100 I=1,50
      IF ((files(I:I) .EQ. ' ') .AND. (INCHECK .EQ. 0)) THEN
       OUT1(I:I+3) = '.RES'
       OUT2(I:I+3) = '.FUL'
       OUT3(I:I+3) = '.DAT'
       STPARA(I:I+3) = '.PAR'
       INFILE(I:I+3) = '.FIL'
       SCALIB(I:I+3) = '.001'
       INCHECK=1
      ENDIF
  100 CONTINUE
     WRITE(*,101)
  101 FORMAT(1X,'OUTPUT WILL BE WRITTEN TO FILES:')
     WRITE(*,110) OUT1, OUT2, OUT3
  110 FORMAT(1X,A50)
```

```
!
! Input the name of the file containing the starting parameters
! Open OUT1 as unit #3, OUT2 as unit #7, and OUT3 as unit #8
!
    OPEN(UNIT=3, FILE=OUT1, STATUS='NEW')
    OPEN(UNIT=7, FILE=OUT2, STATUS='NEW')
    OPEN(UNIT=8, FILE=OUT3, STATUS='NEW')
!
! Write name of output files to top of OUT1, and OUT2:
    WRITE(3, 66) OUT1
    WRITE(7, 66) OUT2
  66 FORMAT(1X, 'Output filename: ',A35,/)
    WRITE(*,*)
!
! Input whether the spectra are from people or phantoms.
!
    WRITE(*,5)
   5 FORMAT(/,1X,'Please indicate whether the spectra are from people o
     1r phantoms.',/,11x,'0 = people',10x,'1 = phantoms')
    READ(5,'(BN,I1)') ISUB
c  comma added in line above by ims, 3/3/99 (was a space)
!
    IF ((ISUB.NE.0) .AND. (ISUB.NE.1)) GOTO 999
!
! Open the data file which contains the filenames, etc.
!
    OPEN(UNIT=4, FILE=INFILE, STATUS='OLD')
!
! Read in the number of data files to be analyzed.
    READ(4,'(BN,I4)') INUM
c  comma added in line above by ims, 3/3/99 (was a space)
    WRITE(*,*)
!
! Read in the file names to the array FNAMS(), the offsets to the
! array OFSETS(), the widths to the array WW() and the heights to
! the array HH(). Write filenames to screen.
!
    WRITE(*,13) INUM
  13 FORMAT(I4,' files will be analyzed. These files are:')
    DO 7, I = 1, INUM
    READ(4,10) FNAMS(I), OFSETS(I), WW(I), HH(I)
  10 FORMAT(A35, 4X, F5.0, 4X, F6.4, 4X, F8.6)
    WRITE(*,11) I, FNAMS(I)
  11 FORMAT(1X, '#',I3,': ',A35)
   7 CONTINUE
    CLOSE(UNIT=4, STATUS='KEEP')
```

```
!
! Input the date (for header)
!
    WRITE(6,439)
 439 FORMAT(' DATE?')
    READ(5,'(A30)') IDTE
!
! Input any comments (for header)
!
    WRITE(6,443)
 443 FORMAT(1X,'Any comments?  Three lines available')
    READ(5,444)(ICOM(I),I=1,36)
 444 FORMAT(36A2)
    READ(5,444)(ICOM(I),I=37,72)
    READ(5,444)(ICOM(I),I=73,108)
!
! Writing information (the header) to the output files OUT1 and OUT2:
!
! Write a blank line and a line of *'s:
    WRITE(3, 445)
    WRITE(7, 445)
 445 FORMAT(/75('*'))
!
! Writing the date:
    WRITE(3,447) IDTE
    WRITE(7,447) IDTE
 447 FORMAT(' DATE:  ',A30)
!
! Writing the comments:
    WRITE(3,887) (ICOM(I),I=1,108)
    WRITE(7,887) (ICOM(I),I=1,108)
 887 FORMAT(1X,36A2)
!
! Writing a line of *'s:
  18 WRITE(3,445)
    WRITE(7,445)
!
! Set counter to use for files equal to 0
    III = 0
!
! Set ITEST = 0 so don't graph
    ITEST = 0
!
! Set NTEST = 1 so keep doing new files with same fit until the last
! file is found at which time NTEST will be changed.
    NTEST = 1
```

```
!-----------------------------------------------------
! WRITE INFORMATION ABOUT THE FITS TO THE FILE OUT2:
! FIND CALIBRATION AND GAIN DATA
      OPEN (UNIT=5, FILE=SCALIB, STATUS='OLD')
      READ(5,*) G
      READ(5,*) SA
      READ(5,*) SAERR
      READ(5,*) BA
      READ(5,*) BAERR
      READ(5,*) COVA
      READ(5,*) SB
      READ(5,*) SBERR
      READ(5,*) BB
      READ(5,*) BBERR
      READ(5,*) COVB
      CLOSE(UNIT=5, STATUS='KEEP')
!
! Open file containing start parameters as unit #4
   OPEN(UNIT=4, FILE=STPARA, STATUS='OLD')
!
! Read the first line telling the length of the measurement that the
! start parameters are for (is a dummy line)
   READ(4,'(A50)') SBNAME
!
   DO 1200, NF = 1, 3
!
   IF (NF.EQ.1) THEN
      NTERMS = 5
      SBNAME = 'COHERENT with fixed width and height          '
   ELSEIF (NF.EQ.2) THEN
      NTERMS = 4
      SBNAME = 'BETA with linked amplitudes, Ca linked to coherent'
   ELSEIF (NF.EQ.3) THEN
      NTERMS = 6
      SBNAME = 'ALPHA with linked amplitudes                  '
   ENDIF
!
! Writing the subroutine to OUT2:
   WRITE(7,448) SBNAME
 448 FORMAT(/,1X,'SUBROUTINE: ',A50,)
!
! Input a dummy character (as are description lines in the file
! with the start parameters)
   READ(4,'(A50)') SBNAME
!
! Input the initial guesses from the file
```

```
1208 DO 1209, I=1, NTERMS
   READ(4,*) AA1(I)
1209 CONTINUE
!
! Input the number of channels and the start channel from the file
   READ(4,*) NPTS,NST
!
! Writing the number of channels and starting channel to OUT2:
   WRITE(7,449) NPTS, NST
 449 FORMAT(10X,I3,' channels starting in channel ',I3)
!
! Write starting parameters to output location:
   WRITE(7,1218)
1218 FORMAT(11X,'The starting parameters are:')
   DO 1203, I = 1, NTERMS
      WRITE(7,1217) I, AA1(I)
1217 FORMAT(16X, 'A(',I2,') = ',G12.5)
1203 CONTINUE
!
! Initialize all deviations, ADEV(), to zero:
   DO 1205, I = 1 , NTERMS
   ADEV(I) = 0.
1205 CONTINUE
!
! Input the number of parameters to be fitted over a restricted range
   READ(4,*) NR
   WRITE(7,1201) NR
1201 FORMAT(10X,I3,' RESTRICTED PARAMETERS:')
!
! Input the deviations for the specific A(I)'s and write to OUT2:
   DO 1202, I = 1 , NR
!  input:
   READ(4,*) IRES , ADEV(IRES)
!  output:
   WRITE(7,310) IRES, AA1(IRES), ADEV(IRES)
 310 FORMAT(16X,'A(',I2,') = ',G12.5,' +/- ',G12.5)
1202 CONTINUE
!
1200 CONTINUE
!
! Write the 2 random numbers to desired output:
   WRITE(7,1211) IH(1), IH(2)
1211 FORMAT(/,1X,'random number entry points ',I5,1X,I5)
!
! Write a line of *'s to OUT2:
   WRITE(7,445)
```

```
!
! Close the start parameters file:
    CLOSE(UNIT=4, STATUS='KEEP')
!-----------------------------------------------------
!
! Here is where the fit to the next file starts
!
! Increment file counter III
!
 998 III = III + 1
!
! Set FNAM to the (next) file in FNAMS(), OFSET to the corresponding
! OFSETS(), W to WW(), and H to HH()
    FNAM = FNAMS(III)
    OFSET = OFSETS(III)
    W = WW(III)
    H = HH(III)
!
! Open file containing start parameters as unit #4
    OPEN(UNIT=4, FILE=STPARA, STATUS='OLD')
!
! Read the first line telling the length of the measurement that the
! start parameters are for (is a dummy line)
    READ(4,'(A50)') SBNAME
!
! Run the programs.  When NF = 1, do the fixed width coherent
! program.  When NF = 2, do the beta program, and when NF = 3, do
! the alpha program.
!
c Call Seed moved from 2pbfit, to ensure changing random numbers are
c generated....
    CALL SEED(IH(1))
    DO 309, NF = 1, 3
!
    IF (NF.EQ.1) THEN
       NTERMS = 5
    ELSEIF (NF.EQ.2) THEN
       NTERMS = 4
    ELSEIF (NF.EQ.3) THEN
       NTERMS = 6
    ENDIF
!
! Input a dummy character (as are description lines in the file
! with the start parameters)
    READ(4,'(A50)') SBNAME
!
```

```
! Input the initial guesses from the file
  8 DO 9 I=1,NTERMS
    READ(4,*) AA1(I)
  9 CONTINUE
!
! Input the number of channels and the start channel from the file
    READ(4,*) NPTS,NST
!
! Set the last channel number (NTOP)
    NTOP=NPTS+NST-1
!
! Initialize all deviations, ADEV(), to zero:
    DO 305 I = 1 , NTERMS
    ADEV(I) = 0.
 305 CONTINUE
!
! Input the number of parameters to be fitted over a restricted range
    READ(4,*) NR
!
! Input the deviations for the specific A(I)'s:
    DO 302 I = 1 , NR
    READ(4,*) IRES , ADEV(IRES)
 302 CONTINUE
!
! Re-initialize FT1 and FT1ERR:
    FT1    = 0.
    FT1ERR = 0.
!
!
! Run the fit program:
    CALL FIT(NTERMS, NPTS, NST, NTOP, NR, AA1, ADEV, IH, ITEST, FNAM,
   1 OFSET, CPOS, FT1, FT1ERR, NF, G, W, H, ISUB, CO1)
!
! Set the peak magnitudes to keep their values
    IF (NF.EQ.1) THEN
       CO1 = FT1
       CO1ERR = FT1ERR
    ELSEIF (NF.EQ.2) THEN
       BE1 = FT1
       BE1ERR = FT1ERR
    ELSEIF (NF.EQ.3) THEN
       AL1 = FT1
       AL1ERR = FT1ERR
    ENDIF
!
 309 CONTINUE
```

```
   CLOSE(UNIT=4, STATUS='KEEP')
!
! Calculate the ratios and their errors.
   RA = AL1/CO1
   RAERR = RA * (((AL1ERR/AL1)**2. + (CO1ERR/CO1)**2.)**0.5)
!
   RB = BE1/CO1
   RBERR = RB * (((BE1ERR/BE1)**2. + (CO1ERR/CO1)**2.)**0.5)
!
! Set parameters (calb. line slope, intercept, etc.) depending
! on which system (tibia or calcaneus) was used
! Note:  ISYS = 4 for calcaneus,  ISYS = 5 for tibia
!
! Calculate Concentrations:
!
! Via Alpha:
   PPMA = (RA - BA) / SA
   PPMAER = RAERR*RAERR + BAERR*BAERR
   PPMAER = PPMAER + PPMA*PPMA*SAERR*SAERR + 2*PPMA*COVA
   PPMAER = (PPMAER**0.5) / SA
!
! Via Beta:
   PPMB = (RB - BB) / SB
   PPMBER = RBERR*RBERR + BBERR*BBERR
   PPMBER = PPMBER + PPMB*PPMB*SBERR*SBERR + 2*PPMB*COVB
   PPMBER = (PPMBER**0.5) / SB
!
! If people (ISUB=0) then multiply these #s by 1.29 to compensate for
! different cross-sections between bone and plaster of paris
!    IF (ISUB.EQ.0) THEN
!       PPMA = PPMA * 1.29
!       PPMAER = PPMAER * 1.29
!       PPMB = PPMB * 1.29
!       PPMBER = PPMBER * 1.29
!    ENDIF
!
!
! If people (ISUB=0) then multiply these #s by 1.29 to compensate for
! different cross-sections between bone and plaster of paris
   IF (ISUB.EQ.0) THEN
      PPMA = 1.29*RA/SA
      PPMAER = PPMA*PPMA*(RAERR*RAERR/RA/RA+SAERR*SAERR/SA/SA)
            PPMAER = (PPMAER)**0.5
      PPMB = 1.29*RB/SB
      PPMBER = PPMB*PPMB*(RBERR*RBERR/RB/RB+SBERR*SBERR/SB/SB)
            PPMBER = (PPMBER)**0.5
```

```
      ENDIF
!
! Weighted mean of these:
      PPMERR = 1/((PPMBER)**2.) + 1/((PPMAER)**2.)
      PPMERR = (1/PPMERR)**0.5
      PPM = (PPMB/((PPMBER)**2.) + PPMA/((PPMAER)**2.)) * (PPMERR**2.)
!
! Write the concentrations to the output files.
!
! To OUT1:
      WRITE(3,460) PPMA, PPMAER
      WRITE(3,461) PPMB, PPMBER
      WRITE(3,462) PPM, PPMERR
  460 FORMAT(/,1X, 'The concentration via alpha 1 is: ', F9.4,
     1 ' +/- ', F9.4, ' ppm.')
  461 FORMAT(1X, 'The concentration via beta 1 is:  ', F9.4,
     1 ' +/- ', F9.4, ' ppm.')
  462 FORMAT(1X, 'The weighted mean concentration is:', F9.4,
     1 ' +/- ', F9.4, ' ppm.'/)
!
! To OUT3:
      WRITE(8,1002) RA, RAERR, RB, RBERR
 1002 FORMAT(4(2X, F12.6))
!
! Write the peak amplitudes and the concentrations to the screen:
!
      WRITE(*,463) FNAM
  463 FORMAT(1X, 'The results of analyzing the file ',A35,' are: '/)
      WRITE(6,303) CO1, CO1ERR
      WRITE(6,304) BE1, BE1ERR
      WRITE(6,306) AL1, AL1ERR
  303 FORMAT(1X, 'Coherent peak amplitude is:',G12.5,' +/- ', G12.5)
  304 FORMAT(1X, 'Beta 1 peak amplitude is:  ',G12.5,' +/- ', G12.5)
  306 FORMAT(1X, 'Alpha 1 peak amplitude is: ',G12.5,' +/- ', G12.5)
!
      WRITE(6,460) PPMA, PPMAER
      WRITE(6,461) PPMB, PPMBER
      WRITE(6,462) PPM, PPMERR
!
 1001 WRITE(*,*)
!
! If have just finished the last data file (ie. III = INUM) then
! stop by setting NTEST = 0
      IF(III.EQ.INUM) THEN
         NTEST = 0
         IFILES = 1
```

```
    ENDIF
!
! If NTEST is 0, go to 1000, if NTEST is 1, go to 998,
! if NTEST is 2 go to 999:
    IF(NTEST-1)1000,998,999
!
! Close the files OUT1 and OUT2:
 1000 CLOSE(UNIT=3, STATUS='KEEP')
    CLOSE(UNIT=7, STATUS='KEEP')
    CLOSE(UNIT=8, STATUS='KEEP')
!
! End of program
    END
```

Subroutine 7:

```
    SUBROUTINE MATINV(ARRAY,NORDER,DET)
    DOUBLE PRECISION ARRAY,AMAX,SAVE
    DIMENSION ARRAY(10,10),IK(10),JK(10)
  10 DET=1.
  11 DO 100 K=1,NORDER
C
C       FIND LARGEST ELEMENT ARRAY(I,J) IN REST OF MATRIX
C
    AMAX=0.
  21 DO 30 I=K,NORDER
    DO 30 J=K,NORDER
  23 IF(DABS(AMAX)-DABS(ARRAY(I,J)))24,24,30
  24 AMAX=ARRAY(I,J)
    IK(K)=I
    JK(K)=J
  30 CONTINUE
C
C     INTERCHANGE ROWS AND COLUMS TO PUT AMAX IN ARRAY(K,K)
C
  31 IF(AMAX)41,32,41
  32 DET=0.
    GOTO 140
  41 I=IK(K)
    IF(I-K)21,51,43
  43 DO 50 J=1,NORDER
    SAVE=ARRAY(K,J)
    ARRAY(K,J)=ARRAY(I,J)
  50 ARRAY(I,J)=-SAVE
  51 J=JK(K)
    IF(J-K)21,61,53
  53 DO 60 I=1,NORDER
```

```
      SAVE=ARRAY(I,K)
      ARRAY(I,K)=ARRAY(I,J)
   60 ARRAY(I,J)=-SAVE
C
C        ACCUMULATE ELEMENTS OF INVERSE MATRIX
C
   61 DO 70 I=1,NORDER
      IF(I-K)63,70,63
   63 ARRAY(I,K)=-ARRAY(I,K)/AMAX
   70 CONTINUE
   71 DO 80 I=1,NORDER
      DO 80 J=1,NORDER
      IF(I-K)74,80,74
   74 IF(J-K)75,80,75
   75 ARRAY(I,J)=ARRAY(I,J)+ARRAY(I,K)*ARRAY(K,J)
   80 CONTINUE
   81 DO 90 J=1,NORDER
      IF(J-K)83,90,83
   83 ARRAY(K,J)=ARRAY(K,J)/AMAX
   90 CONTINUE
      ARRAY(K,K)=1./AMAX
  100 DET=DET*AMAX
C
C        RESTORE ORDERING OF MATRIX
C
  101 DO 130 L=1,NORDER
      K=NORDER-L+1
      J=IK(K)
      IF(J-K)111,111,105
  105 DO 110 I=1,NORDER
      SAVE=ARRAY(I,K)
      ARRAY(I,K)=-ARRAY(I,J)
  110 ARRAY(I,J)=SAVE
  111 I=JK(K)
      IF(I-K)130,130,113
  113 DO 120 J=1,NORDER
      SAVE=ARRAY(K,J)
      ARRAY(K,J)=-ARRAY(I,J)
  120 ARRAY(I,J)=SAVE
  130 CONTINUE
  140 RETURN
      END
```